Evaluation of Impact of Nanoparticle Pollutants on Water Reclamation

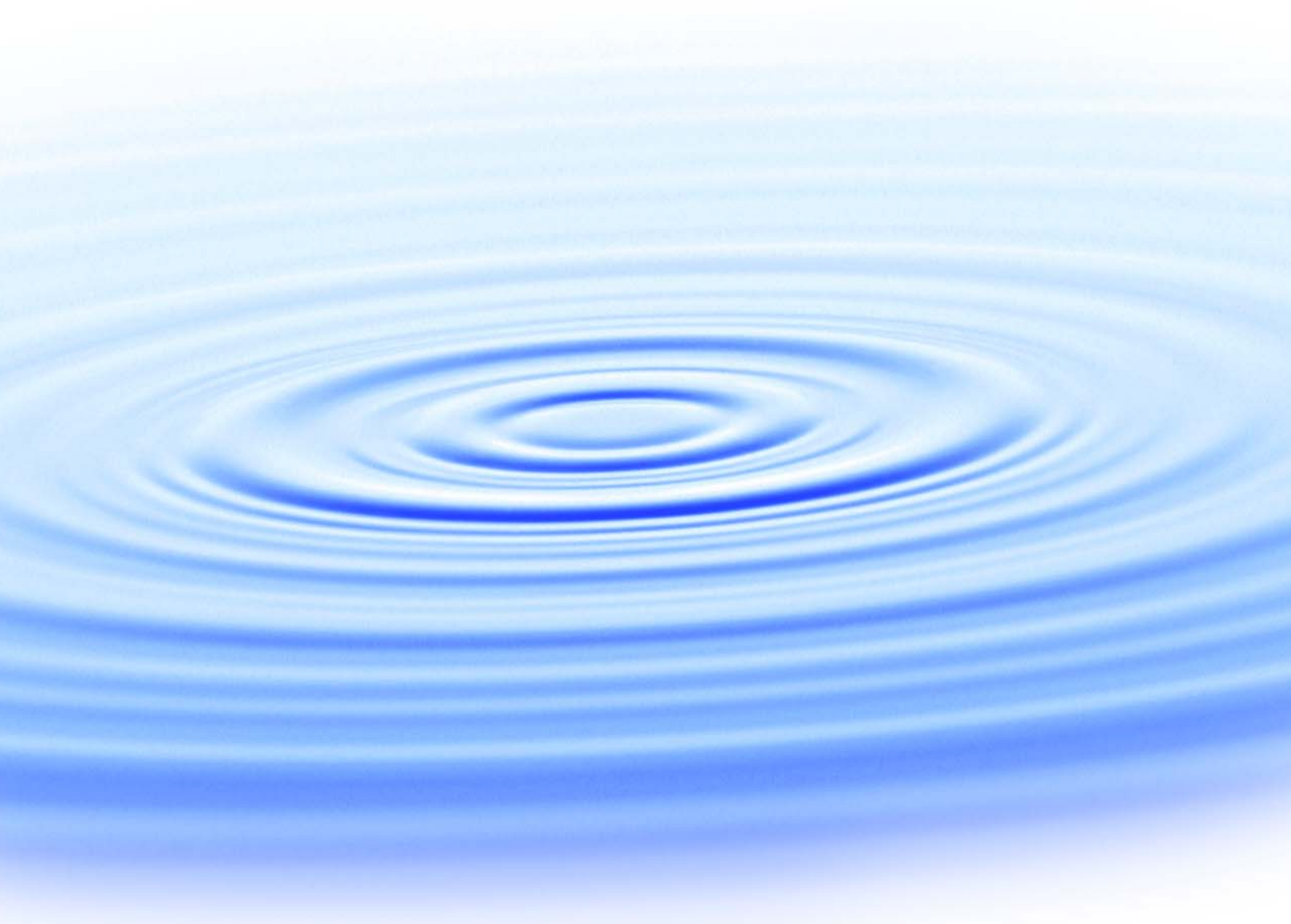

WateReuse Research Foundation

Evaluation of Impact of Nanoparticle Pollutants on Water Reclamation

About the WateReuse Research Foundation

The mission of the WateReuse Research Foundation is to conduct and promote applied research on the reclamation, recycling, reuse, and desalination of water. The Foundation's research advances the science of water reuse and supports communities across the United States and abroad in their efforts to create new sources of high quality water through reclamation, recycling, reuse, and desalination while protecting public health and the environment.

The Foundation sponsors research on all aspects of water reuse, including emerging chemical contaminants, microbiological agents, treatment technologies, salinity management and desalination, public perception and acceptance, economics, and marketing. The Foundation's research informs the public of the safety of reclaimed water and provides water professionals with the tools and knowledge to meet their commitment of increasing reliability and quality.

The Foundation's funding partners include the Bureau of Reclamation, the California State Water Resources Control Board, the California Energy Commission, and the California Department of Water Resources. Funding is also provided by the Foundation's Subscribers, water and wastewater agencies, and other interested organizations.

Evaluation of Impact of Nanoparticle Pollutants on Water Reclamation

Dr. Rajagopalan Ganesh
Kennedy/Jenks Consultants

Dr. Diego Rosso
University of California, Irvine

Cosponsors
Bureau of Reclamation
South Bay Water Recycling (CA)

WateReuse Research Foundation
Alexandria, VA

Disclaimer

This report was sponsored by the WateReuse Research Foundation. The Foundation, its board members, and the project cosponsors assume no responsibility for the content of this publication or for the opinions or statements of facts expressed in the report. The mention of trade names of commercial products does not represent or imply the approval or endorsement of the WateReuse Research Foundation, its board members, or the cosponsors. This report is published solely for informational purposes.

For more information, contact:
WateReuse Research Foundation
1199 North Fairfax Street, Suite 410
Alexandria, VA 22314
703-548-0880
703-548-5085 (fax)
www.WateReuse.org/Foundation

WateReuse Research Foundation Project Number: WRF-07-04
WateReuse Research Foundation Product Number: 07-04-1

ISBN 978-1-934183-85-4
Library of Congress Control Number: 2013945358

Printed in the United States of America

Printed on Recycled Paper

Contents

Figures

Tables

Acronyms

Ag	nanosilver
BET	Brunauer, Emmett, and Teller method
BOD	biochemical oxygen demand
C60	fullerene
COD	chemical oxygen demand
CdTe	cadmium telluride
CuNP	copper nanoparticles
CuO	nanocopper oxide
DI	deionized
DLS	dynamic light scattering
DLVO	Derjaguin-Landau-Verwey-Overbeek
DO	dissolved oxygen
DOC	dissolved organic carbon
EDS	energy dispersive X-ray spectroscopy
EPA	Environmental Protection Agency
F/M	food-to-microorganism ratio
ICP	inductively coupled plasma
ISO	International Organization for Standardization
kCPS	kilo counts per second
MLSS	mixed liquor suspended solids
MLVSS	mixed liquor volatile suspended solids
MPN	most probable number
NaCl	sodium chloride
NNI	National Nanotechnology Initiative
NO_3^-	nitrate
NO_2^-	nitrite
NOM	natural organic matter
NTU	nephelometer turbidity units (turbidity)
OCSD	Orange County Sanitation District
PSD	particle size distribution
ROS	reactive oxygen species
sCOD	soluble chemical oxygen demand
SEM	scanning electron microscopy
SVI	sludge volume index
TDS	total dissolved solids
TEM	transmission electron microscopy
TiO_2	titanium dioxide
TSS	total suspended solids
UCI	University of California, Irvine
UCLA	University of California, Los Angeles
UV	ultraviolet
WWICS	Woodrow Wilson International Center for Scholars
ZnO	nanozinc oxide

Foreword

The WateReuse Research Foundation, a nonprofit corporation, sponsors research that advances the science of water reclamation, recycling, reuse, and desalination. The Foundation funds projects that meet the water reuse and desalination research needs of water and wastewater agencies and the public. The goal of the Foundation's research is to ensure that water reuse and desalination projects provide high quality water, protect public health, and improve the environment.

An Operating Plan guides the Foundation's research program. Under the plan, a research agenda of high priority topics is maintained. The agenda is developed in cooperation with the water reuse and desalination communities including water professionals, academics, and Foundation Subscribers. The Foundation's research focuses on a broad range of water reuse research topics including:

- Definition of and addressing emerging contaminants
- Public perceptions of the benefits and risks of water reuse
- Management practices related to indirect potable reuse
- Groundwater recharge and aquifer storage and recovery
- Evaluation and methods for managing salinity and desalination
- Economics and marketing of water reuse

The Operating Plan outlines the role of the Foundation's Research Advisory Committee (RAC), Project Advisory Committees (PACs), and Foundation staff. The RAC sets priorities, recommends projects for funding, and provides advice and recommendations on the Foundation's research agenda and other related efforts. PACs are convened for each project and provide technical review and oversight. The Foundation's RAC and PACs consist of experts in their fields and provide the Foundation with an independent review, which ensures the credibility of the Foundation's research results. The Foundation's Project Managers facilitate the efforts of the RAC and PACs and provide overall management of projects.

The Foundation's primary funding partners include the Bureau of Reclamation, the California State Water Resources Control Board, the California Energy Commission, Foundation Subscribers, water and wastewater agencies, and other interested organizations. The Foundation leverages its financial and intellectual capital through these partnerships and other funding relationships.

The widespread use of nanomaterials in everyday products has increased the concerns about their potential release into the environment. The objective of this study was to obtain preliminary information on the fate and impact of manufactured nanomaterials in three key water reclamation unit processes (biological treatment, media filtration, and disinfection). This report documents the results of bench-scale studies that were performed to meet the project's objective.

Richard Nagel
Chair
WateReuse Research Foundation

G. Wade Miller
Executive Director
WateReuse Research Foundation

Acknowledgments

This project was funded by the WateReuse Research Foundation in cooperation with the City of San Jose and the Orange County Sanitation District.

This study would not have been possible without the insights, efforts, and dedication of many individuals and organizations. These include the members of the research team and PAC members; the WateReuse Research Foundation's project manager, Julie Minton; and many key individuals at the participating utilities and related organizations. In particular, the project team would like to thank laboratory and operational staff at Orange County Sanitation District for their help with nanomaterial analyses and wastewater sample collection and characterization.

The research team would like to thank immensely Dr. Eric Hoek and Dr. Mingua Li at NanoMeTeR Lab in the Department of Civil and Environmental Engineering at the University of California, Los Angeles, for their help with analyses and characterization of nanomaterial.

The research team would like to thank the WateReuse Research Foundation for funding this applied research project, as well as the following organizations for their in-kind contributions: the Orange County Sanitation District, Fountain Valley, CA, and the City of San José – South Bay Water Recycling, San Jose, CA.

Principal Investigator and Project Manager

Rajagopalan Ganesh, Ph.D., *Kennedy/Jenks Consultants*

Co-Principal Investigator

Diego Rosso, Ph.D., *University of California at Irvine*

Research Project Team

William J. Cooper, Ph.D., *University of California at Irvine*
Betty H. Olson, Ph.D., *University of California at Irvine*
Leila Khatib, Ph.D., *Kennedy/Jenks Consultants*
Joshua Smeraldi, *University of California at Irvine*
Turaj Hosseini, *University of California at Irvine*

Project Advisory Committee

James (Chip) Kilduff, Ph.D., *Rensselaer Polytechnic Institute*
Yuliana Porras, *U.S. Bureau of Reclamation*
Nora Savage, Ph.D., *U.S. Environmental Protection Agency*
Paul G. Tratnyek, Ph.D., *Oregon Health & Science University*
Paul Westerhoff, Ph.D., *Arizona State University*

Executive Summary

Project Background and Objectives

In the very near future, the water reclamation industry will have to address an entirely new family of pollutants, *manufactured nanomaterials*. Manufactured nanomaterials (nanomaterials) are extremely small in size (1–100 nm in at least one dimension), are potentially highly reactive, and are often manipulated at the molecular level to generate "new" types of compounds (National Nanotechnology Initiative [NNI], 2011). Although the source elements for most nanomaterials are often the same as the chemicals (e.g., inorganic ions) already used in commercial products, at nanoscale size, many materials have been shown to be far more reactive and to possess unique physical and chemical characteristics compared to their ionic counterparts (Rolison 2003; USEPA, 2007). As a result, nanomaterials behave very differently than their conventional counterparts and offer superior product performance. Furthermore, the same nanomaterials are shown to exhibit different behavior at different size ranges. In recent years, more than 1000 everyday products containing nanomaterials have been introduced into the market. The world market for products containing nanomaterials is expected to increase to more than 2.5 trillion in less than 10 years (Maynard et al., 2006).

With increasing use of nanomaterials in products, it is conceivable that some of these materials will end up in the wastewater streams. Presence of nanomaterials in biosolids and model wastewater effluents has already been reported (Kiser et al., 2009; Limbach et al., 2008). Simultaneously, potential adverse effects to human health and environment because of exposure to nanomaterials have also been reported (Long et al., 2006). Currently, limited information is available on the fate and transport of nanomaterials in wastewater treatment/water reclamation processes, or on any adverse effect of nanomaterials to the existing treatment systems. In particular, information regarding their fate and effects compared to their ionic counterparts (e.g., ionic copper versus nanocopper) is not available.

The objective of this study is to obtain preliminary information on the fate and impact of manufactured nanomaterials in three key water reclamation unit processes (biological treatment, media filtration, and disinfection). Bench-scale studies were performed to evaluate the following:

- Do nanomaterials behave differently than conventional (dissolved ionic) constituents in water reclamation processes?
- What is the impact of size of nanomaterials on water reclamation?
- Do different nanomaterials behave similarly in these treatment processes?

Three metal (oxide) nanomaterials (nanocopper, zinc oxide, and nanosilver) of varying size ranges were selected for this study. Their fate and effects were compared with those of their ionic salts. These nanomaterials were added to filtered or unfiltered wastewaters from the Orange County Sanitation District (OCSD), Fountain Valley, CA for these evaluations.

The fate and effects of nanomaterials during biological treatment were evaluated through:

- Determination of nanomaterials removal by abiotic and biomass mediated processes in wastewater,
- Microbial growth (most probable number [MPN]) tests, and
- Gross process parameters (e.g., organic degradation, nitrate [NO_3^-] and nitrite [NO_2^-] production) in bioreactors.

The fate of nanomaterials during media filtration was evaluated through column studies using sand media of different sizes and different effluent loading rates. Finally, the disinfection studies addressed the chlorine demand in the presence or absence of nanomaterials.

Results and Implications

Characterization of nanomaterials using scanning electron microscopy (SEM), energy dispersive X-ray spectroscopy (EDS), and other techniques indicated that the primary size of the nanomaterials used varied from 50 to 500 nm. These dimensions are larger than those indicated by the vendors at the time of procurement (Table ES-1). Note that the SEM and other in-house characterizations of the nanomaterials were performed after almost all of the fate and transport studies were completed (i.e., nearly 2 years after the material procurement). Such long storage time can potentially alter nanomaterials' characteristics. Hence, future studies to investigate environmental and other effects of nanomaterials should perform in-house characterization soon after (e.g., within a few weeks of) procurement. In aqueous suspensions, the nanomaterials aggregated to a larger size range (125–3000 nm).

Table ES.1. Nanozinc Oxide and Silver Materials Suspensions (1%) Procured for this Study

Sample ID	Nanomaterial	Size Indicated by Vendor (nm)	Measured Particle Size (nm)
ZnO-A	Zinc Oxide	40-100	100
ZnO-B	Zinc Oxide	30	300
ZnO-C	Zinc Oxide	<10	50–300
CuNP	Copper	50	100–200
Ag-A	Silver	<100	100
Ag-B	Silver	150	ND
Ag-C	Silver	<120	20–400

Note. ND =Not Determined

Studies were performed to evaluate removal of nanomaterials in the presence and absence of activated sludge biomass (mixed liquor suspended solids [MLSS] ~ 650 mg/L). These studies were performed using an initial concentration of 2 to 10 mg/L. Currently, no data are available on current or projected concentrations of the nanomaterials in actual wastewaters. A maximum concentration of 10 mg/L was selected for this study since it is unlikely that concentrations higher than this will enter wastewater treatment plants. Nanomaterials removed in the absence of biomass (0.45 µm filtrate using Fisher Brand Nitrocellulose

Filters) were assumed to represent the fraction removed by abiotic processes such as precipitation, aggregation, and settling. The nanomaterials removed in the presence of sludge biomass would include the fraction removed by biosorption and possible uptake, in addition to that removed by aggregation and sedimentation processes. The data using filtered wastewater showed some differences in the removal of nano and ionic copper as well as copper and zinc removal. In general, nanomaterials were removed more effectively than their ionic counterparts in the filtered wastewater. Approximately 80% of the added nanocopper (10 mg/L) and 60% of the ionic copper were removed in the filtered wastewater. Approximately 55% of the ionic zinc was removed whereas the removal of three different nanozinc oxides varied from 55 to 75%. Copper (nano or ionic form) was removed more effectively than respective forms of zinc. Limited tests were performed to evaluate removal of nanosilver in the wastewater. The filtrate samples contained less than 10% of the added silver. However, the difficulties encountered in nanosilver analyses rendered interpretation of the silver data difficult. The relatively higher removal of copper compared to zinc was consistent with that predicted by a chemical speciation model (MINTEQ) for the ionic constituents. SEM analyses of the removed solids showed distinctly different morphologies for nano and ionic materials. The nano materials appeared to have aggregated to larger size (> 1 µm) during their removal. Ionic salts precipitated from the wastewater as finer solids, completely covering the filter surface. These observations support the hypothesis that the mechanisms governing the removal of nano and ionic constituents are different, thus potentially resulting in the differences in the extent of their removal from the wastewater. Analyses of nanoscale suspended particles by Dynamic Light Scattering (DLS) technique also showed differences in size distribution and count rates for the ionic and nanomaterial filtrates. In the presence of activated sludge biomass, removal of copper and zinc increased by 5 to 20%.

Most Probable Number (MPN) tests were performed to evaluate potential inhibitory effects of nanomaterials to key wastewater microorganisms (coliform bacteria and ammonia oxidizing bacteria; Halvorson and Ziegler, 1933). The data indicated that at 10 mg/L concentration, ionic copper and ionic zinc inhibited microbial growth while no inhibition was observed in the presence of nanocopper or zinc oxide. At 2 mg/L, ionic zinc temporarily inhibited growth of ammonia oxidizing bacteria. No such inhibition was observed for coliform bacteria. Nanozinc oxide did not inhibit coliform or ammonia oxidizing bacteria. The nanomaterial removal studies indicated that more ionic copper or zinc than their nanoscale counterparts remained in the wastewater suspensions. These observations seem to indicate that dissolution of nanomaterial to ionic form may be a key mechanism of toxicity when nanomaterials are released into the environment. However, in the studies using nanosilver, growth of ammonia oxidizing bacteria was delayed in the presence of nanosilver whereas no such delay was observed in the presence of ionic silver. This data suggested that nanomaterial could interact directly (i.e., without undergoing dissolution) with microorganisms and cause inhibition.

Bioreactor studies performed to evaluate impact of nanomaterial on key process parameters (e.g., organic degradation, biomass levels, dissolved oxygen levels, pH, nitrite, and nitrate transformations) did not yield any significant differences between nano and ionic materials spiked (0.2 or 2 mg/L) samples.

Column tests performed to evaluate the transport of nanomaterial in media filter indicated that nanomaterial tend to aggregate and deposit more than ionic salts in the media filters. Ionic zinc breakthrough occurred early and the peaks were higher than with nanomaterial. The differences in the breakthrough patterns were more pronounced for larger media (0.45

mm) than for smaller media (0.175 mm). Columns packed with larger media provide larger pore space for ionic zinc to move freely, while nanozinc oxides are still captured. The smaller media provides smaller pore space that in turn increases capture of ionic zinc and nanozinc oxide.

Finally, the evaluation of chlorine demand in ionic zinc and nanozinc oxides indicated no significant differences. The chlorine demands for these samples were similar to those observed with the control samples.

In summary, the results from this study indicated significant differences in the fate and transport behavior of nanomaterials compared to their ionic forms in water reclamation processes. More nanomaterial than ionic salts were removed from wastewater and accumulated in biosolids. Although most of the observed toxic effects were associated with the ionic constituents, some evidence of direct nanomaterial toxicity was also observed. More nanomaterial was captured in the media filters than ionic salts.

Recommendations for Future Studies

The data from this study indicated that future studies should investigate the toxicity effects of nanomaterial in detail using continuous flow reactors and thorough field investigations. Initial toxicity studies must include (1) nanomaterials such as silica that do not aggregate under Derjaguin-Landau-Verwey-Overbeek (DLVO) forces thus tending to remain in suspension; (2) nanomaterials with novel structures and those with molecular level changes (e.g., new carbon-based nanomaterials), and (3) nanomaterials such as silver or copper that are known to cause toxic effects in their ionic form. Furthermore, future studies should investigate the impact that is due to long-term release of nanomaterial in wastewater facilities. Also, because more nanomaterials are likely to be in the biosolids, the fate of nanomaterials in biosolids should be investigated. Finally, although not addressed in this study, preliminary data from other studies indicate that suspended particles in nanoscale size (biogenic or otherwise) can enter membrane pores and cause fouling during membrane-based water reclamation processes (Safarik and Phipps, 2006). Hence, detailed investigations must be performed to evaluate the impact of nanomaterial on membrane filtration processes.

Chapter 1

Introduction

1.1 Background

The widespread use of nanomaterials in everyday products has increased the concerns about their potential release into the environment (Maynard et al., 2006). Nanoscale materials (or nanomaterials) are characterized by extremely small size (i.e., particles with a size of 1 to 100 nm at least in one dimension) and commensurately high surface area (National Nanotechnology Initiative (NNI), 2011). Although the source elements for most nanomaterials are often the same as the ions already used in commercial products, at nanoscale size, many materials have been shown to be far more reactive than their ionic counterparts and to possess more unique physical and chemical characteristics than their ionic counterparts (Rolison, 2003). Furthermore, nanomaterials lend themselves to surface functionalization, thereby facilitating interactions with the surrounding medium in ways not possible with micron-sized particles. Consequently, new mechanisms of interactions between nanoparticles and the surrounding environment are now possible. It has already been demonstrated that at nanoscale size properties such as color, conductivity, solubility, and reactivity may differ from ionic or larger counterparts (Rolison, 2003; U.S. Environmental Protection Agency [EPA], 2007; NNI, 2011).

Because of their beneficial characteristics, nanomaterials are currently used in a number of commercial and industrial products. According to a nanomaterials products survey by the Woodrow Wilson International Center for Scholars (WWICS, 2011), there are currently more than 1000 products containing nanomaterials in the market. Nanomaterials in these products are made of a variety of metals, metal oxide, and organic compounds. They are used in a variety of shapes and forms (e.g., rods, powders, or fibers). Depending on the application, nanomaterials are used as free powders, functionalized with organic or inorganic ligands to form stable suspensions, or loosely or tightly incorporated into a fixed matrix (Gottschalk and Nowack, 2011).

With increasing use of nanomaterials in products, it is conceivable that some of these materials will end up in the wastewater streams. Presence of nanomaterials in biosolids and model wastewater effluents has already been reported (Kiser et al., 2009; Limbach et al., 2008). Simultaneously, potentially adverse effects to human health and the environment because of exposure to nanomaterials have also been reported (Long et al., 2006). Hence, when new types of materials such as nanomaterials enter wastewater or water reclamation systems, the water reclamation industry needs to understand the fate of these materials during wastewater treatment and inhibitory effects of these materials to the current treatment processes. For nanomaterials in particular, information regarding their fate and effects compared to their ionic counterparts (e.g., ionic copper versus nanocopper) is critically required.

For example, when nanomaterials enter biological treatment systems, questions regarding of their fate and removal may include the following: Do the nanomaterials behave differently than their ionic counterparts? If yes, at what size range? How much of these materials are

removed? How does functionalization alter their removal? How are the materials removed through abiotic processes by wastewater constituents? How does the presence of biomass alter their removal? How rapidly are they being removed? Do the nanomaterials desorb and redissolve after their initial removal?

The evaluation of inhibitory effects of nanomaterials may include the following: Are these materials toxic to any specific group of microorganisms (e.g., most prevalent group, most sensitive group)? Is the effect lethal or transient in nature? Is the harm primarily caused by shock load or continuous release? What is the best method to identify the inhibitory effects caused by these materials (e.g., growth, respiration, community change, DNA damage studies)? How do these results translate from one nanomaterial to another?

Research studies about the fate and effect of nanomaterials are just beginning to be produced. Very limited information is currently available on many of these issues. This study was performed to obtain preliminary information through laboratory bench-scale studies to address some of these questions. The results from this study, along with other ongoing and future studies, will provide information for water reclamation utility managers and regulators to deal with the release of these new types of materials into wastewaters.

1.2 Objective

The objective of this study is to obtain preliminary information on the fate and impact of manufactured nanomaterials in three key water reclamation unit processes (**biological treatment, media filtration, and disinfection**). Bench-scale studies were performed to evaluate the following:

- Do nanomaterials behave differently than conventional (dissolved / ionic) constituents in water reclamation processes?
- What is the impact of size of nanomaterials on water reclamation?
- Do different nanomaterials behave similarly in these treatment processes?

1.3 Approach

Three metal (oxide) nanomaterials (nanocopper, zinc oxide, and nanosilver) of varying size ranges were selected for this study. Their fate and effects were compared with those of their ionic salts.

The fate and effects of nanomaterials during biological treatment were evaluated through

- determination of nanomaterials removal by abiotic and biomass mediated processes in wastewater,
- MPN tests, and
- gross process parameters (e.g., organic degradation, nitrate and nitrite production) in bioreactors.

The fate of nanomaterials during media filtration was evaluated through column studies using sand media of different sizes and different effluent loading rates. Finally, the disinfection studies addressed the chlorine demand in the presence or absence of nanomaterials.

1.4 Report Organization

This report is organized into ten chapters. Chapter 1 provides a background of the issue and study objectives. Chapter 2 presents a brief summary of current state of knowledge. Chapter 3 discusses the approach and methods used in this study. Chapters 4 through 9 present and discuss the results of this study. Chapter 4 presents data on characterization of various nanomaterials used. Chapter 5 presents results from studies on removal of nanomaterials. Chapter 6 provides data from microbial growth and respiration studies. Chapter 7 presents data on gross operational parameters in bioreactors in the presence of nanomaterials. Chapters 8 and 9 present data from media filtration and chlorine demand evaluation studies. Finally, Chapter 10 provides a summary of the results and recommendations for the next steps.

Chapter 2

State of Knowledge

2.1 Background

A number of review articles are available on the human health effects, risk assessment, and environmental fate of manufactured nanomaterials. This chapter provides an overview of available information of the fate and effect of manufactured nanomaterials during biological treatment, media filtration, and disinfection processes.

2.2 Fate and Effect in Biological Treatment Process

2.2.1 Nanomaterial Removal During Biological Treatment

The removal of nanomaterials during biological wastewater treatment may occur through abiotic processes such as aggregation and settling or through biomass-mediated processes such as biosorption or uptake. Removal by abiotic processes may be dictated by wastewater constituents (e.g., dissolved salts, organic content, and pH) as well as by properties of nanomaterials (e.g., type, size, zeta potential). In general, the stability or removal of charged particles such as nanomaterials appear to be affected by various forces of attraction or repulsion (e.g., electrostatic repulsion, steric stabilization, van der Waals forces of attraction) occurring in the aqueous suspension as defined by Derjaguin-Landau-Verwey-Overbeek (DLVO) theory and relevant extensions (Derjaguin and Landau, 1941; Verwey and Overbeek, 1948). Accordingly, high dissolved salt concentration (i.e., higher ionic strength) in the wastewaters will suppress the electric double layer of the particles. This, in turn, will lower the electrostatic repulsion, promote aggregation of the particles, and facilitate their removal. Changes in pH or other water quality parameters in the wastewater that will cause charge neutralization can facilitate removal of nanomaterials. Organic or inorganic chelating agents such as humic acid can enhance stabilization of nanomaterials and lower their removal (Fortner et al., 2005; Limbach et al., 2008; Klaine et al., 2008; Zhang et al., 2009).

Several studies have addressed abiotic forces affecting stability of manufactured nanomaterials using synthetic waters. A recent study by Bien et al. (2011) provides a detailed overview of the various factors that affect the stability or removal of nanomaterials. Their study compared removal of nanozinc oxide (primary size 4–240 nm) in aqueous solutions of varying ionic strength, pH, and organic content. Their study indicated that an increase in ionic strength from 0 to 0.04 M (NaCl) increased the removal of nanomaterials significantly. The authors suggested that high ionic strength possibly compressed the repulsive electric double layer, in accordance with DLVO theory, and caused increased aggregation and sedimentation of nanozinc oxide. Concurrently, the zeta potential of the materials decreased from approximately 35 mV at an ionic strength of 0 to 15 mV at 0.04 M (NaCl). Some of the added nanomaterials dissolved, and the extent of dissolution varied with the solution pH. Dissolution was more pronounced at acidic and alkaline conditions. Nearly 100% dissolution of the zinc oxide (100 mg/L) was observed at pH 1, and dissolution decreased to approximately 15% at pH 6. Up to 10% dissolution of zinc oxide occurred at alkaline conditions (pH 9 and 11). Little or no dissolution was predicted at pH range of 6 to 9. The

addition of 100 mg/L of humic acid did not enhance dissolution of zinc oxide nanomaterials at acidic conditions. Under alkaline conditions, the addition of humic acid (100 mg/L) increased nanozinc oxide dissolution by 5 to 10%. A decrease in the size of nanozinc oxide increased its dissolution in aqueous solutions. At pH 7.5, approximately 5.7, 2.2, and 1% dissolution was observed for zinc oxide nanomaterial of 4 nm, 15 nm, and 240 nm diameter, respectively. Similarly, studies by Jiang et al. (2010) using ZnO nanoparticles (primary size 20 $\pm$ 5 nm) showed that increasing the ionic concentration from 1 to 100 mM increased the rate of deposition (on silica surfaces) approximately four-fold.

Zhang et al. (2008; 2009) evaluated the stability of engineered nanomaterials (ZnO, NiO, TiO_2, and Fe_2O_3) in aqueous suspensions in the presence of natural organic matter (NOM) and divalent cations. The size of the nanomaterials ranged from 10 nm (SiO_2) to 50 to 70 nm (ZnO). Their data indicated that most of the nanomaterials readily settled even at an electrolyte concentration of 0.01 M. The addition of NOM increased the negative charge of the nanomaterials which, in turn, increased their stability. Subsequent addition of Ca^{2+} neutralized the charge causing the nanomaterials to precipitate.

Gao et al. (2009) evaluated dispersion and toxicity of CuNP in three different Suwannee River water samples (headwaters, river midsection, and off-delta). Their study showed that aggregation and settling of CuNP was lower in headwaters that had higher organic content and low ionic strength (dissolved organic carbon [DOC] 45.7 mg C/l; I 0.94 mM and residual CuNP 12.58 mg/L). Removal of CuNP increased with an increase in ionic strength and decrease in organic content (DOC 10.18 mg C/l, I 3.34 mM, residual CuNP 1.45 mg/L for midsection; and DOC 2.3 mg C/l, I 475 mM, residual CuNP 0.51 mg/L for off-delta sample).

Similar trends in nanomaterial aggregation and removal were observed with other nanomaterials. He et al. (2008) evaluated stability of hematite nanomaterials of size (hydrated radius) 12 to 65 nm. Their study indicated that the aggregation and settling of hematite nanomaterials increased with the ionic strength of the solution. At ionic strengths of up to 20 mM (NaCl), little or no aggregation of the nanomaterials occurred. At ionic strengths of 20 to 50 mM, the particles aggregated at a slower rate. The rate of aggregation increased significantly at ionic strengths higher than 50 mM. Their study also indicated that the rate of aggregation for smaller nanomaterials (12 and 32 nm) was higher than that of larger nanomaterials (65 nm). Their study further indicated that the concentration of dissolved salt required to destabilize the nanomaterials (critical coagulant concentration) decreased with decreasing size of the nanomaterials. Approximately 70, 54, and 45 mM of NaCl were required to destabilize hematite nanomaterials of 65, 32, and 12 nm size, respectively, at pH 5.7. Similar trends were observed in studies by French et al. (2009), Fortner et al. (2005), and Klaine (2008) using titanium dioxide, fullerene (C60), and other nanomaterials.

The one exception to this trend was observed with silicon dioxide (SiO_2) nanomaterials. Zhang et al. (2008; 2009) observed that SiO_2 nanomaterials remained in a stable, dispersed form in aqueous media in the presence or absence of NOM or Ca^{2+}. The authors suggested that the lower Hamaker constant of the SiO_2 particles facilitated their stability in aqueous suspensions containing high dissolved salts.

Although most of the previously mentioned studies were performed using synthetic waters, few studies have evaluated nanomaterials removal in wastewater matrices. Liang et al. (2010) evaluated removal and toxicity of silver nanomaterials to wastewater microorganisms. Their data indicated that a significant portion of the nanosilver (> 90%) added to the activated sludge ended up in the biosolids. Their study, however, did not identify the fraction of silver

removed by abiotic process and the fraction removed by biosorption. Deposition of titanium oxide nanomaterials in biosolids was identified by Kiser et al. (2009) also. Limbach et al. (2009) evaluated removal of metal oxide nanomaterials in a model wastewater system. Their study indicated that most of the cerium nanomaterial was removed to the biomass. However, a small portion (approximately 6%) of the nanocerium was not removed in the treatment unit and remained in the treated effluent.

In summary, higher dissolved salt concentrations in wastewaters are likely to promote aggregation and deposition of nanomaterials, whereas the dissolved organic content would improve their stability. Nanomaterials with a lower Hamaker constant will be less influenced by these constituents compared to other nanomaterials.

2.2.2 Nanomaterial Toxicity to Wastewater Microorganisms

The factors influencing toxicity of nanomaterials to microorganisms appear to be complex and currently not fully understood. Whether toxic effects occurred because of direct interactions of the nanomaterials or the observed toxic effects are due to the dissolution of nanomaterials to ionic form is still a topic of great debate. Generally, reports discussing the toxic effects of these specific nanomaterials have not all been in agreement.

For example, Griffit et al. (2008) evaluated the toxicity of copper nanomaterials to a variety of aquatic species that represented different trophic and taxonomic levels. Their studies indicated that nanocopper was less toxic to most of the species (except juvenile zebra fish) than ionic copper. More than 80% of the added CuNP aggregated or settled in their studies. In another study by Fabrega et al. (2009), ionic silver appeared to inhibit the growth of *P. fluorescens* more than did nanosilver (average size ~ 70 nm), suggesting that dissolution of silver may be required to induce microbial toxicity. However, in the same study, at a higher silver concentration (2000 ppb), the toxicity effect of nanosilver was different from that of ionic silver, suggesting that a nanomaterial-specific toxicity may also be involved. Also, in a different study (Choi et al., 2008), nanosilver inhibited the respiration rate of ammonia oxidizing bacteria (86%) more than did ionic silver (42%). This suggested that nanomaterials directly interacted with the wastewater microorganisms to induce toxicity.

Studies evaluating the effect of different size of nanomaterials appear to indicate that nanomaterials of smaller average size are more toxic to microorganisms than larger size nanomaterials. For example, in one study, nanosilver stock containing a larger amount of smaller size (< 5 nm) particles inhibited the growth of nitrifying bacteria more than the stock containing more of the larger size (> 5 nm) nanoparticles (Choi and Hu, 2009). Similarly, Liu et al. (2010) evaluated antimicrobial characteristics of three different sizes of nanosilver to *E. coli*. Their study showed that nanomaterials with the smallest average size (~ 5 nm) had the highest toxicity. Similar results were shown by Schwegmann et al. (2010) in a study using iron oxide nanomaterial and *E. coli*. However, these studies did not evaluate possible dissolution of nanomaterials in the test matrix. It is possible that nanomaterials of smaller size can more readily dissolve compared to larger size nanomaterials and cause toxicity.

In wastewater systems, Liang et al. (2010) evaluated toxicity of ionic and nanosilver to heterotrophic and nitrifying bacterial communities in the wastewater using batch and continuous bioreactors. Their study indicated that at concentrations of 1 mg/L, nanosilver was not inhibitory to heterotrophic bacteria in the batch reactors. However, both nano and ionic silver inhibited growth of enriched nitrifying bacteria. In a continuous reactor using activated sludge biomass, nanosilver affected nitrifying bacterial activity more than the ionic silver.

Inhibition of ammonia oxidizing bacteria was observed through a reduction in the extent ammonia oxidation, accumulation of nitrite, and a reduction in nitrate level. Evaluation of microbial community structure indicated a reduction in *Nitrospira* and *Nitrosomonas* communities and a complete washout of *Nitrobacter* from this reactor. The authors suggested that exposure to nanomaterials in a continuous reactor facilitated slower kinetics of metal internalization and "an exacerbation effect" (p. 5433) on bacteria that was due to continued metal exposure, causing microbial toxicity. These results supported the idea that some nanomaterials directly interacted with sensitive microbial communities causing inhibition.

In summary, information on toxicity of nanomaterials is still evolving. Some evidence of direct toxic effects caused by nanomaterials to wastewater microorganisms exists. Some studies point to the toxic effects to the presence of dissolved ion in the samples. In many other studies, complete information on the state of nanomaterials (e.g., dissolved, settled, associated with microorganisms) is lacking.

2.3 Removal of Nanomaterials During Granular Filtration

In general, filtration or transport of nanomaterials through filtration media appear to be affected by the same factors (pH, NOM, ionic strength, nanomaterial size, and zeta potential) that facilitate the aggregation and settling of nanomaterials in aqueous solutions (Petosa, 2010). However, forces other than those explained by DLVO theory have also been reported to affect nanomaterials transport in columns (Tian, 2010).

Torkzaban et al. (2010) evaluated transport of cadmium telluride quantum dots (CdTe nanomaterials) in different types of sand media. Their study showed that complete breakthrough (i.e., the effluent concentration equaled the influent concentration) of quantum dots in silica sand (Accusand, Unimin Corporation, Le Sueur, MN) and ultrapure quartz occurred within 1 to 2 pore volumes. However, in the column packed with goethite-coated sand, the initial breakthrough was observed after approximately 8 pore volumes and complete breakthrough occurred after approximately 34 pore volumes. Accusand and ultrapure quartz materials are homogeneously made of negatively charged materials. These characteristics were reported to facilitate smooth passage of the negatively charged quantum dots. It was suggested that goethite-coated sand, however, has microscale heterogeneity with intermittent positive charges. The delayed breakthrough of quantum dots is attributed to destabilization of the nanomaterials caused by the interaction of positive charges in the goethite with the negatively charged quantum dots.

In a separate study, Liu et al. (2009) evaluated the effect of ionic strength and flow rates on the transport of boron nanoparticles on quartz media. Their data showed that at an ionic strength of 0.01 M (NaCl), the peak effluent boron concentration was nearly 80% of the influent boron concentration. However, at an ionic strength of 0.4 M, the effluent boron concentration did not exceed 10% of the influent concentration. These trends are consistent with predictions of DLVO theory and observations by others using different nanomaterials. Evaluation of nanoboron breakthrough at different flow rates indicated that the peak effluent concentrations were higher (80% of the influent) at higher flow rates (8 mL/min) compared to that (50% of the influent) at lower flow rates (2 mL/min). A similar role of flow rate on nanomaterial filtration has been reported in other studies. Evaluation of copper oxide nanoparticles in a porous medium by Jeong and Kim (2009) showed that at lower velocity a larger number of aggregates were formed, and they deposited over a larger area. It appears that slower flow rates can enhance deposition of nanomaterials because the time scale of

transport through the column may be closer to the time scale for the attachment of the particles to the media (Lecoanet and Wiesner, 2004; Ben-Moshe, 2010; Petosa, 2010).

2.4 Effect of Nanomaterials on Disinfection Processes

Currently there are no systematic studies that quantify any adverse effects that nanomaterials may pose to the disinfection process. Possible effects of nanomaterials during disinfection may include exertion of chlorine demand by reactive nanomaterials and nanoscale suspended particles providing shelter from disinfection agents (acting similar to turbidity-causing constituents).

A few studies, however, reviewed the use of nanomaterial as a disinfectant. A review by Li et al. (2008) provides a compilation of several nanomaterials that may be used in water and wastewater disinfection. It was found that zinc oxide nanomaterial can exhibit antimicrobial effects, but the mechanism is not well understood. It was suggested that in the disinfection process, the photocatalytic generation of hydrogen peroxide and dissolution of the zinc particles act as the primary mechanisms. Overall, the use of nanozinc oxide as a disinfectant is limited.

Silver, on the other hand, is known to have antimicrobial properties and has been used in a variety of applications, including water disinfection (Li et al., 2008). The mechanisms are only partially understood but include the dissolution of the silver particles releasing antimicrobial silver ions or the silver particles penetrating the bacterial wall causing DNA damage. In one study, silver nanoparticles were attached to polymeric microspheres and used as a bactericidal agent for water disinfection (Gangadharan, 2010). It was found to be highly effective against both gram-negative and gram-positive bacteria, and there was no bacterial adhesion or adsorption on the polymeric beads.

Titanium dioxide nanomaterial (TiO2) may be most suitable for water disinfection due to its stability in water, lack of toxicity following ingestion, and low cost. In addition, several studies on photocatalytic disinfection of TiO_2 have shown promise in the disinfection process (Li et al., 2008; Brunet, 2009). Generally, disinfection using TiO_2 nanomaterial is related to the production of reactive oxygen species (ROS) under UV radiation, which effectively inactivates viruses and cleaves DNA. Fullerenes also have been show to have similar effects when photosensitized (Badireddy, 2007).

Chapter 3

Methods and Materials

This chapter provides details of the approach used in this study to investigate the effects of nanomaterials on wastewater microorganisms and the techniques used to measure various parameters to investigate the effects.

3.1 Project Approach

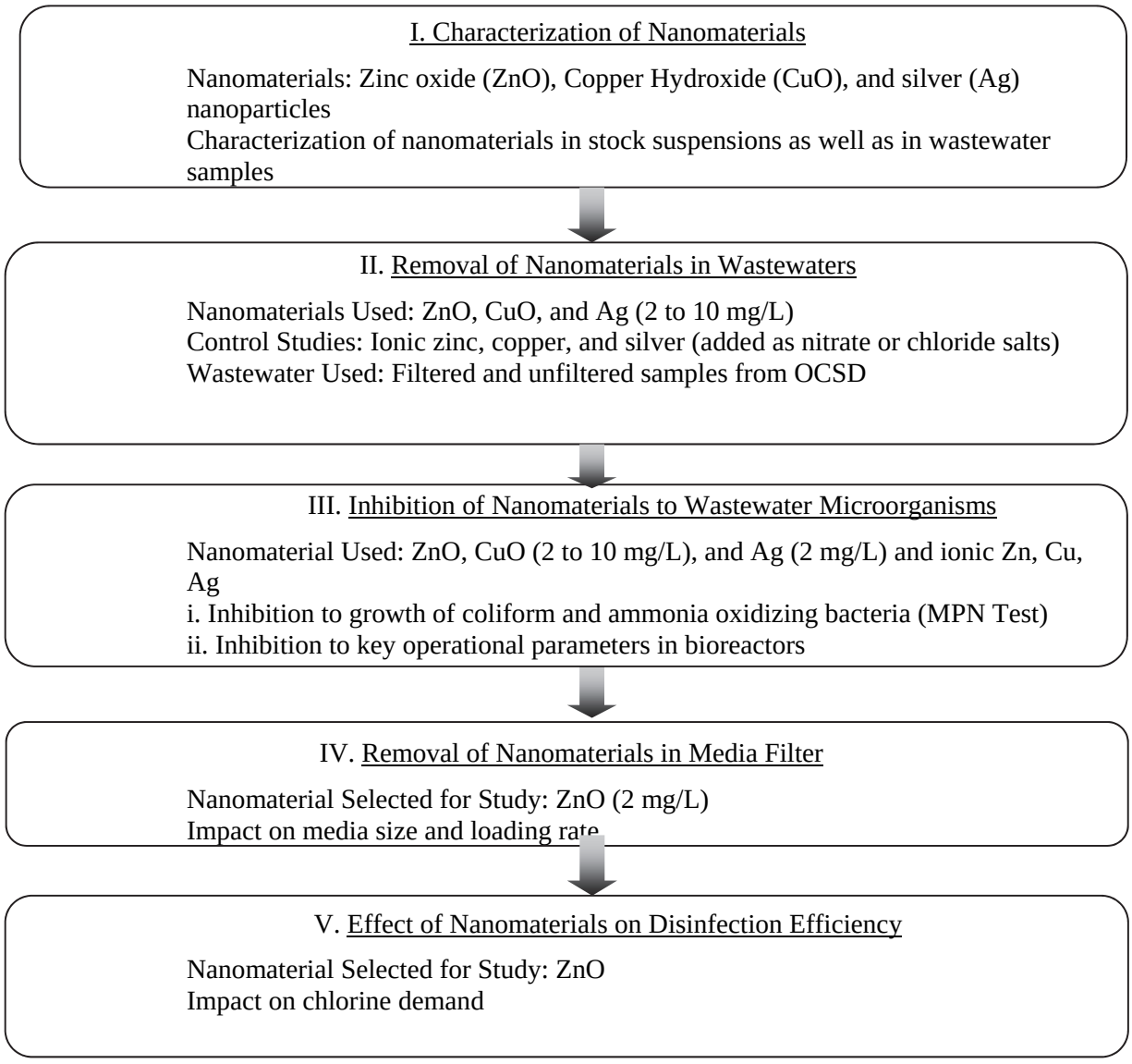

Figure 3.1. Project approach to investigate fate and transport of nanomaterials.

The flow chart in Figure 3.1 illustrates the step-by-step approach followed in this study to investigate the fate and effect of nanomaterials during wastewater treatment. Such a systematic approach will provide detailed information on the fate of nanomaterials during

water reclamation. Brief descriptions of the approach are given in each step in the flow chart, and complete details of each method are given in the following subsections.

3.2 Wastewater Characteristics

Primary effluent and activated sludge samples were collected from OCSD Plant 1. Initially, wastewater from the headworks is treated in the primary settling tank. The typical chemical oxygen demand (COD) of the primary effluent was approximately 150 mg/L. Subsequently, an activated sludge process was used for secondary treatment of the wastewater. The activated sludge process was operating in ammonia bypass mode (i.e., carbon oxidation only) with 1.2 day sludge retention time with an average MLSS of 650 mg/L and average COD of approximately 45 mg/L. Activated sludge effluent characteristics are provided in Table 3.1.

Table 3.1. Typical Water Quality Characteristics of OCSD Activated Sludge

Parameter Value	Value
Total BOD (mg/L)	7–8.5
Carbonaceous BOD (mg/L)	4–5
TSS, (mg/L)	5.5–7.6
COD (mg/L)	35–50
Ammonia-N (mg/L)	23–30
Turbidity (NTU)	2–3.5
F/M(#BOD/#MLVSS)	1–1.3
MLSS (mg/L)	650–750
MLVSS (mg/L)	600–670
Sludge Volume Index	310–475
TDS (mg/L)	750–850

3.3 Nanomaterials and Characterization

Three nanomaterials—nanozinc oxide, nanocopper oxide, and nanosilver—were selected for this study. Nanozinc oxide is selected for this study because of its use in sunscreens, cosmetics, solar cells, and electronic materials (Zhou and Keller, 2010; Bian et al., 2011). Nanocopper is currently used in applications including fungicides, cosmetics, printers, and electronics (WWICS, 2011). Nanosilver, among other uses, is widely used as an antimicrobial agent in pesticides, fungicides, washing machines, and hair sprays (WWICS, 2011). The following sections discuss the methods used to characterize ionic and nanomaterial solutions in this study. All stock nanomaterial solutions were well-mixed and sonicated (VWR 75T Aquasonic Sonicator) for 1 hour prior to use.

3.3.1 Zinc and Silver Nanoparticle Suspensions

Zinc oxide and silver nanoparticles were obtained in 1% suspensions from NEI Corporation, Somerset, NJ. Three zinc oxide (ZnO-A, ZnO-B, and ZnO-C) and silver (Ag-A, Ag-B, and Ag-C) nanomaterials that differed in particle size, surface area, and zeta potential were

procured for this study. The zinc and silver nanomaterials were also functionalized by the vendor using ammonium polyelectrolyte and a sulfate-based anionic surfactant, respectively. Table 3.2 summarizes the characteristics of the 12 nanomaterial suspensions, as indicated by the vendor. Upon receipt, the nanomaterials were further characterized by various techniques at NanoMeTeR Lab in the Department of Civil and Environmental Engineering at UCLA. These techniques included SEM, EDS, transmission electron microscopy (TEM), and particle size distribution (PSD) in solution. The details of these analyses follow.

3.3.1.1 Scanning Electron Microscopy (SEM)

The primary size of nanoparticles in the stock solutions was determined using a JEOL JSM-67 Field Emission Scanning Electron Microscope. Samples were prepared by adding several drops of a specific undiluted (1%) stock solution onto a nitrocellulose filtration membrane and dried such that the top of the filter was visibly coated with the nanomaterial. After drying, each membrane was then cut and attached, using conductive carbon adhesive, to aluminum SEM stubs. Before analysis all samples were coated with gold/platinum (Au/Pd). The SEM was set to a voltage of 10 kV and a working distance of 7.8 mm.

3.3.1.2 Energy Dispersive X-ray Spectroscopy (EDS)

EDS analysis was also completed on the samples using the same SEM (JEOL JSM-67 Field Emission Scanning Electron Microscope) to confirm the composition and purity of the samples. The SEM was set to a voltage of 15 kV and a working distance of 5.6 mm. Data was collected over a period of 5 minutes for each sample in order to determine the composition of the particles.

3.3.1.3 Transmission Electron Microscopy (TEM)

TEM analysis was performed using a JEOL 100CX unit by diluting stock solutions with MilliQ water to 10 mg/L and adding drop-wise to a TEM tray to determine individual and aggregate particle size.

3.3.1.4 Aggregated Nanoparticle Size Distribution

Because of the high potential for nanomaterials to agglomerate in solution, it is important to determine changes in average particles size when in solution. Stock solutions were diluted with MilliQ water to 10 mg/L, and the diluted samples were immediately sonicated for 1 hour using a Fisher Scientific FS30H sonicator at a 100W and 42kHz setting, prior to analysis. Then a 3 mL sample was added to a plastic cuvette and immediately analyzed with Brookhaven ZetaPALS (Holtsville, NY) to determine particle size distribution in a solution. The instrument was set at 25 ^{o}C and the refractive index was set at 2.004. The differences in primary particle sizes measured by SEM analyses and the aggregated particle size measured by ZetaPALS yielded information on changes that occurred to the nanoparticles when suspended in solution.

Table 3.2. Nanozinc Oxide and Silver Materials Suspensions (1%) Procured for this Study[a]

Sample ID	Nanomaterial	Surface Area (m2/g)	Average Particle Size (nm)	pH[b]	Zeta Potential at pH 7 (mV)[c]
ZnO-A	Zinc Oxide	10–25	40–100	7.1	
ZnO-B	Zinc Oxide	35	30	8.7	+ 40.6
ZnO-C	Zinc Oxide	70	< 10	9.0	
Fn-ZnO-A	Functionalized Zinc Oxide	10–25	40–100	8.3	
Fn-ZnO-B	Functionalized Zinc Oxide	35	30	8.8	- 7.8
Fn-ZnO-C	Functionalized Zinc Oxide	70	< 10	9.2	
Ag-A	Silver	5	<100	4.2	
Ag-B	Silver	3	150	5.8	- 9.1
Ag-C	Silver	4	<120	5.2	
Fn-Ag-A	Functionalized Silver	5	<100	4.2	
Fn-Ag-B	Functionalized Silver	3	150	5.9	- 16.8
Fn-Ag-C	Functionalized Silver	4	<120	4.3	

[a]Properties of stock nanomaterials indicated are as received from the supplier.

[b]Manufacturer's Note: All dispersions were prepared in water that had been adjusted to pH 7–8. Any change in pH would then presumably be due either to a chemical reaction between the particles (and/or accompanying impurities) and the water (including dispersant if applicable), or to the particles interfering with the pH measurement. The reported values could not be verified with a paper indicator, so their accuracy is not certain. Values of pH listed were measured directly in the 1 wt% slurry using an Orion pH/ATC Gel Triode (9107BN). A significant dilution of these dispersions in pH neutral water should yield a dispersion with pH in the range of 6–8.

[c]Manufacturer's Note: Zeta potential was measured by adding several drops of each dispersion to 200 mL of pH 7 water. To ensure that the surface modifier would remain bound to the particles' surface upon dilution, dispersants were selected based on the degree of change observed in the particles' surface charge. A change of at least 8–10 mV was considered to be sufficient evidence of retained surface modifier.

3.3.2 Nanocopper Suspensions and Characterization

Copper nanoparticles were obtained from QSI Company (Santa Ana, CA). The material obtained from the vendor is a mixture of copper and copper oxide particles with a copper content of approximately 51%. The reported particle size of the nanocopper was 20 to 50 nm. The nanomaterials received were further characterized by Nanotech Analytics Lab, NEI Corporation, Somerset, NJ. SEM was used to analyze particle size. Specific surface area was measured with the Brunauer, Emmett and Teller method. Quantachrome Autotap (Syossett, NY) measured particle density based on International Organization for Standardization (ISO) method 3953 (2011). Stock solutions of 200 mg/L Cu were prepared by adding the

nanomaterials to deionized (DI) water (preadjusted to pH 8). Chemical composition of the powder and stock suspensions were determined using X-ray diffraction. Zetasizer Nano (Malvern Instruments) was used to determine particle size distribution in the solution by dynamic light scattering method.

3.3.3 Ionic Solutions

A zinc standard in a 2% HNO_3 matrix was obtained from VHG Labs at a concentration at 1 g/L. A silver standard made of $AgNO_3$ in a 2% HNO_3 matrix was obtained from Ricca Chemical (CAS 7761-88-8) with a 10 g/L concentration. Ionic copper solutions were made from $CuCl_2$ salt dissolved in DI water.

3.4 Removal of Nanomaterials in Wastewater Samples

3.4.1 Experimental Approach

These studies were performed to evaluate removal of nanomaterials in the presence and absence of activated sludge biomass. Nanomaterials removed in the absence of biomass were assumed to represent the fraction removed by abiotic processes such as settling and aggregation. The nanomaterials removed in the presence of sludge biomass would include the fraction removed by biosorption and possible uptake, in addition to that removed by the abiotic process. The intent of these tests is to estimate the amount of nanomaterials in suspension (dissolved or nanosuspended forms), the fraction of the material that is directly associated with biomass, and the fraction that is settled, but not associated with the biomass. This information can then help explain any toxic effects occurring in the presence of these materials.

To evaluate nanomaterials removal by abiotic processes, activated sludge samples collected from OCSD were filtered using 0.45 µm filters and spiked with 2 or 10 mg/L of nanomaterials or ionic salts. The typical concentrations of zinc and silver ions in OCSD primary treated OCSD wastewater are 175 and 6 ug/L, respectively. Currently no data are available on current or projected concentrations of the nanomaterials in actual wastewaters. A maximum concentration of 10 mg/L was selected for this study since it is unlikely that concentrations higher than this will enter typical wastewater treatment plants. Samples (100 mL) were then equilibrated in 250 mL flasks for 20 hours at 25 °C, at 100 rpm using a Gyratory Water Bath shaker. The addition of either the nanoparticle or the ions altered the pH within 0.2 units. No further pH adjustments were made. After equilibration, samples were then filtered by 0.45 µm filters, and the filtrate was analyzed by inductively coupled plasma (ICP). Figure 3.2 illustrates the various steps.

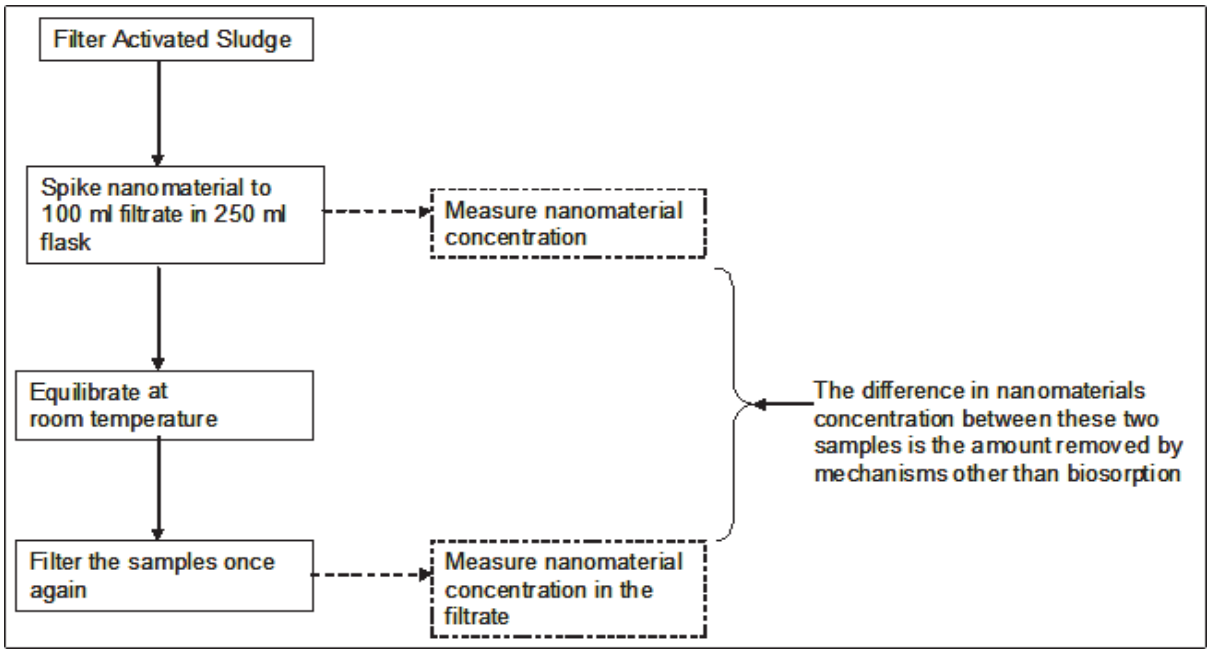

Figure 3.2. Procedure used to evaluate removal of nanomaterials by abiotic processes in wastewater

Note that this experiment measures the nanomaterials removal by filtration, which under certain circumstances may overestimate the removal by aggregation and settling process. Hence, the removal estimated from this study is likely to represent the maximum potential abiotic removal.

Subsequently, the procedure was repeated using unfiltered activated sludge samples. After equilibration, the samples were filtered (0.45 μm Fisherbrand Nitrocellulose Filteres) and analyzed by ICP. The difference in the amount of nanomaterials removed in the presence of biomass and in the absence of biomass was assumed to be the fraction removed by biomass mediated processes such as biosorption.

3.4.2 Measurement of Nanomaterials Concentration in Aqueous Samples

For this and other tasks throughout this study, concentrations of zinc oxide nanoparticles were measured by ICP (EPA Method 200.7) at the analytical laboratory at OCSD and at the Department of Civil and Environmental Engineering at UCI. Nanosilver concentrations were measured at OCSD according to ICP (EPA Method 200.7). The reporting limit for the analyses of zinc and silver by ICP (EPA Method 200.7) at OCSD is 0.02 mg/L. Copper ions as well as copper nanoparticles in the filtrates were analyzed by ICP (EPA Method 200.7), by an external, California state-certified laboratory. The samples were digested using EPA Method 200.2 prior to ICP analyses. The reporting limit for copper analysis is 0.01 mg/L.

3.4.3 Analyses of Nanoscale Suspended Particles by Dynamic Light Scattering (DLS) Methods

A Zatasizer Nano (Malvern Instruments, Westborough, MA) was used to analyze submicrometer/nanoscale particle size distribution and particle count in the filtrate (0.45 μm) samples in this task and throughout this study. The instrument uses a dynamic light scattering (DLS) technology to measure particle distribution in the range 0.6 nm to 6 μm. Statistical analyses performed using the photon count rate data indicated that this data could be a useful technique to qualitatively measure relative nanoparticle removal in wastewaters (Smeraldi et al., 2009, 2012). Hence, the photon count rate measured during particle analyses was used to determine relative particle count in various samples. The submicrometer particles measured during the filtrate analyses include naturally occurring submicrometer particles in the wastewater, nanoparticles, and colloidal fraction of the added salts.

3.4.4 Speciation Modeling to Predict Removal of Nanomaterials

Finally, the experimental data from nanomaterial removal studies were compared with the predictions for ionic species (i.e., ionic zinc, copper, and silver) using a chemical speciation model (MINTEQA2). MINTEQA2 is a multimedia equilibrium speciation model developed by the United States Environmental Protection Agency's (U.S. EPA) Center for Exposure Assessment Modeling (CEAM). The model is useful for calculating the equilibrium mass distribution among dissolved species, adsorbed species, and multiple solid phases under a variety of conditions including a gas phase with constant partial pressures. The model contains a comprehensive database (e.g., known solubility products for most inorganic salts) that is adequate for solving a broad range of problems without need for additional user-supplied equilibrium constants. If required, the model facilitates incorporation of solubility products that are not already in the model's database. The model's existing database contains equilibrium constants for the key inorganic constituents present in OCSD wastewater (Table 3.1) and those added (i.e., zinc, copper, and silver ions) to the test solutions. Equilibrium constants for nanomaterials are not currently available. For this study, the input to the model runs included the concentration of inorganic salts in OCSD wastewater, the concentration of the added inorganic salts, and the equilibrium-solution pH observed during the removal of these salts. The output from the model runs included predictions for the equilibrium-dissolved concentration of various salts and the mass and speciation of various solids likely to form. The model output is then used to compare the equilibrium concentration predicted by the model to that observed in the tests for the inorganic salts and the concentration predicted for inorganic salts to that measured for nanomaterials, to infer additional information on the fate of nanomaterials in wastewaters.

Note that this analysis is limited by a lack of equilibrium constants for any complexes formed by nanomaterials and a lack of data on the organic species in the wastewater and their equilibrium constants. Hence, this analysis is performed only to obtain qualitative information on the fate of nanomaterials.

3.5 Inhibitory Effects of Nanomaterials During Biological Wastewater Treatment

Possible inhibitory effects that are due to release of nanomaterials were studied by evaluating the growth of key microbial communities (coliform and ammonia oxidizing bacteria) using

MPN tests, the respiration rate of wastewater microorganisms, and the critical process/operational parameters (e.g., COD, MLSS) that may affect biological treatment processes. The experimental approach for each of these studies follows.

3.5.1 Most Probable Number (MPN) Tests

MPN tests were performed to determine whether the presence of nanomaterials adversely affects the growth of coliform and ammonia oxidizing bacteria populations in activated sludge. This technique involves a pattern of positive and negative test results based on pH-sensitive dye. Coliform bacteria were chosen for this study because they are more prevalent in wastewater and other aquatic environments. *Lauryl Tryptose* growth media was used to evaluate the coliform growth with Brilliant Green Bile Broth used as the confirmation stage (Eaton et al., 2005). This broth required an incubation time of 24 to 48 hours for each step at 25 °C. The growth of coliform bacteria is identified by visual inspection (samples turn cloudy upon microbial growth) and gas production that is due to microbial respiration. Ammonia oxidizing bacteria were used because they were more sensitive than coliform and most other common bacterial communities in the wastewaters to upsets during wastewater treatment (Kowalchuk and Stephen, 2001). *Nitrosomonas* media was used to determine the growth of nitrifying microorganisms and requires incubation at 35 °C (Atlas, 2004). The color of the media changes from pink to yellow upon growth of ammonia oxidizers. After the specified times, the MPN was calculated for both the nitrifying and coliform bacteria based on a procedure described by Halvorson and Ziegler (1933). Tests were performed using nanomaterials as well as ionic salts.

Initially, copper and zinc nanomaterial inhibition of coliform bacteria was tested by spiking the media with 10 or 2 mg/L concentration of nanocopper, nanozinc oxide material, or their ionic salts. Nanomaterials (or salts) were added to a batch bioreactor containing activated sludge samples and equilibrated for 4 hours. Subsequently, well-mixed samples were collected from the reactors, diluted to predetermined ratios, and added to the spiked growth media in triplicate. Preliminary screening studies indicated that up to 10^{-6} of dilution is required to monitor growth of coliform bacteria and 10^{-2} dilution was required to monitor the growth of ammonia oxidizing bacteria. Figure 3.3 shows the procedure used to obtain the required dilution for MPN values. Microbial growth was analyzed for each dilution over a period of several days, and MPN was calculated. Subsequently, experiments were conducted using 2 mg/L of zinc and silver nanomaterials to evaluate inhibition to coliform and ammonia oxidizing bacteria.

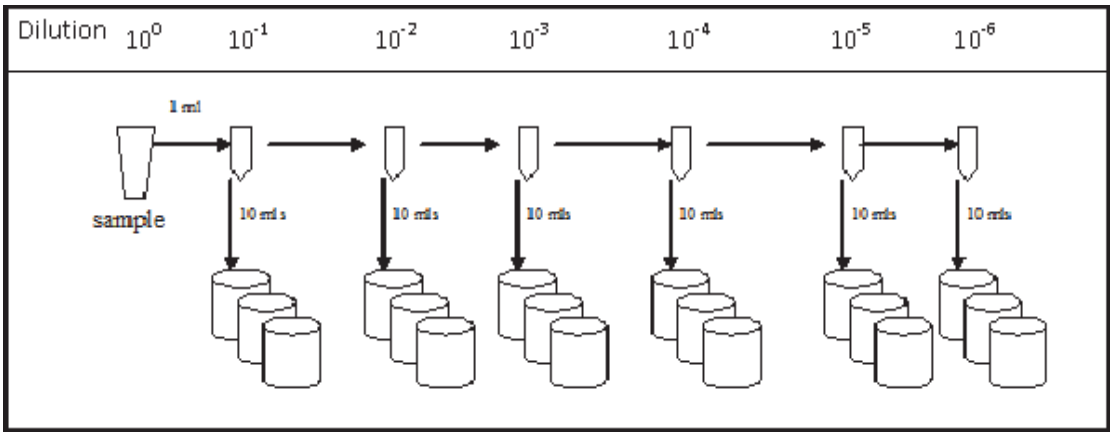

Figure 3.3. Illustration of sample dilution for MPN test.

3.5.2 Inhibition of Key Operational Parameters

This task evaluated the effect of nanomaterial on several commonly tested parameters during biological treatment. Figure 3.4 shows the batch bioreactor setup used for this task. Whereas the MPN test provided the effect of nanomaterials for a specific group of microorganisms, the evaluation of operating parameters such as COD and MLSS in a bioreactor system provides insight into the collective response of the microbial population to these materials.

In the bioreactor setup, air is initially passed through a glass column filled with activated carbon to remove oil and dust particles. It is then saturated by passing through a flask filled with water. A manifold is used to distribute the air between 5 bioreactors. An air stone attached to the end of the tube facilitates distribution of air evenly within the reactors. A magnetic stirrer is used in each reactor to keep the biomass in suspension.

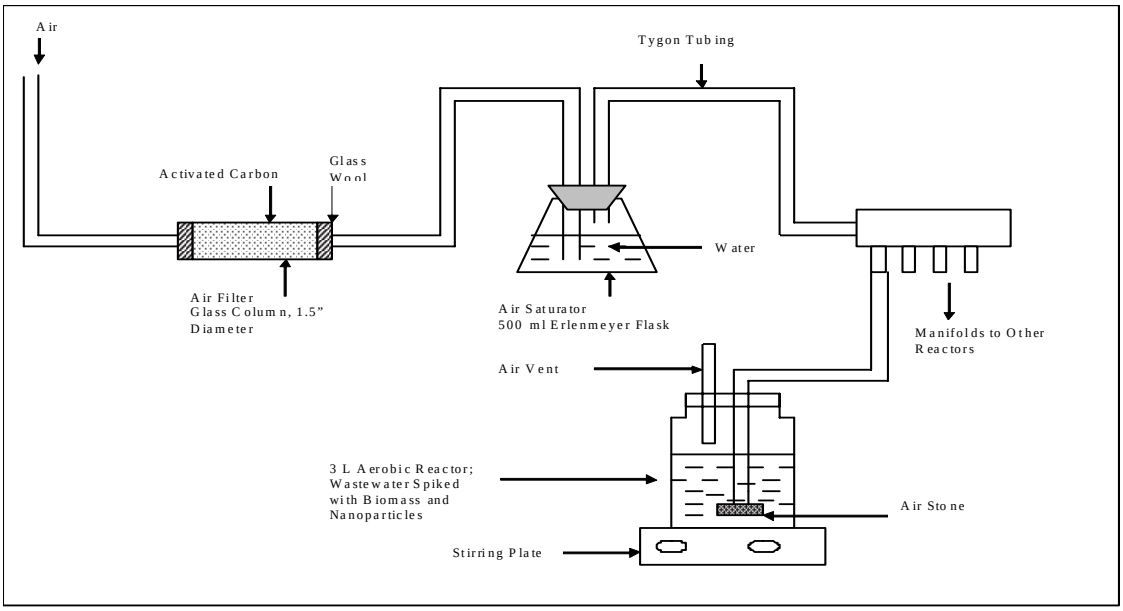

Figure 3.4. Experimental setup of batch bioreactors.

For the bioreactor studies, activated sludge collected from OCSD was allowed to settle for 1 hour, and the supernatant was decanted and was then replaced by an equal volume of primary effluent. This was done in an attempt to replicate the treatment process with the combination of return activated sludge and primary effluent. Then 3 L of the mixture was distributed to each of the 5 batch reactors. Zinc oxide or silver nanomaterials (2 or 0.2 mg/L) were added to the bioreactors. Table 3.3 summarizes the batch reactor studies performed under this task. The bioreactors were operated for up to 7 days. Initial samples were collected at 0 and 4 hours after setting up the reactors. Subsequently, samples were collected and analyzed once each day or once every 2 days depending on the trends observed. Table 3.4 shows the parameters analyzed and the frequency of analyses. Sample analyses included soluble chemical oxygen demand (sCOD), MLSS, pH, nitrite, nitrate, and metals. Except for MLSS, all the other analyses were performed on filtered (0.45 μm) samples.

Table 3.3. Batch Bioreactor Tests Performed

Batch Test	Spiked with	Initial Conc	Surface Treatment	Reactor 1	Reactor 2	Reactor 3	Reactor 4	Reactor 5
1	Zinc Oxide	0.2 mg/L	Functionalized	(ZnO-A / Fn-ZnO-A)	(ZnO-B / Fn-ZnO-B)	(ZnO-C / Fn-ZnO-C)	Dissolved Metal	Control – No spike
2		0.2 mg/L[a]	No Functionalization				Polymer Only	2 mg/L (1 size from Batch #1)
3		2 mg/L	Functionalized				Dissolved Metal	Control – No spike
4	Silver	0.2 mg/L	Functionalized	(Ag-A / Fn-Ag-A)	(Ag-B / Fn-Ag-B)	(Ag-C / Fn-Ag-C)	Dissolved Metal	Control – No spike
5		0.2 mg/L[a]	No Functionalization				Polymer Only	2 mg/L (1 size from Batch #4)
6		2 mg/L	Functionalized				Dissolved Metal	2 mg/L (1 size from Batch #5)

[a]Except in Reactor 5, where the initial concentration was 2 mg/L.

Table 3.4. Frequency of Sample Analyses During Activated Sludge Studies

Parameter	Sampling Frequency
COD[a], pH, Zinc, Silver, DLS	1D
MLSS, Nitrate, Nitrite, Ammonia	2D

Notes. 1D = One sample/day. 2D = One sample/2 days.
[a]COD was analyzed twice (immediately after starting the reactors and after 4 hours of operation on the first day).

3.5.2.1 Bioreactor Samples Analyses

COD was measured by Hach Method 8000 where exactly 2 mL of the filtered sample was added to a premade Hach COD vial. The vial was then digested at 150 ºC for 2 hours and allowed to cool to room temperature before analysis. After the vials reached room temperature, they were placed in a Hach colorimeter (DR/890), and the COD concentrations were measured.

MLSS (Standard Method 2540C) was measured using a 50 mL sample and filtered with a preweighed 934-AH Whatman filter. The filter was then placed in a oven at 103 ºC for 1 hour and then cooled in a dessicator for 30 minutes. Once cooled, the final measurement was made and the MLSS calculated:

MLSS = (“final weight” – “initial weight”) / volume

A Thermo Scientific Orion 9157 pH probe was used to measure sample pH. The pH probe was calibrated before each use with 4.01, 7.0, and 10.01 standards and rinsed with DI water between each measurement. Samples were continuously stirred while pH was measured.

Nitrate and nitrite were both measured by ion chromatography using a Dionex DX120 Ion Chromatograph and an IonPac AS14 column. Before analysis all samples were filtered on a 0.45 micron filter to prevent clogging the instrument. Standards and calibration curves were used to accurately calculate the anions within the samples.

Measurement of metals concentration and DLS analyses of the samples were performed using the procedures described in sections 3.4.2 and 3.4.3.

3.6 Removal of Nanomaterials in a Media Filter

Column studies were performed to evaluate the fate of nanomaterials during media filtration during wastewater treatment. A glass column (10 cm length, 1 cm diameter) was packed with 5 cm of sand with grain sizes of either 0.175 or 0.45 mm. A protocol shown in Figure 3.5 was followed to minimize clogging of the media filter by presettled nanomaterials. Briefly, secondary effluent samples from the OCSD plant were spiked with 2 mg/L nanozinc oxide or ionic salt and allowed approximately 1 hour for any solids formed to settle. The supernatant was then collected, analyzed for metals concentration, and used as the feed water for media filtration studies. Select studies were performed by suspending nanozinc oxide or ionic zinc in DI water also.

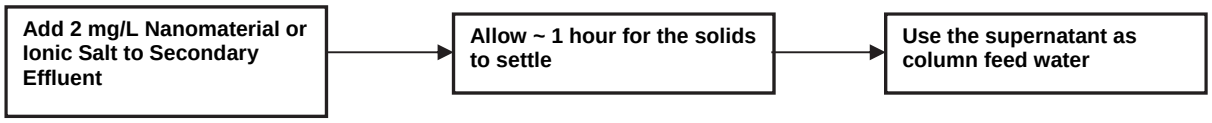

Figure 3.5. Preparation of feed water for media filtration studies.

A peristaltic pump (Dynamax, Model RP-1) was used to maintain flow rates of 0.98 mL/min or 0.49 mL/min (loading rates of 0.15 and 0.3 gpm/ft^2) through the column. The column operating parameters are provided in Table 3.5. In addition, Table 3.6 summarizes the various column runs. Figure 3.6 shows the column setup used in this study.

Table 3.5. Filtration Design and Operational Conditions

Parameter	Value
Packing Height (cm)	5
Column Diameter (cm)	1
Media Material	Sand
Media Size (mm)	0.175, 0.45
Porosity	0.43
Flow Rate (mL/min)	0.98, 0.49
Surface Loading Rate (gpm/ft^2)	0.3, 0.15
Empty Bed Contact Time (min)	4, 8
Initial Concentration (mg/L)	2
Initial pH	7
Initial Temperature (C^o)	25

Note. The initial concentration of 2 mg/L was spiked in the wastewater. However, the sample was then mixed well and settled for 1 hour in order to remove readily settable particles so they would not clog the sand column. The feed concentrations were approximately 1.8 mg/L.

Table 3.6. Summary of the Column Runs for Evaluation of Nanomaterials in Media Filtration

Spike Material	Flow Rate (mL/min)	Average Media Size (mm)
Ionic Zn, ZnO-A, ZnO-B and ZnO-C	0.49 mL/min, 0.98 mL/min	0.175 mm, 0.45 mm

Note. Overall, there was a total of 16 column runs.

Figure 3.6. Column setup used to evaluate nanomaterials removal.

3.7 Effect of Nanomaterials on Disinfection Efficiency

This study was performed to determine whether the presence of nanomaterials could affect the disinfection of secondary effluents. To this end, the chlorine demand was estimated for effluents spiked with 2 mg/L of nanozinc oxide or ionic zinc. Secondary effluents with no added nano or ionic zinc were used as controls. A procedure based on Standard Method 2350 B (Chlorine Demand) was used. Triplicate samples (50 mL) of OCSD secondary effluent was transferred to a 150 mL flask and spiked with 2 mg/L of nano or ionic zinc. A 2 mg/L concentration of chlorine (sodium hypochlorite) was added to each flask. Each flask was then covered in foil and placed in a dark room to prevent exposure to light. The samples were incubated at room temperature for 1 hour using a Gyratory Water Bath shaker set to 100 rpm. After incubation the samples were analyzed for total chlorine with Hach Colorimetric (N,N-Diethyl-p-phenylenediamine [DPD], Hach Method 8167, Loveland, CO). The demand was estimated using the following formula:

$$\text{Chlorine Demand (mg/L)} = (D_s - R_s) - (D_c - R_c)$$

where

D_s = initial chlorine dose in the nanomaterial-containing sample (mg/L)
R_s = residual chlorine in the nanomaterial-containing sample after the contact time (mg/L)
D_c = chlorine dose in the control sample (unspiked OCSD effluent) (mg//L)
R_c = residual chlorine in the control sample after the contact time (mg/L)

Chapter ***4***

Characterization and Analysis of Nanomaterials

4.1 Introduction

This chapter presents data from the characterization of nanomaterials and efforts to measure nanomaterials in aqueous samples.

Nanomaterials in stock suspensions and upon their addition to wastewater samples were characterized by SEM, EDS, TEM, DLS, and other techniques. Table 4.1 summarizes various analyses performed on these samples. Results from these efforts are presented in sections 4.2 through 4.6.

Table 4.1. Summary of Nano ZnO and Ag Characterization Analyses Completed[a]

	Stock Solution						2 mg/L Spiked in Secondary Effluent					
	CuNP[b]	ZnO-A	ZnO-B	ZnO-C	Ag-A	Ag-C	CuNP[b]	ZnO-A	ZnO-B	ZnO-C	Ag-A	Ag-C
SEM	x	x	x	x	x	x	x	x	x	x	x	x
EDS	x	x	x	x	x	x		x	x	x	x	x
TEM		x	x	x	x	x						
PSD[c]	x	x	x	x	x	x	x	x	x	x	x	x
BET[d]	x											

[a]Many analyses were performed on ionic salt samples also.

[b]10 mg/L CuNP conc.

[c]Additional DLS analyses were performed during nanomaterials removal, toxicity, and filtration evaluations. These data are presented throughout Sections 4.5 through 4.8.

[d]Brunauer, Emmett, and Teller test for surface area analyses.

Prior to evaluating the fate and effect of nanomaterials in wastewaters, tests were performed to determine if analytical techniques such as ICP, often used to measure dissolved metals are capable of measuring nanomaterials also. Undigested and predigested samples were measured by ICP and other methods to determine percent recovery of added nanomaterials. DLS and matrix spike tests were also performed on select samples to determine pretreatment requirements. Results from these efforts are summarized in Sections 4.7 and 4.8.

4.2 Characterization of Zinc Oxide Nanomaterials

Characterization of zinc oxide and silver nanomaterials was performed at NanoMeTeR Lab, at the Department of Civil and Environmental Engineering, UCLA. Copper oxide nanomaterials were characterized at Nanotech Analytical Lab, Somerset, NJ. Characterization included SEM, TEM, EDS, and particle size distribution analyses of stock suspension. The stock suspensions (1% of ZnO and Ag) were diluted and sonicated for 1 hour prior to analyses. A 1 mg/L nanocopper stock was prepared for characterization.

4.2.1 SEM Analysis of Stock Nanomaterials

SEM results for ZnO-A nanomaterial is shown in Figure 4.1. A wide range of particle sizes and a variety of shapes were in the images. The average particle size appeared to be approximately 100 nm. Few particles larger than 500 nm were also observed. The particles predominantly appeared to be circular.

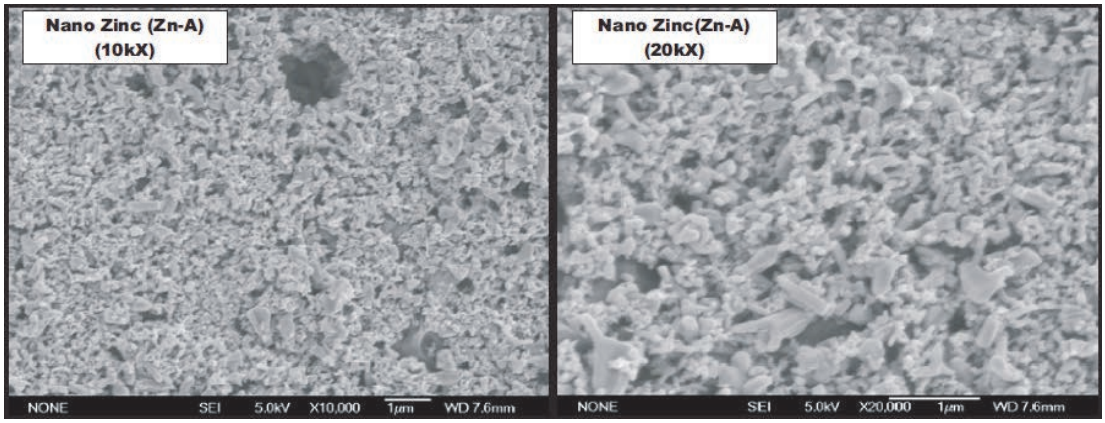

Figure 4.1. SEM images of the stock zinc oxide (ZnO-A) nanomaterial on a membrane filter.

SEM results for ZnO-B nanomaterial is shown in Figure 4.2. These particles again have a large variety of shapes, and the average particle size is approximately 300 nm, which is larger than ZnO-A nanomaterial. Again, there appear to be a few particles larger than 1 micron.

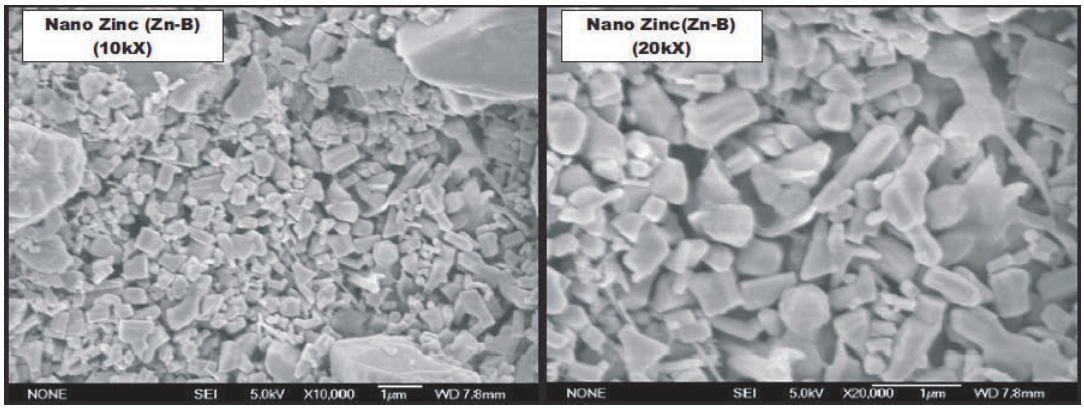

Figure 4.2. SEM images of the stock zinc oxide (ZnO-B) nanomaterial on a membrane filter.

SEM results for ZnO-C nanomaterial are shown in Figure 4.3. The distinctive shapes observed in the images of the other two zinc nanomaterials are absent. Upon closer inspection this nanomaterial appears to be more flake-like in structure than the other nanomaterials tested. In a separate sample (Figure 4.17) where ZnO-C was added to wastewater we again do not see defined particle shapes (this figure will be discussed in more detail later). The diameter appears to vary from 50 nm to larger than 1 micron. The average size is very difficult to determine but the best estimate would be approximately 300 nm.

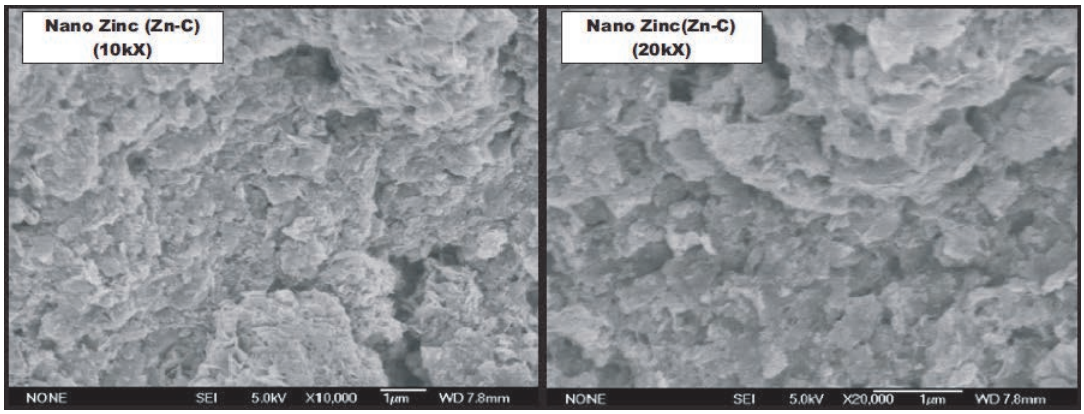

Figure 4.3. SEM images of the stock zinc oxide (ZnO-C) nanomaterial on a membrane filter.

4.2.2 EDS Analysis of Stock Zinc Oxide Nanomaterial

For EDS analyses, three replicates were analyzed for each sample. Table 4.2 shows the EDS results of the stock solutions of ZnO-A, ZnO-B, and ZnO-C nanomaterials. Some elements are not included in all samples because of low concentrations. Generally, the major elements found are C, O, Pd, Au, and Zn. In addition, calcium was found in ZnO-B samples. This may be because some adhesive was exposed in the area analyzed or the sample was contaminated. Carbon is seen because of the membrane; Pd and Au are due to the coating placed on the samples, which is needed for SEM EDS analysis. The percent of pure Zn in pure ZnO is approximately 80.3%. The observed percentage of Zn in ZnO-A, ZnO-B, and ZnO-C samples

(i.e., Wt% Zn/(Wt%Zn + Wt%O) in Table 4.2) were 87.6%, 80.9%, and 81.8%, respectively. These results show that the stock solutions contained fewer impurities with zinc levels within 10% of the expected values.

Table 4.2. EDS Analysis Indicating Composition of Stock Zinc Oxide Nanomaterials

ZnO-A			ZnO-B			ZnO-C		
Element (Shell) [a]	**Wt%**	**At%**	**Element (Shell)** [a]	**Wt%**	**At%**	**Element (Shell)** [a]	**Wt%**	**At%**
C (K)	4.25		C (K)	7.82	23.61	C (K)	3.54	14.87
O (K)	10.9	30.1	O (K)	14.47	32.8	O (K)	11.4	35.97
Na (K)	0	0	Na (K)	0	0	Na (K)	0	0
Cl (K)	0.07	0.09	Cl (K)	0.22	0.22	Cl (K)	0	0
K (K)	0.18	0.2	K (K)	0.15	0.14	K (K)	0.12	0.16
Pd (M)	7.07	1.6	Ca (K)	8.59	7.77	Ca (K)	0.43	0.54
Zn (L)	77.53	52.38	Pd (M)	7.12	1.32	Pd (L)	21.84	5.65
			Zn (L)	61.33	34.03	Au (M)	11.16	2.86
						Zn (K)	51.28	39.58
Total	100	100	Total	100	100	Total	100	100

[a]K, L, and M are the respective electron shells used to identify the element by the instrument.

4.2.3 TEM Analysis of Stock Zinc Oxide Nanomaterial

EDS analyses were performed using a JEOL 100CX unit. This analysis required a 1000-fold dilution of the 1% stock nanomaterial solution. The stock solutions were sonicated for 1 hour. The diluted sample of each nanomaterial was added to a TEM cartridge for TEM analysis. TEM results for ZnO-A nanomaterial can be seen in Figure 4.4. The particles appear to have the same characteristics seen in the SEM results. There are a variety of shapes with the average size approximately 100 nm.

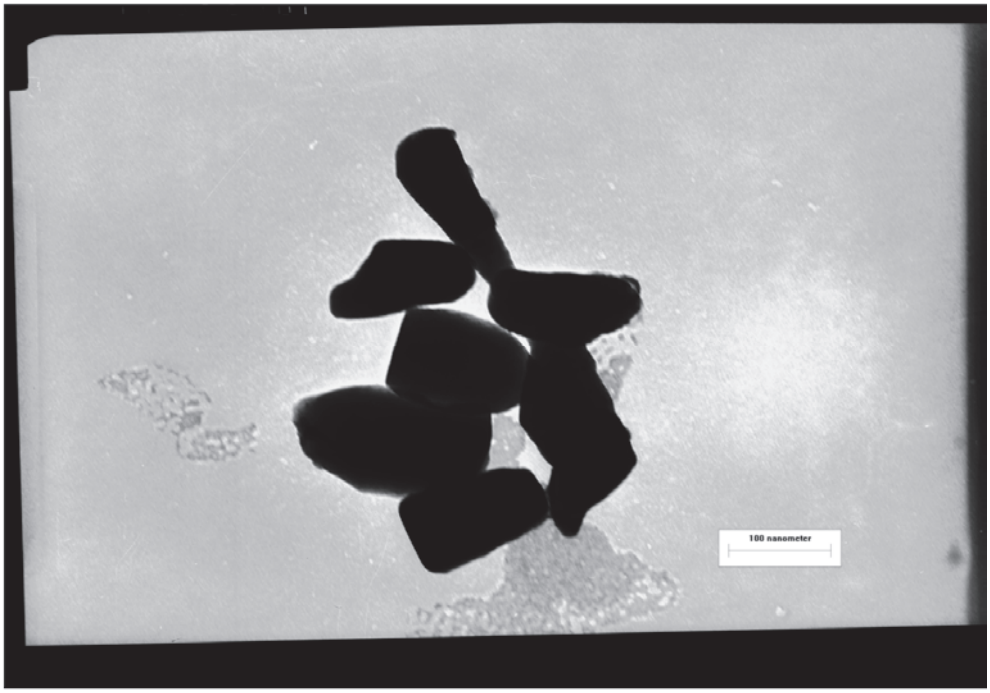

Figure 4.4. TEM images of the stock zinc oxide (ZnO-A) nanomaterial.

Figure 4.5 shows the TEM image for ZnO-B nanomaterial. Again, the particles appear to have the same characteristics seen in the SEM results. There are a large variety of shapes seen in this sample varying between 100 and 500 nm diameters. The average size appears to be 300 nm.

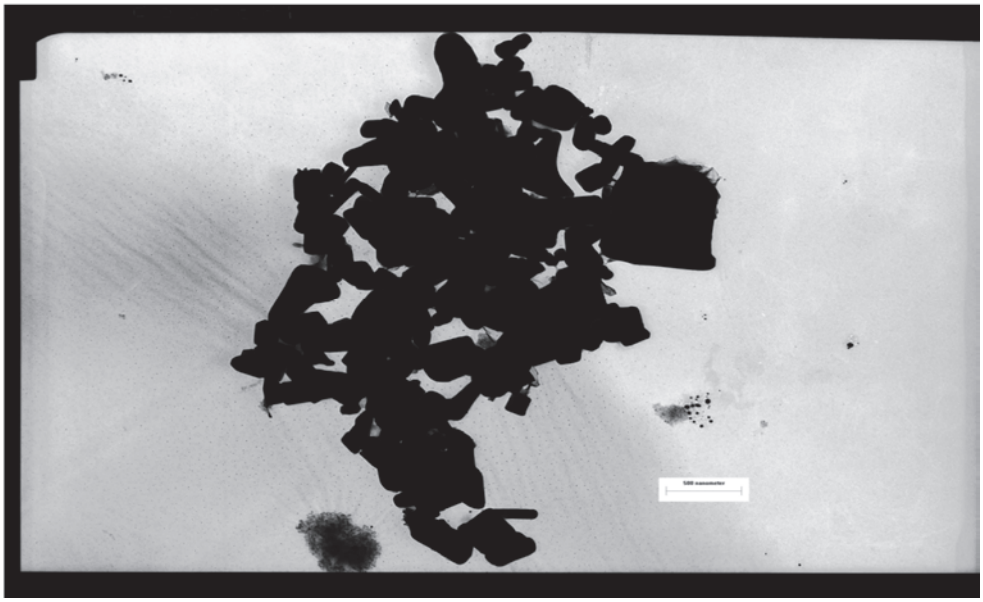

Figure 4.5. TEM images of the stock zinc oxide (ZnO-B) nanomaterial.

ZnO-C was difficult to find in the TEM results seen in Figure 4.6. The particle appears to have the same characteristics as previous zinc oxide nanomaterial and has a diameter of approximately 500 nm. However, only the “shadow” of the particle is seen in TEM, whereas SEM analysis provides more of a three-dimensional appearance. The size of the particle appears to agree with what was seen in the SEM image, but it cannot be determined if the particle is flake-like as seen using the SEM.

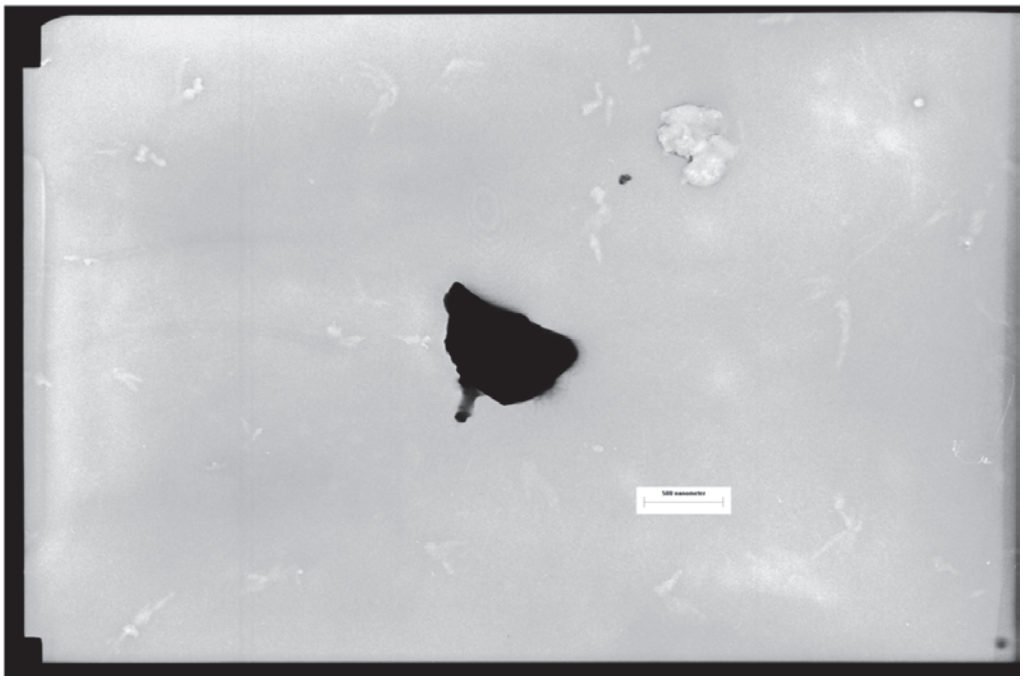

Figure 4.6. TEM images of the stock zinc oxide (ZnO-C) nanomaterial.

4.2.4 Particle Size Analysis of Zinc Oxide Stock Nanomaterial

The stock solution was sonicated for 1 hour, and then a 1000-fold dilution of the 1% stock solution was made. The diluted solution was then sonicated again for 15 minutes prior to particle size analysis. Exactly 3 mL of the diluted solution was added to a disposable cuvette and then placed in Brookhaven ZetaPALS particle sizing instrument. This was repeated for each nanomaterial.

Particle size results of zinc oxide nanomaterial can be seen in Table 4.3. SEM results for ZnO-A showed an average diameter of 100 nm, but when in a DI water suspension, the average effective diameter was 240 nm. This indicated possible agglomeration of the nanomaterial in DI water. Both ZnO-B and ZnO-C appeared to have a diameter of 300 nm. Particle size analysis of ZnO-B determined the average diameter of 336 nm, which relates very well with the SEM images. ZnO-C had large variances between repetitions and resulted in an average diameter of 874 nm. Based on the SEM images, it is possible the particles aggregated and altered the effective diameter when in solution.

Table 4.3. Particle Size Analysis Using Brookhaven ZetaPALS of 10 mg/L Dilution of Stock Zinc (Oxide) Nanomaterial

	ZnO-A		ZnO-B		ZnO-C	
	Eff. Dia. (nm)	Poly-dispersity	Eff. Dia. (nm)	Poly-dispersity	Eff. Dia. (nm)	Poly-dispersity
Rep 1	242.1	0.083	339.0	0.195	1433.7	0.346
Rep 2	241.8	0.122	328.9	0.179	551.7	0.261
Rep 3	237.8	0.149	340.4	0.135	638.6	0.208
Average	240.57	0.118	336.10	0.170	874.67	0.272

4.3 Characterization of Silver Stock Nanomaterial

4.3.1 SEM Analysis of Stock Silver Nanomaterial

SEM results for Ag-A nanomaterial is shown in Figure 4.7. These particles are much more uniform when compared to the nanozinc stock solutions. The particles are spherical and have an average diameter of 100 nm.

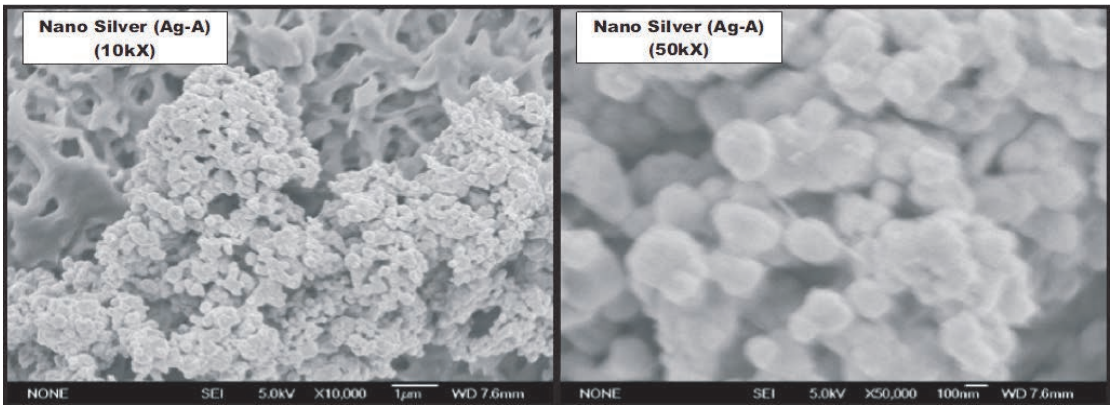

Figure 4.7. SEM images of the stock silver (Ag-A) nanomaterial on a membrane filter.

SEM results for Ag-C nanomaterial are shown in Figure 4.8. Again, these particles are much more uniform when compared to the nanozinc stock solutions. The particles are disk-shaped, and the size varies a little more than Ag-A (20–400 nm). The average size appears to be approximately 100 nm.

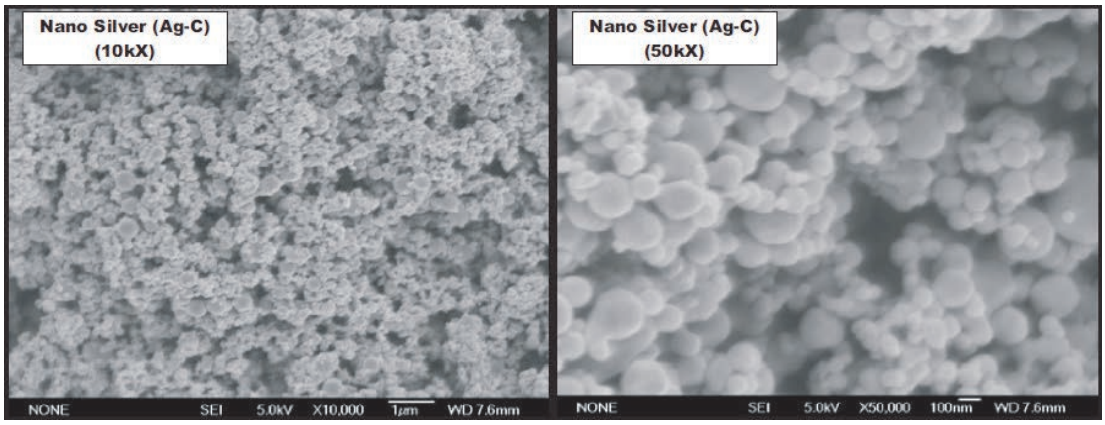

Figure 4.8. SEM images of the stock silver (Ag-C) nanomaterial on a membrane filter.

4.3.2 EDS Analysis of Stock Silver Nanomaterial

Table 4.4 shows the EDS results of the stock solutions of Ag-A and Ag-C nanomaterials. Generally, the major elements are C, Pd, Au, and Ag. Again, carbon is seen because of the membrane and Pd/Au because of the coating placed on the samples. Silver is the main element seen in these results making up 70% of the total composition. A small amount of Zn is found, the origin of which is currently unknown. Graphical results can be seen in Figures 4.9 and 4.10 for Ag-A and Ag-C, respectively. These results show that the silver stock solutions are relatively pure.

Table 4.4. EDS Analysis Indicating Composition of Stock Silver Nanomaterial

Ag-A			Ag-C		
Element (Shell) [a]	**Wt%**	**At%**	**Element (Shell) [a]**	**Wt%**	**At%**
C (K)	6.68	38.53	C (K)	4.99	31.7
O (K)	1.22	5.27	O (K)	0.87	4.15
Na (K)	0.44	1.33	Na (K)	0.88	2.9
P (K)	0.33	0.73	P (K)	0.2	0.5
Cl (K)	0.31	0.61	Cl (K)	0.11	0.24
K (K)	0	0	K (K)	0	0
Ca (K)	0	0	Ca (K)	0	0
Zn (K)	1.5	1.59	Zn (K)	2.29	2.67
Pd (L)	11.61	4.13	Pd (L)	12.05	4.71
Au (M)	7.73	2.72	Au (M)	7.69	2.98
Ag (L)	70.18	45.09	Ag (L)	70.91	50.15
Total	100.00	100.00	Total	100.00	100.00

[a]K, L, and M are the respective electron shells used to identify the element by the instrument.

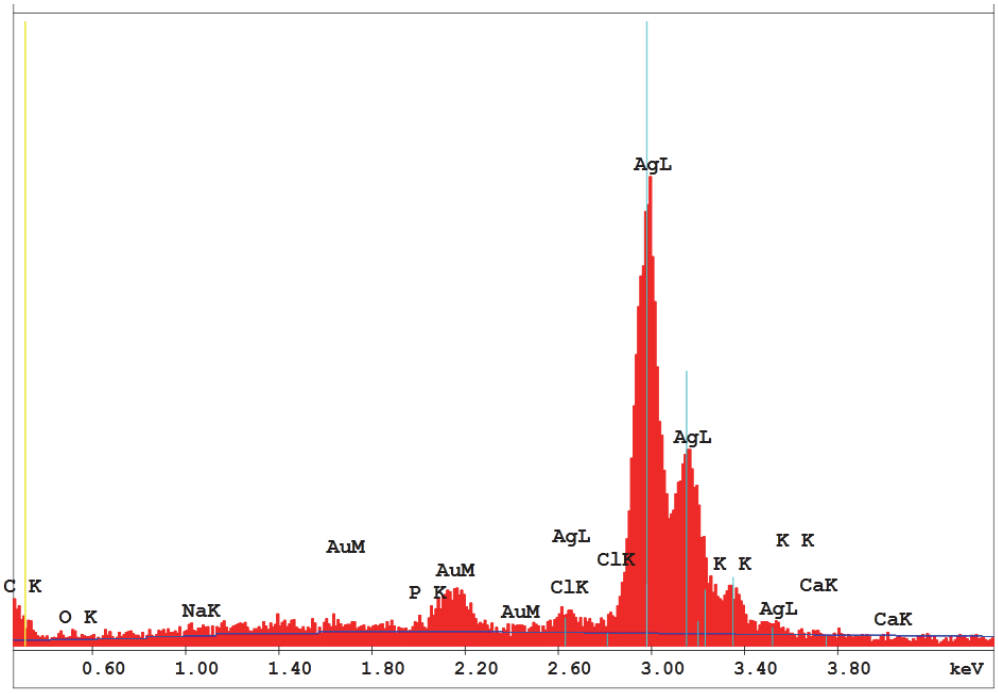

Figure 4.9. Graphical output of EDS analysis using SEM of stock Ag-A solution on a filtration membrane and sputter-coated with Au/Pd.

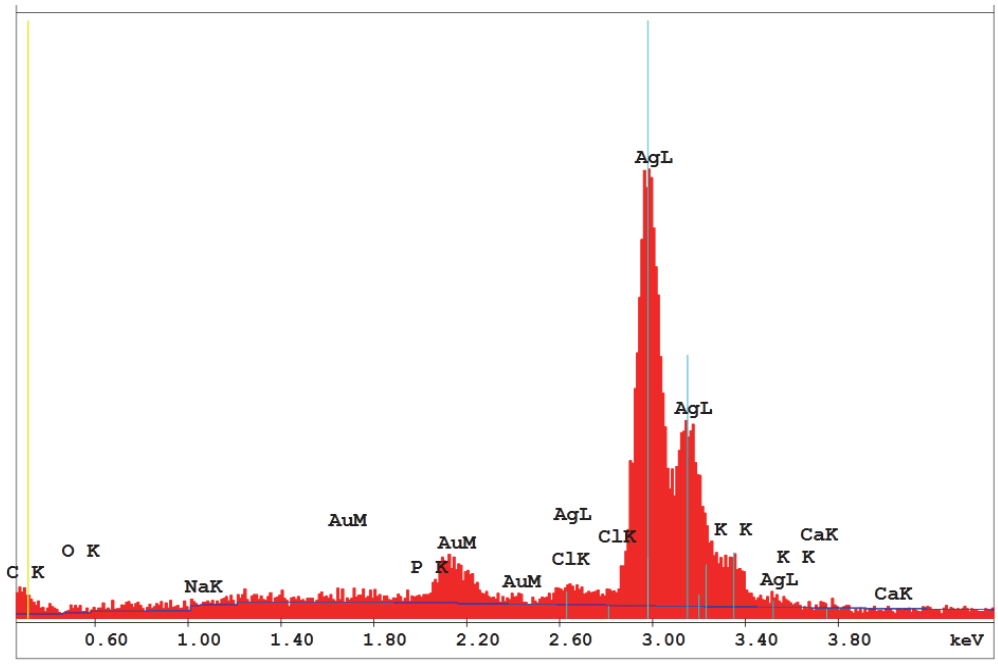

Figure 4.10. Graphical output of EDS analysis using SEM of stock Ag-C solution on a filtration membrane and sputter-coated with Au/Pd.

4.3.3 TEM Analysis of Stock Silver Nanomaterial

TEM results for Ag-A nanomaterial can be seen in Figure 4.11. The particles appear to be 100 nm in diameter and more uniform compared to the zinc nanomaterial.

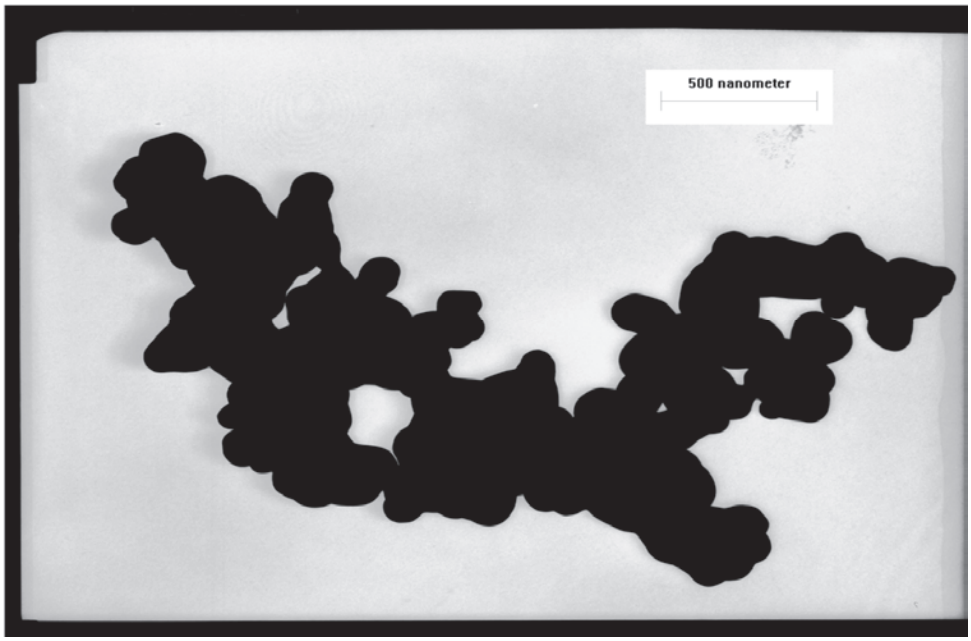

Figure 4.11. TEM images of the stock silver (Ag-A) nanomaterial.

TEM results for Ag-C nanomaterial can be seen in Figure 4.12. Particles are highly agglomerated and appear to vary slightly more in size relative to the Ag-A sample. The average particle size appears to be approximately 100 nm.

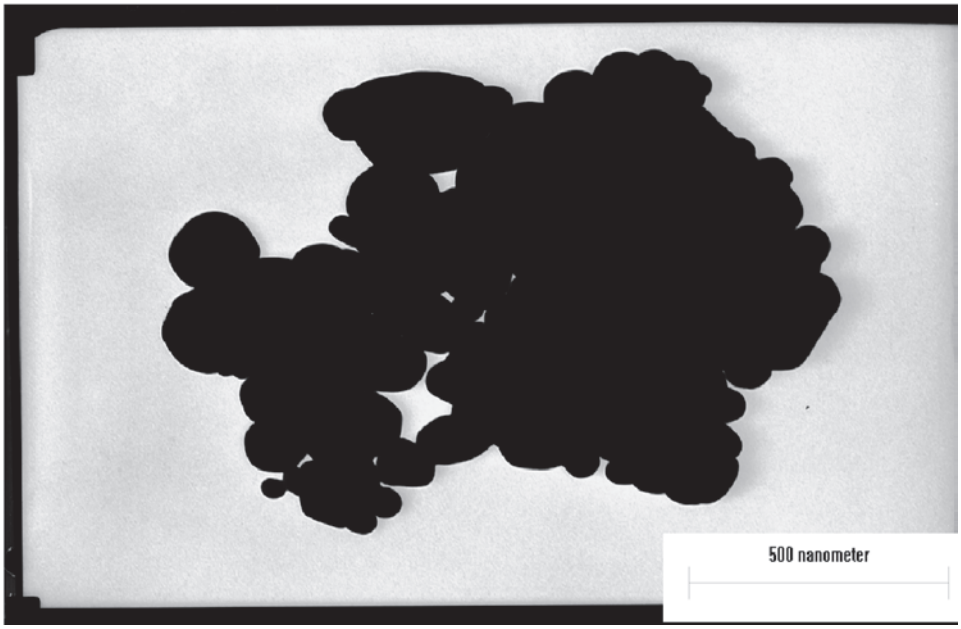

Figure 4.12. TEM images of the stock silver (Ag-C) nanomaterial.

4.3.4 Particle Size Analysis of Zinc Oxide Stock Nanomaterial

SEM results for Ag-A showed an average diameter of 100 nm, but when in a DI water solution, the particles are highly agglomerated increasing the effective diameter to more than 2000 nm (Table 4.5). Ag-C diameter in a DI water solution was found to be 132 nm. The results relate well to the SEM images where the diameter was found to be approximately 100 nm. However, it is possible that some of the particles rapidly agglomerated and settled out of solution prior to the analysis.

Table 4.5. Particle Size Analysis Using Brookhaven ZetaPALS of 10 mg/L Dilution of Stock Silver Nanomaterial

	Ag-A		Ag-C	
	Eff. Dia. (nm)	**Polydispersity**	**Eff. Dia. (nm)**	**Polydispersity**
Rep 1	3628.4	0.331	133.4	0.238
Rep 2	519.2	0.282	128.0	0.266
Rep 3	2859.0	0.233	135.5	0.247
Average	2335.53	0.282	132.30	0.250

4.4 Characterization of Copper Oxide Stock Nanomaterial

Table 4.6 summarizes data from CuNP characterization. SEM analyses of the copper nanomaterial showed an average particle size of about 50 to 100 nm (Figure 4.13). X-ray diffraction analyses indicated the presence of copper and copper oxide in the CuNP particles (Figure 4.14). The predominant copper oxide phases are CuO and $Cu^{2+1}O$.

During the preparation of stock suspensions, the dark brown elemental CuNP oxidized to copper oxides within 30 minutes of sonication, as indicated by the green color and X-ray diffraction analyses. Analyses of these suspensions by Zetasizer indicated that the particles aggregated to a size (measured as hydrodynamic diameter) distribution of 100 to 200 nm with an average particle size of approximately 125 nm. BET analyses of the nanomaterial yielded an average surface area of 14.27 m^2/g.

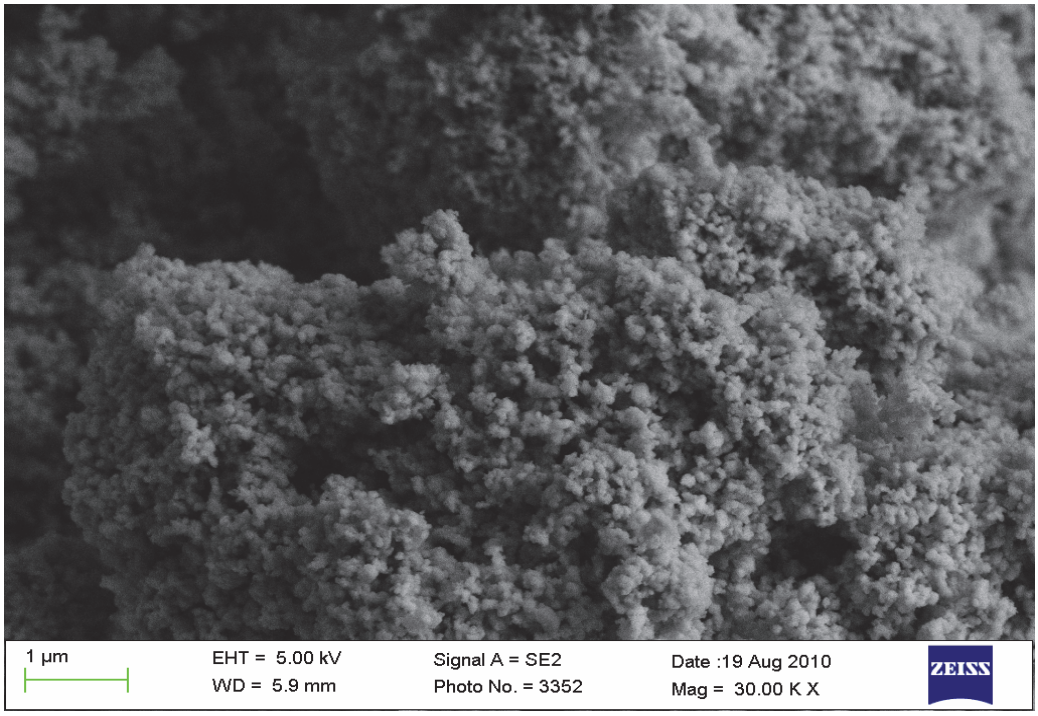

Figure 4.13. SEM images of the stock copper nanomaterial.

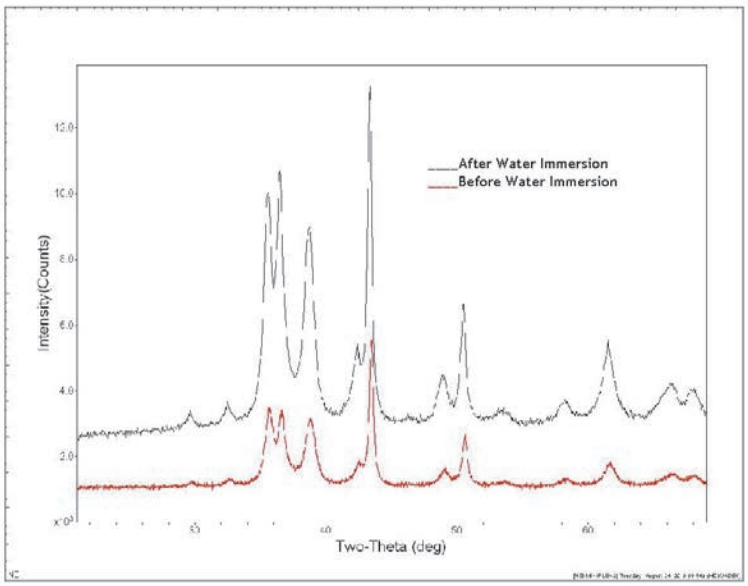

Figure 4.14. X-ray diffraction images of the stock copper nanomaterial.

4.5 Characterization of Nanomaterial Spiked in Unfiltered and Filtered Activated Sludge Samples

4.5.1 SEM Analysis of Nanomaterials in Wastewater Samples

Activated sludge samples from OCSD were used in these analyses. Approximately 200 mL of unfiltered wastewater was spiked with 2 mg/L of stock nanomaterial and distributed to a flask. Additional analyses were also performed with filtered (0.45 µm) samples. The flasks were then incubated in a shaker for 4 hours at room temperature. After 4 hours, 50 mLs of samples were collected from each flask and filtered using 0.2 micron nuclepore filters. All the nuclepore filters were air-dried, and then an appropriate size was cut out of the filter paper and attached to SEM aluminum stubs with conductive carbon adhesive and again air-dried. The samples were sputter-coated with gold/palladium and analyzed by SEM.

Figures 4.15 to 4.17 show several images of a specific nanomaterial spiked (2 mg/L) with the biomass (A, B, and C) and without the biomass (D, E, and F). Comparison of images in Figure 4.15 (ZnO-A spiked) to the pure stock SEM images (Figure 4.1) yielded some similarities in the particle structures. It appears that the nanomaterial retains its structure within and without the biomass. Because of the amount of organic material seen in the images with the biomass, it is difficult to see smaller structures, but in the filtered samples, they are clearly visible. It appears that the size and the amount of nanomaterial particles are the same with and without the biomass. Generally, the sizes of the particles appear similar to the stock solution with the average size of 100 nm.

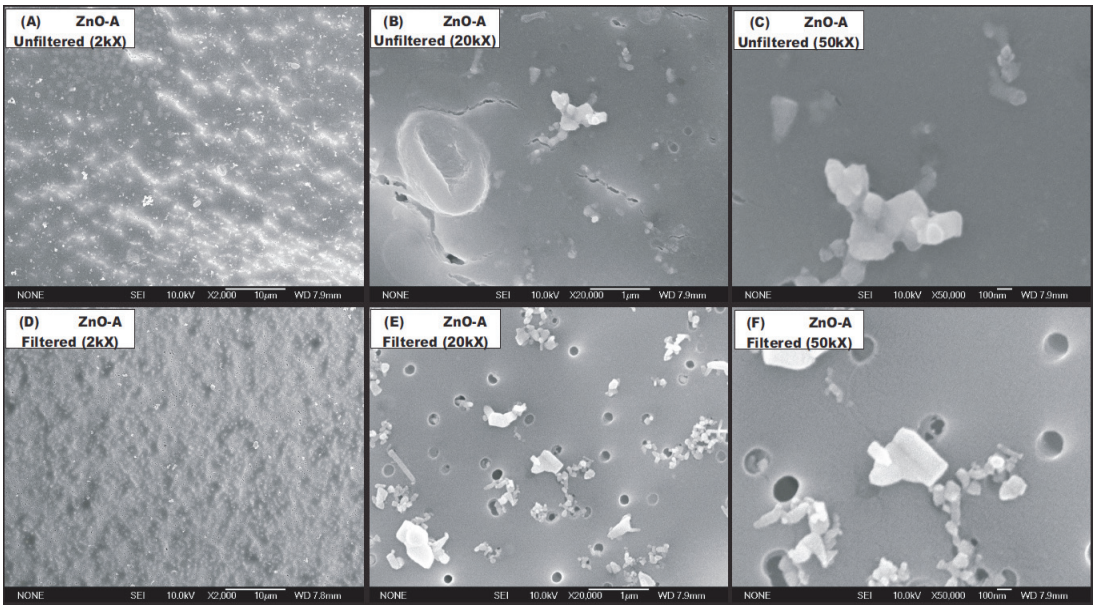

Figure 4.15. SEM images of ZnO-A nanomaterial spiked with the biomass (A, B, C) and without the biomass (D, E, F).

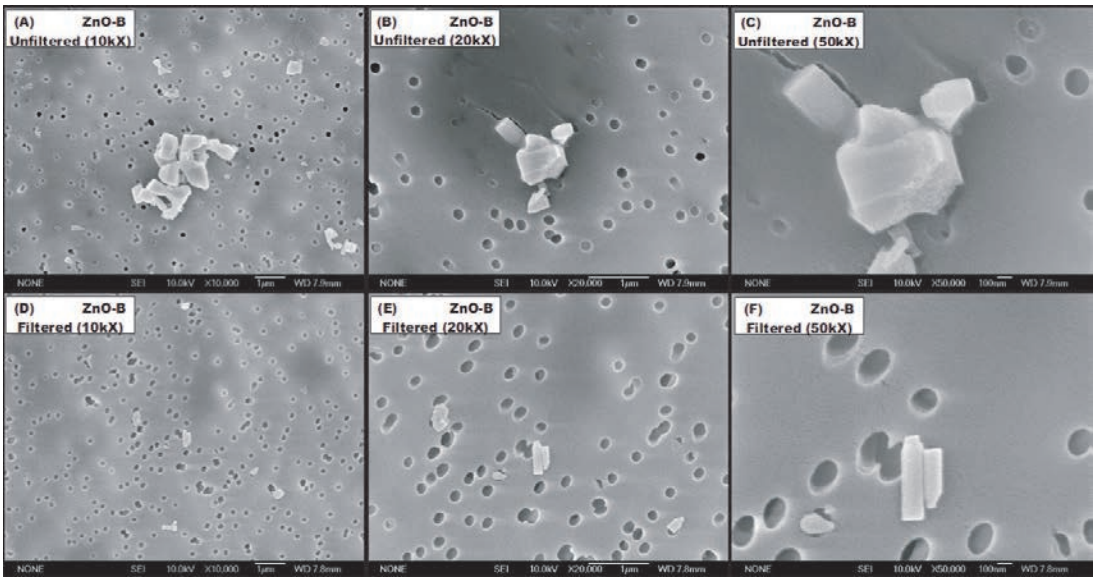

Figure 4.16. SEM images of ZnO-B nanomaterial spiked with the biomass (A, B, C) and without the biomass (D, E, F).

Images in Figure 4.16 (ZnO-B spiked) appear to have similar results seen in Figure 4.15 with ZnO-A. The size and amount of particles appear to be similar between the filtered and unfiltered samples. However, there are relatively fewer particles seen in the images. The

structures of the particles have the same characteristics observed with the stock SEM images (Figure 4.2). Because of the larger size, the particles probably settled out of solution more readily, which may explain the low number of particles seen in the sample.

Figure 4.17 has SEM images of wastewater spike with ZnO-C. As observed with the stock suspension images (Figure 4.3), no clear definition of size or shape was obtained from these images. In the presence of biomass it appears that the nanomaterials were covered by the sample constituents, preventing them from being seen in the images. Without the biomass the nanomaterial is visible (compared to stock solution) but highly agglomerated, and individual particles are indistinguishable. It is very difficult to make any conclusions based on these images.

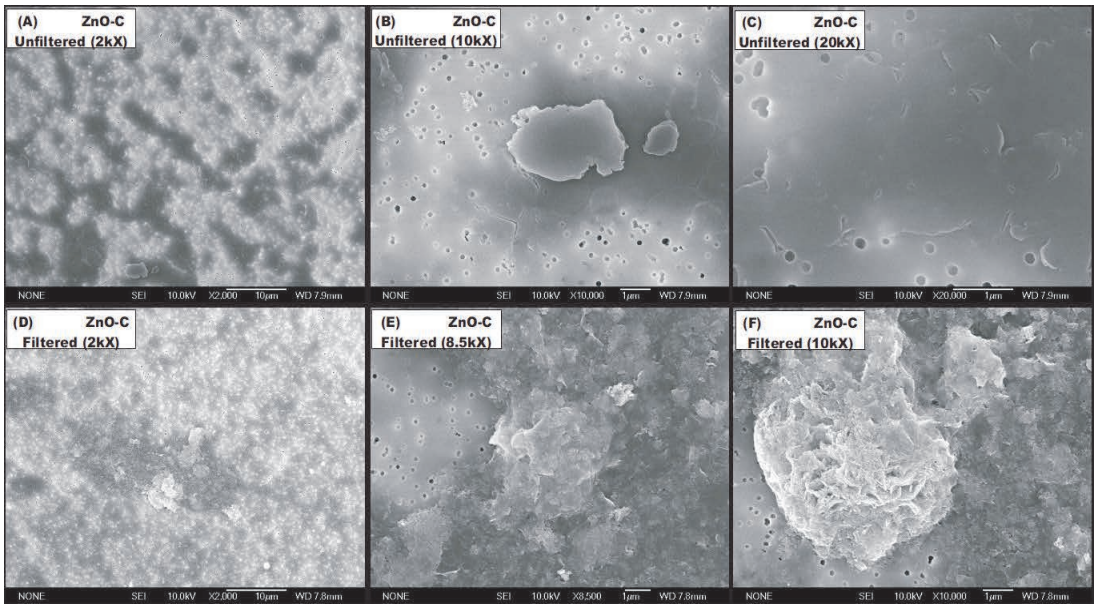

Figure 4.17. SEM images of ZnO-C nanomaterial spiked with the biomass (A, B, C) and without the biomass (D, E, F).

Figure 4.18 shows SEM images of Ag-A nanomaterial spiked in wastewater. Both samples (with and without the biomass) show that the particles are highly agglomerated resulting in an overall size of 1 micron or larger. The particles within the agglomerates appear to have the same characteristics seen in the stock SEM images (Figure 4.7). The individual particle size appears to be approximately 100 nm.

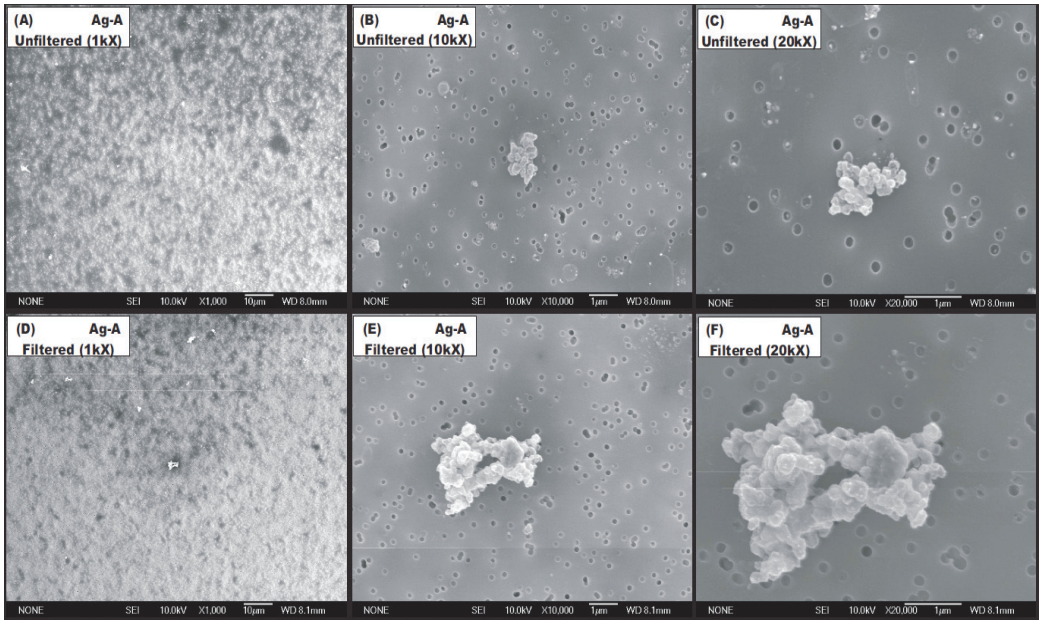

Figure 4.18. SEM images of Ag-A nanomaterial spiked with the biomass (A, B, C) and without the biomass (D, E, F).

Figure 4.19 has SEM images of Ag-C nanomaterial spiked in wastewater. In images with the biomass the particles are highly agglomerated resulting in an overall size of over 1 micron. The individual particles appear to be about 100 nm. Unfortunately, there were no agglomerates found in the sample without the biomass.

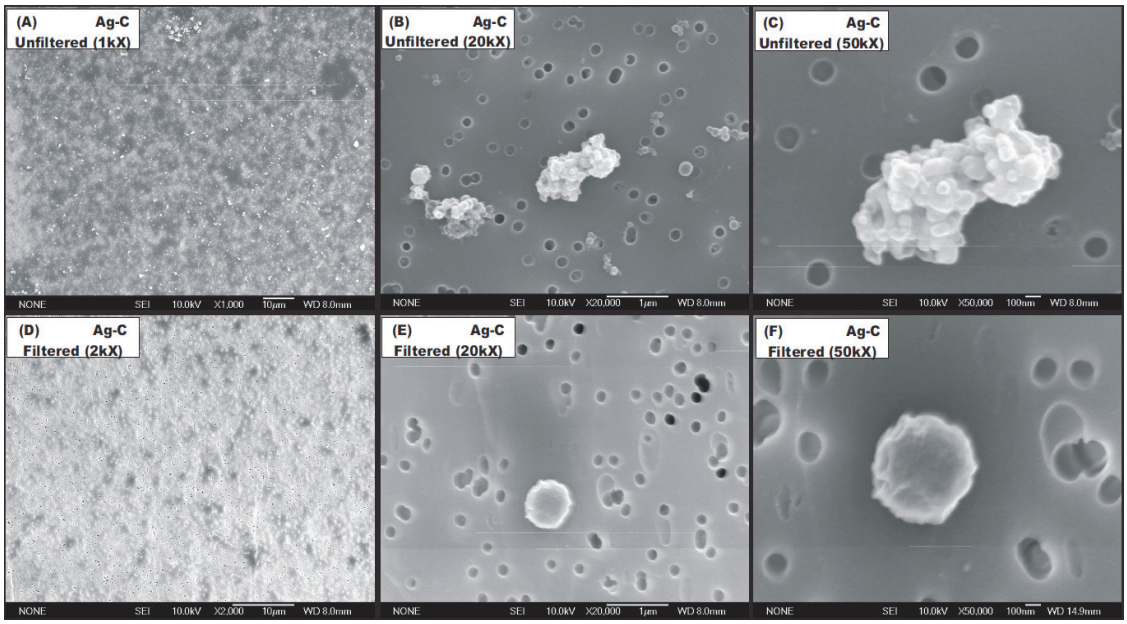

Figure 4.19. SEM images of Ag-C nanomaterial spiked with the biomass (A, B, C) and without the biomass (D, E, F).

Figure 4.20 shows the picture of copper nanoparticles after 4 hours of incubation in the filtrate. The particles appeared to have transformed to larger size aggregates (> 1 µm) during their removal.

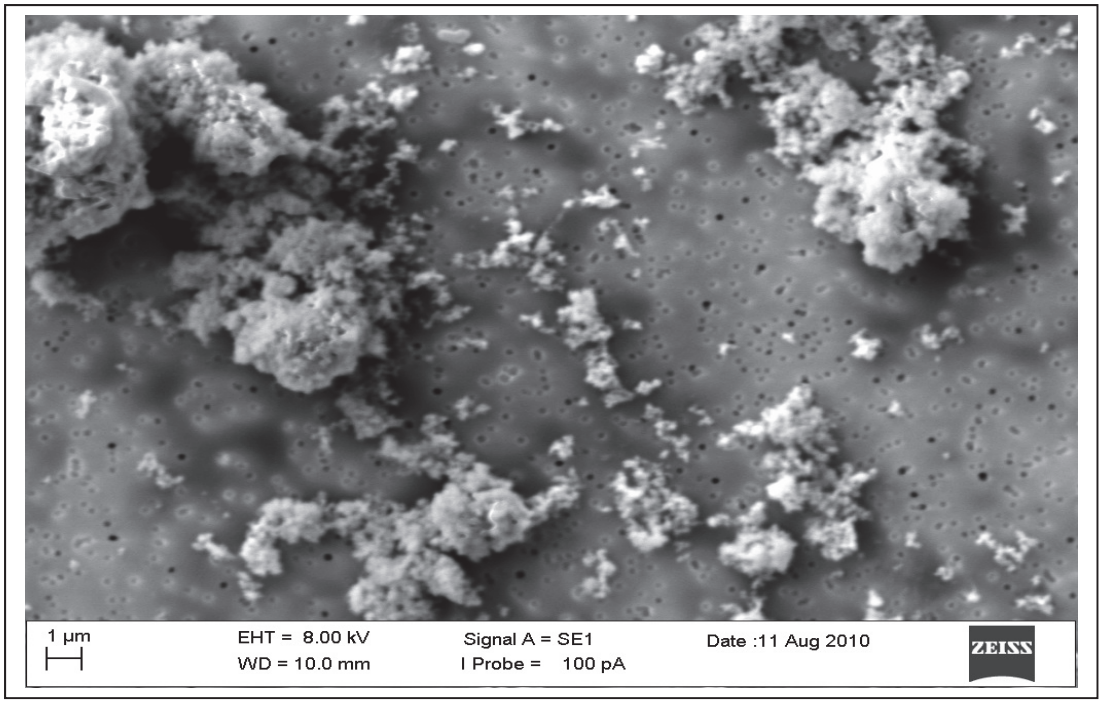

Figure 4.20. SEM image of nanocopper in filtered wastewater.

4.5.2 EDS Analysis of Nanomaterials in Wastewater Samples

For this analysis the secondary effluent from OCSD was obtained and filtered with a 0.45 µm filter. Approximately 200 mL of the filtered wastewater was distributed to several flasks and spiked with 2 mg/L concentration of a nanomaterial. The flasks were then incubated in a shaker for 4 hours at room temperature. After 4 hours, 500 mLs of each sample were collected and filtered using 0.2 micron nuclepore filters. All the nuclepore filters were air-dried, and then an appropriate size was cut out of the filter paper and attached to SEM aluminum stubs with conductive carbon adhesive and again air-dried. The samples were sputter-coated with gold/palladium and analyzed for composition with EDS using the SEM.

Table 4.6 shows the composition of zinc-spiked samples in wastewater filtrate (graphical results can be seen in Figures 4.21 to 4.23). The results are consistent for all three types of zinc nanomaterial. Major components are C, O, Au, Pd, and Zn. Au/Pd is due to the coating added to the sample for analysis. Overall, ~15% of the composition is made of zinc, ~17% is oxygen, and ~45% is carbon. The ratio of zinc and oxygen is not the same as the stock sample because of organic material in the filtrate. In combination with the SEM results, it appears the composition of the zinc nanomaterial is unaffected.

Table 4.6. EDS Analysis of Zinc Oxide (2 mg/L) in Filtered Secondary Effluent

ZnO-A			ZnO-B			ZnO-C		
Element (Shell) [a]	**Wt%**	**At%**	**Element (Shell) [a]**	**Wt%**	**At%**	**Element (Shell) [a]**	**Wt%**	**At%**
C (K)	45.87	71.57	C (K)	50.76	74.31	C (K)	41.95	70.88
O (K)	18.35	21.49	O (K)	17.49	19.22	O (K)	15.7	19.92
Na (K)	0	0	Na (K)	0	0	Na (K)	0	0
P (K)	0.48	0.29	P (K)	0.47	0.27	P (K)	0.76	0.5
Au (M)	9.1	0.87	Au (M)	6.91	0.62	Au (M)	7.69	0.79
Cl (K)	0.42	0.22	Cl (K)	0.11	0.05	Cl (K)	0.56	0.32
K (K)	0.36	0.17	K (K)	0	0			
Ca (K)	0.74	0.35	Ca (K)	2.24	0.98	Ca (K)	0.86	0.44
Zn (K)	14.02	4.02	Zn (K)	14.33	3.85	Zn (L)	18.27	5.67
Pd (L)	10.67	1.03	Pd (L)	7.69	0.69	Pd (L)	14.21	1.48
Total	100	100	Total	100	100	Total	100	100

[a]K, L, and M are the respective electron shells used to identify the element by the instrument.

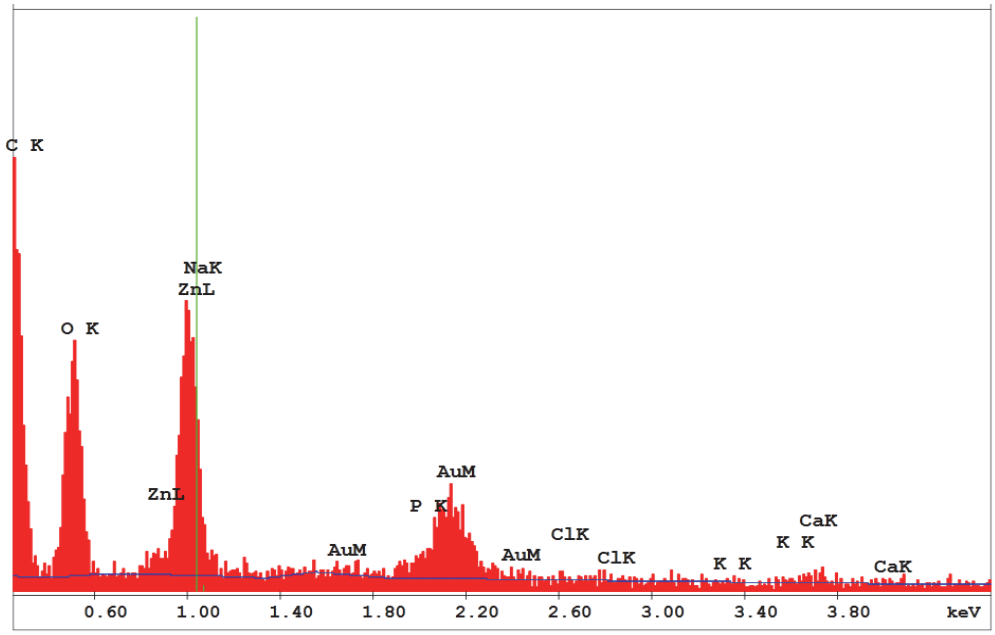

Figure 4.21. Graphical EDS results using SEM of secondary effluent filtrate spiked with 2 mg/L ZnO-A on a filtration membrane and sputter-coated with Au/Pd.

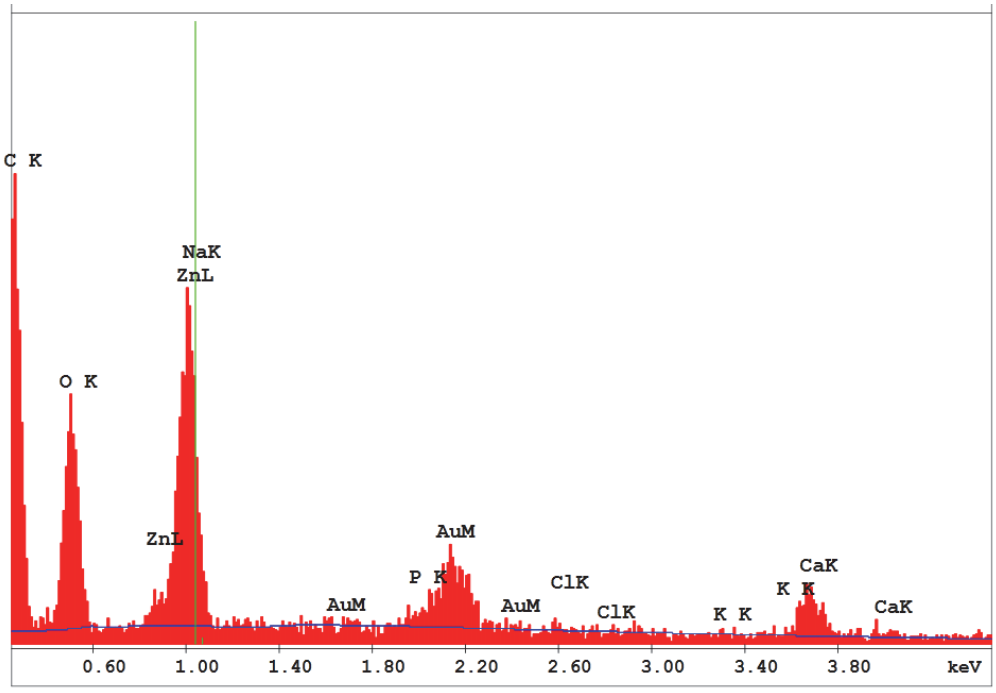

Figure 4.22. Graphical EDS results using SEM of secondary effluent filtrate spiked with 2 mg/L ZnO-B on a filtration membrane and sputter-coated with Au/Pd.

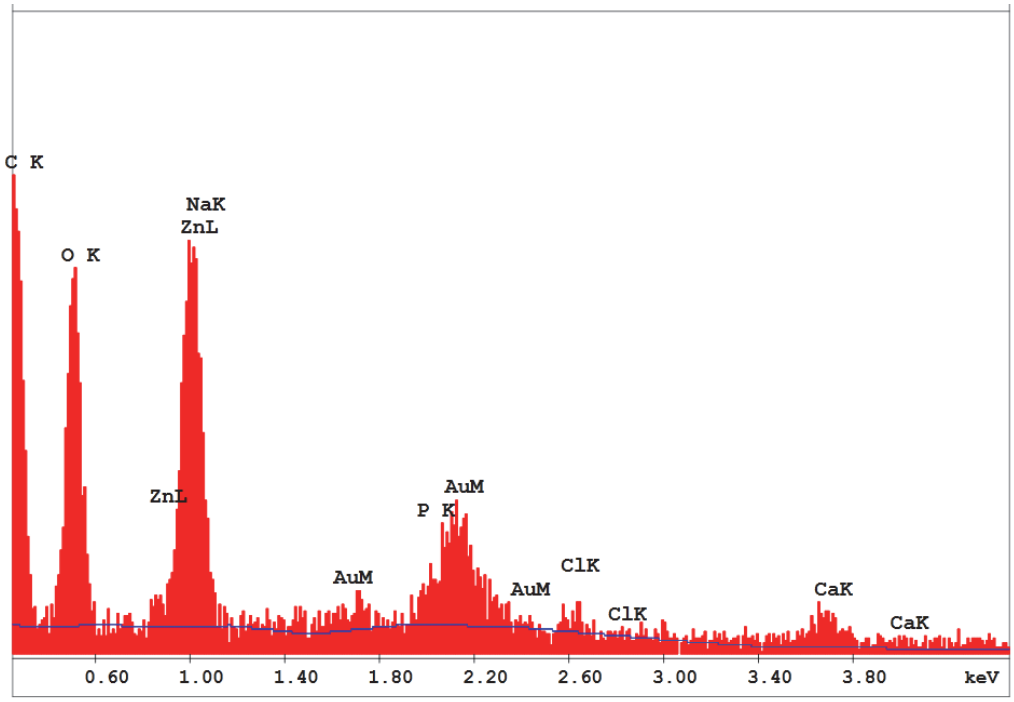

Figure 4.23. Graphical EDS results using SEM of secondary effluent filtrate spiked with 2 mg/L ZnO-C on a filtration membrane and sputter-coated with Au/Pd.

Table 4.7 shows the composition of silver-spiked samples in secondary effluent filtrate (graphical results can be seen in Figure 4.24 and 4.25). Again, the results are consistent between samples. Major components are C, O, Au, Pd, and Ag. Au/Pd is due to the coating added to the sample for analysis. Overall, ~50% of the composition is made of silver, ~20% carbon, and only ~5% oxygen. Again, in combination with the SEM results, it appears the composition of the silver nanomaterial is unaffected.

Table 4.7. EDS Analysis Using SEM in Secondary Effluent without the Biomass Spiked with 2 mg/L of Ag-A and Ag-C Nanomaterials

Ag-A			Ag-C		
Element (Shell) [a]	**Wt%**	**At%**	**Element (Shell) [a]**	**Wt%**	**At%**
C (K)	19.75	63.75	C (K)	23.63	67.11
O (K)	4.61	11.18	O (K)	5.95	12.68
Na (K)	0.71	1.2	Na (K)	0.61	0.91
P (K)	0.35	0.43	P (K)	0.14	0.15
Au (M)	7.63	1.5	Au (M)	8.03	1.39
Cl (K)	0.31	0.34	Cl (K)	0.13	0.12
Ag (L)	51.89	18.66	Ag (L)	48.23	15.25
K (K)	0	0	K (K)	0	0
Ca (K)	0	0	Ca (K)	0.09	0.08
Pd (L)	14.75	2.93	Pd (L)	13.19	2.31
Total	100	100	Total	100	100

[a]K, L, and M are the respective electron shells used to identify the element by the instrument.

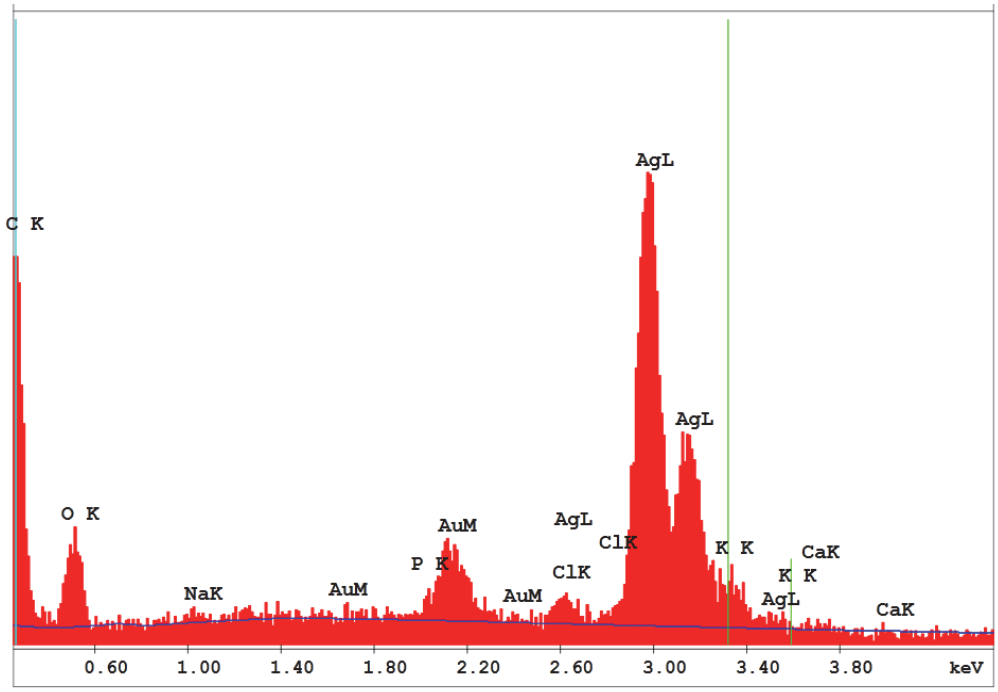

Figure 4.24. Graphical EDS results using SEM of secondary effluent filtrate spiked with 2 mg/L Ag-A on a filtration membrane and sputter-coated with Au/Pd.

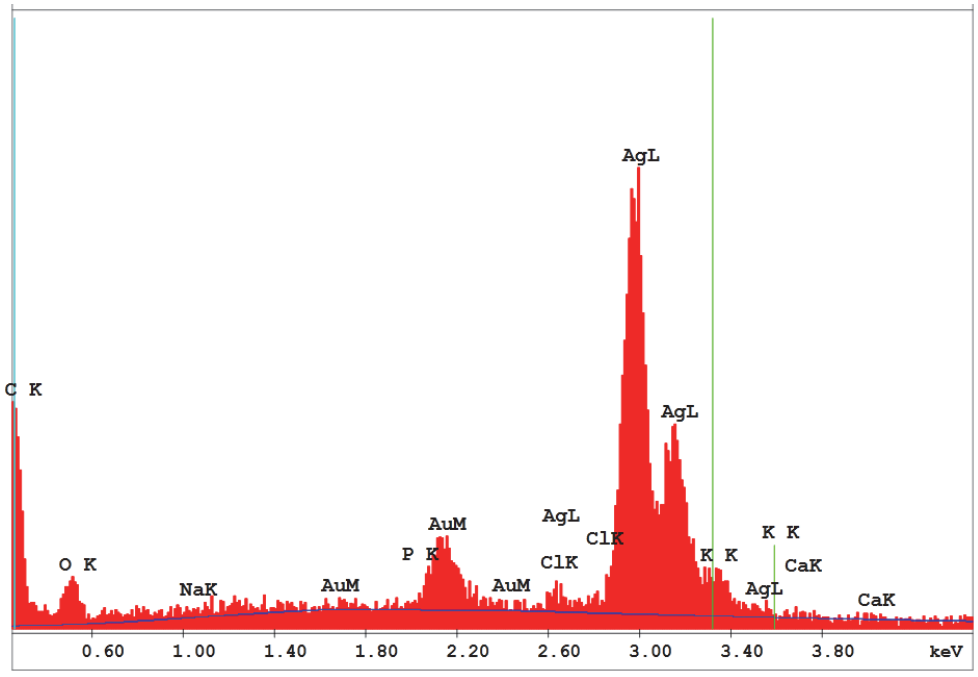

Figure 4.25. Graphical EDS results using SEM of secondary effluent filtrate spiked with 2 mg/L Ag-C on a filtration membrane and sputter-coated with Au/Pd.

4.6 Summary of Nanomaterials Characterization

Table 4.8 summarizes the nanomaterials characteristics in stock suspensions provided by the vendor as well as those determined independently. Table 4.9 provides a summary of nanoparticles added to wastewater samples.

In general, the sizes of the nanomaterials measured (100–500 nm) in the stock suspensions were larger than the vendor-reported size range (10–150 nm). It must be noted that, because of various instrument malfunctions and the eventual closure of the Zeiss Nanomaterials Lab at UCI, the nanomaterials characterization was performed near the end of the project period rather than upon immediate receipt of the nanomaterials stock suspensions. As a result, the nanomaterials stock suspensions were stored for nearly 2 years prior to characterization. Nanomaterials are known to aggregate to a larger size or to dissolve and precipitate over time. Indeed, some of the DLS analyses performed on filtrate samples during an earlier part of the study showed a particle size distribution smaller than those measured during characterization studies.

Table 4.8. Summary of Nanomaterial Composition in Stock Suspensions

Nanomaterial	Primary Particle Size (nm) (SEM)		Aggregated Particle Size (nm) (SEM)	EDS/XRD Analyses	Zeta Potential[b]	Surface Area[b]
	Vendor Information	*Lab Characterization*[a]				
ZnO-A	40–100	100	241	87.6% Zn[c]	+ 40.6	10-25
ZnO-B	30	300	336	80.9 Zn[c]		35
ZnO-C	< 10	50–300	875	81.8% Zn[c]		70
Ag-A	<100	100	2335	70% Ag[d]	- 9.1	5
Ag-B	150	ND	ND	ND		3
Ag-C	<120	20–400 nm	132	71% Ag[d]		4
CuNP	20–40 nm	50–100 nm	125	50% CuO, $Cu^{2+1}O$[e]	ND	14.27

[a]Some particles as large as 1 µm were also observed.

[b]Vendor provided information.

ND = not determined.

[c]Expected Composition 80.3%.

[d]Expected Composition ~100%.

[e]Expected Composition 53%.

Table 4.9. Summary of Nanomaterial Characteristics in Wastewater Samples

Nanomaterial	SEM: Primary Particle Size (nm)	EDS: Chemical Comp
ZnO-A	100	45%C, 14%Zn, 18% O
ZnO-B	300–500	50%C, 14%Zn, 17% O
ZnO-C	50	42%C, 18%Zn, 17% O
Ag-A	100	19% C, 52% Ag
Ag-C	100	23% C, 48% Ag
CuNP	Not Determined	Not Determined

4.7 Analyses of Nanomaterials

Several tests were performed to verify if ICP and other analyses used to measure nanomaterials yielded good recovery of the added nanomaterials. These analyses were performed by the OCSD analytical laboratory staff and the UCI Department of Civil and Environmental Engineering laboratory staff. Select samples were analyzed by external certified laboratories also. A brief summary of the analyses follow.

Initially, analyses of nanozinc oxide and nanosilver were performed at the OCSD analytical laboratory. The 1% stock suspensions obtained from the vendor were diluted, sonicated, and analyzed by ICP (EPA Method 200.8). Samples were analyzed with and without digestion (5.4% HNO_3 + 3.6% HCl) prior to ICP analyses. A summary of initial results is shown in Table 4.10.

Table 4.10. Recovery of Nanozinc Oxide and Nanosilver from Diluted Stock Suspension

Nanomaterial	Percent Recovery	
	Undigested Sample	Digested Sample[a]
Nanozinc Oxide	89%	91%
Functionalized Nanozinc Oxide	97%	99%
Nanosilver	8%	10%
Functionalized Nanosilver	9%	14%

[a]Digestion matrix: 5.4% HNO_3 + 3.6% HCl.

As shown in Table 4.10, more than 90% of nanozinc oxide in the suspensions was recovered during analyses. In general, high levels of zinc oxide (90–105%) were recovered from wastewater samples throughout this study. However, less than 10% of nanosilver was recovered during the initial analyses. Hence, additional analyses were performed using a fresh batch of nanosilver stock, simultaneous DLS analyses of the digested and undigested samples, and spike analyses using ionic silver standards. These data are presented in the Tables 4.11 to 4.13.

Table 4.11. Nanosilver Analyses in Original and Newer Stock Suspensions

Analyses Date	Sample ID	Anticipated Concentration	Measured Concentration	% Recovery
8/28/09	Fn-Ag-A	1	0.43	43.0%
8/28/09		1	0.447	44.7%
8/28/09		1	0.417	43.4%
8/28/09		0.5	0.22	44.0%
8/28/09		0.5	0.213	42.6%
9/24/09		0.5	0.208	41.6%
9/24/09		0.5	0.196	39.2%
9/24/09		1	0.45	45.0%
10/23/09		1	0.42	42.0%
10/23/09		1	0.39	39.0%
9/24/09	Fn-Ag-C	0.5	0.287	57.4%
9/24/09		1	0.585	58.5%
9/24/09	Fn-Ag-B	0.5	0.03	6.0%
9/24/09		1	0.094	9.4%
10/23/09	Fn-Ag-B[a]	0.5	0.05	5.0%
10/23/09		1	0.08	8.0%

[a]Fresh batch made a week prior to analyses.

As indicated in the Table 4.11, poor recoveries (5 to 58%) of nanosilver were observed with all of the stock suspensions tested. In particular, nanosilver stock B (Fn-Ag-B) had recoveries below 10%. Subsequently, the 1% nanosilver (Fn-Ag-A) stock was diluted to an anticipated concentration of 1 mg/L, sonicated and analyzed by ICP with and without digestion. In this test, the digested and undigested samples were simultaneously analyzed by Malvern Zetasizer for nanoscale particles distribution and count rate. A high particle count rate would indicate that the nanomaterials were not digested well and may explain the poor recovery. The results from these analyses are shown in Table 4.12. The data indicated that approximately 19 and 42% of nanosilver were recovered in the undigested and digested samples. Furthermore, a large photon count rate (a surrogate for nanoscale particle count) was obtained in the undigested samples. However, the count rate decreased significantly (38 kilo counts per second (kCPS), which is the approximate particle count for many drinking water samples) in the digested samples, which indicated that most of the nanosuspended silver particles were indeed digested. A poor recovery of the nanosilver in these digested samples pointed to the

difficulty of analyzing the nanosilver in our studies. It is possible that some of the nanosilver precipitated out of the solution and was not captured for analyses. Finally, matrix spike analyses were performed by spiking 0.5 mg/L of ionic silver standard in the diluted nanosilver stock. Analyses of the spiked samples yielded silver recoveries of 92 to 102% (Table 4.13). This indicated that the problems encountered with silver analysis were primarily caused by the nanosilver components rather than other constituents in the stock solution.

Table 4.12. Percent Silver Recovery and Photon Count Rate of Diluted Nanosilver Stock

	Undigested Sample	Digested Sample
Anticipated Concentration	1	1
Measured Concentration	0.19	0.42
% Recovery	19%	42%
Photon Count Rate (kCPS)	3175	38

Table 4.13. Matrix Spike Analyses Data for Nanosilver (FTmS-A)

Sample	Nanosilver Conc. Before Spike (mg/L)	Conc. of Ag Std Added (mg/L)	Conc. After Spike (mg/L)	% Recovery
1	0.42	0.5	0.93	102%
2	0.39	0.5	0.85	92%

Table 4.14 summarizes evaluation of 10 mg/L nanocopper stock with and without digestion, using Hach Bicinchoninate Method (Method #8506). DLS analyses were also performed on the samples. The undigested samples yielded a low recovery of copper (16%). Furthermore, the photon count rates of these samples were significantly higher (320 kCPS), indicating the presence of a large number of nanoscale suspended particles. The acid-digested samples, however, yielded approximately 95% recovery. Furthermore, the photon count rate of the sample was significantly low (27 kCPS), indicating dissolution of the copper nanoparticles.

Table 4.14. Percent Silver Recovery and Photon Count Rate of Diluted Nanocopper Stock

Sample	Measured Concentration (mg/L)[a]	Photon Count Rate (kCPS)[b]
Ionic copper	9.55 (95.5%)	23.9
Nanocopper without digestion	1.6 (16%)	320
Nanocopper after digestion	9.5 (95%)	27

[a] Values in the parentheses indicate percent recovery.

[b] The samples were diluted with MilliQ water (1:10) prior to DLS analyses.

4.8 Summary of Nanomaterials Characterization and Analyses

The data from the efforts to analyze nanomaterials in stock suspensions are summarized as follows:

- Compared to manufacturer-indicated concentration, a good recovery (90% or more) of nanozinc oxide was observed using ICP analyses even without predigestion of the samples.

- Nanocopper samples required acid predigestion for recoveries above 90% of the manufacturer-indicated concentrations.

- ICP analyses of nanosilver used in this study continued to yield concentrations significantly lower than those indicated by the vendor even after sample preparation by acid digestion. Hence, it was difficult to make meaningful inference from the subsequent fate and removal tests using nanosilver.

- The nanoscale particle size distribution and photon count rate data from DLS analyses complemented ICP data for nanocopper oxide and nanosilver well. The photon count rates of the undigested copper and silver samples were much higher than those of the acid-digested samples. The copper and silver concentration of the undigested samples measured by ICP was lower than those of the acid-digested samples. The photon count rate can be a measure of the amount of nanoscale suspended particles in the samples. It appears that acid digestion facilitates dissolution of nanocopper and silver samples resulting in a higher recovery (i.e., measured concentration) during ICP analyses and a lower photon count rate during DLS analyses.

- Primary particle size of the nanomaterials measured in the lab using SEM analyses was larger than that specified by the vendors. Note that the SEM and other in-house characterizations of the nanomaterials were performed after almost all of the fate and transport studies were completed (i.e., nearly 2 years after the material procurement). Such long storage time can potentially alter the characteristics of nanomaterials.

Based on these observations, all the zinc oxide nanomaterials analyzed by the OCSD were analyzed without predigestion. The zinc oxide samples analyzed at UCI laboratories (most of

the column studies) were analyzed after predigestion of the samples. All of the nanocopper and silver samples were analyzed after predigestion in our study.

Chapter 5

Removal of Nanomaterials in Wastewaters

This chapter presents and discusses data from studies performed to evaluate removal of nanomaterials in wastewaters. Nanocopper and zinc oxide were equilibrated in unfiltered or filtered (0.45 µm) activated sludge samples (100 mL in 250 mL flasks) from the OCSD wastewater treatment plant. After equilibration, the supernatant samples were collected and filtered again using 0.45 µm filters prior to analysis. For select samples, the unfiltered supernatants were also analyzed for metals concentration. Parallel tests were performed using ionic salts. The supernatant samples were analyzed for concentration of metals by ICP and the nanoscale particles distribution and levels by DLS techniques. Furthermore, precipitates from select samples were analyzed by SEM to evaluate the nature of the precipitated solids.

5.1 Analyses of Metals Concentrations

Figure 5.1 shows the concentration of nanocopper and nanozinc remaining in the supernatant when equilibrated in the activated sludge filtrates (i.e., biomass-free samples). In these tests, the filtrate samples were spiked with approximately 10 mg/L of nanocopper (CuNP), nanozinc (ZnO-A, ZnO-B, ZnO-C), or copper/zinc salts. The supernatant samples were collected after equilibration and filtered again. The percentage of copper or zinc remaining in the filtrate is shown in the text box above the bars. The removal of copper or zinc in these studies would represent the fraction removed by an abiotic process such as precipitation or settling.

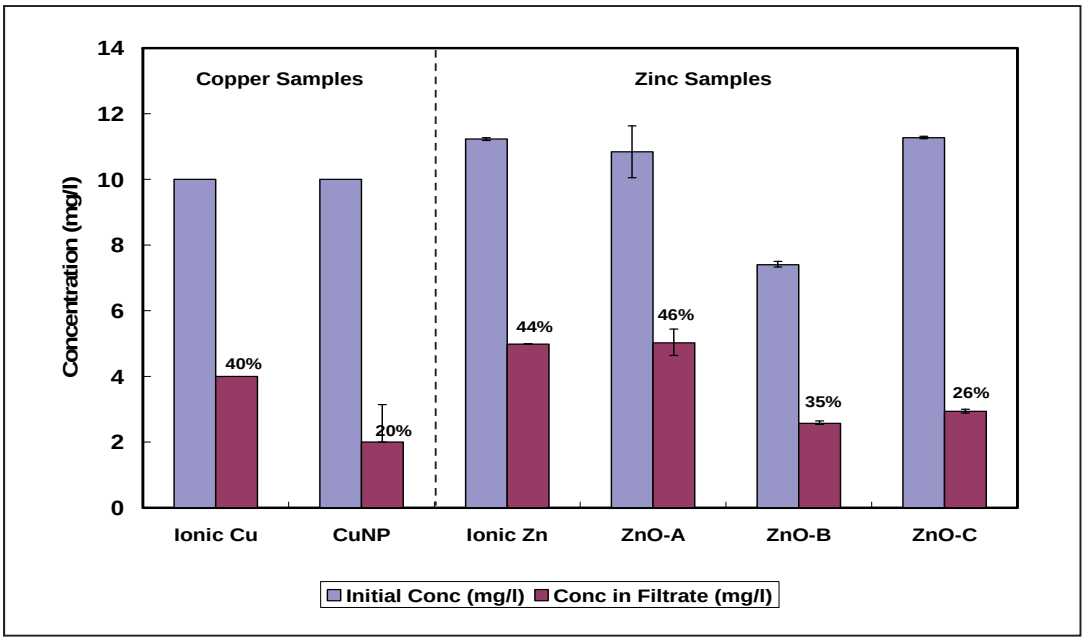

Figure 5.1. Concentrations of ionic copper, nanocopper, ionic zinc, and nanozinc added and that remained in the filtrate after equilibration with filtered OCSD wastewater. The percentage of copper or zinc remaining in the filtrate is shown above the columns.

The data from this test showed some differences between nano and ionic copper as well as copper and zinc removal. For example, compared to ionic copper, nanocopper was removed more effectively in the OCSD effluent. Nearly 40% of the added ionic copper was in the suspension (i.e., approximately 60% was removed), whereas only about 20% of the nanocopper was in suspension (i.e., approximately 80% was removed) in the filtered effluent. Furthermore, copper (nano or ionic) appeared to be more effectively removed than zinc from the wastewater samples. Nearly 44% of the ionic zinc remained in suspension (i.e., approximately 56% was removed) after equilibration. Nanozinc removal varied from 26 to 46% in the effluent. Two nanozinc oxides (ZnO-B, ZnO-C) were removed more effectively than ionic zinc, and removal of one nanozinc oxide (ZnO-A) was not substantially different from ionic zinc. In general, the data from these tests indicate that copper (nano or ionic) is removed more effectively than zinc, and nanomaterials (copper or zinc) are generally removed more effectively than their ionic salts.

Subsequently, an equilibrium speciation model was run using 10 mg/L of zinc (or copper), other inorganic salts at concentrations indicated in Table 3.2, and a final pH of 8 as (approximately) observed in the removal studies. No limitations were imposed on the type of solids to precipitate or to remain in solution or redox conditions. Predictions from equilibrium speciation model (MINTEQ) indicated removal of almost all of the added copper and approximately 81.6% of zinc from solution. The model predicted all of copper to precipitate as tenorite (CuO) and 81.6% of the zinc to precipitate as zinc oxide (ZnO) solids (Appendix). The percentage distribution of zinc species in solution included Zn^{2+} (88.8%), ZnOHCl (aq) (2.2%), $ZnOH^{+}$ (6.2%), and $ZnCl^{+}$ (1.9%). These predictions pertain to the removal of ionic copper or zinc only. Currently, no information is available regarding the solubility products of nanomaterials. The higher removal of copper compared with that of zinc observed in this

study is consistent with the model-predicted trends. However, the amounts of copper or zinc removed were less than that predicted by the model. This may be due to the complexation of copper or zinc with the organic materials (which are not included in the model) in the wastewater or because of nonattainment of equilibrium conditions.

The previous studies using zinc samples (initial concentration ~ 10 mg/L) were extended to 7 days to investigate possible redissolution over time. Figure 5.2 shows the zinc levels in the supernatant after 1 and 7 days of equilibration. The data indicated that the ionic and nanozinc did not redissolve; rather, they continued to be removed over the 7-day period. Approximately 26% of the ionic zinc and 12 to 18% of the nanozinc remained in the filtrate after 7 days. These data again indicated that nanozinc was removed more effectively than ionic zinc in the OCSD effluent. Again, the amount of ionic zinc remaining in the solution was higher than the model-predicted concentrations (~ 18.4%).

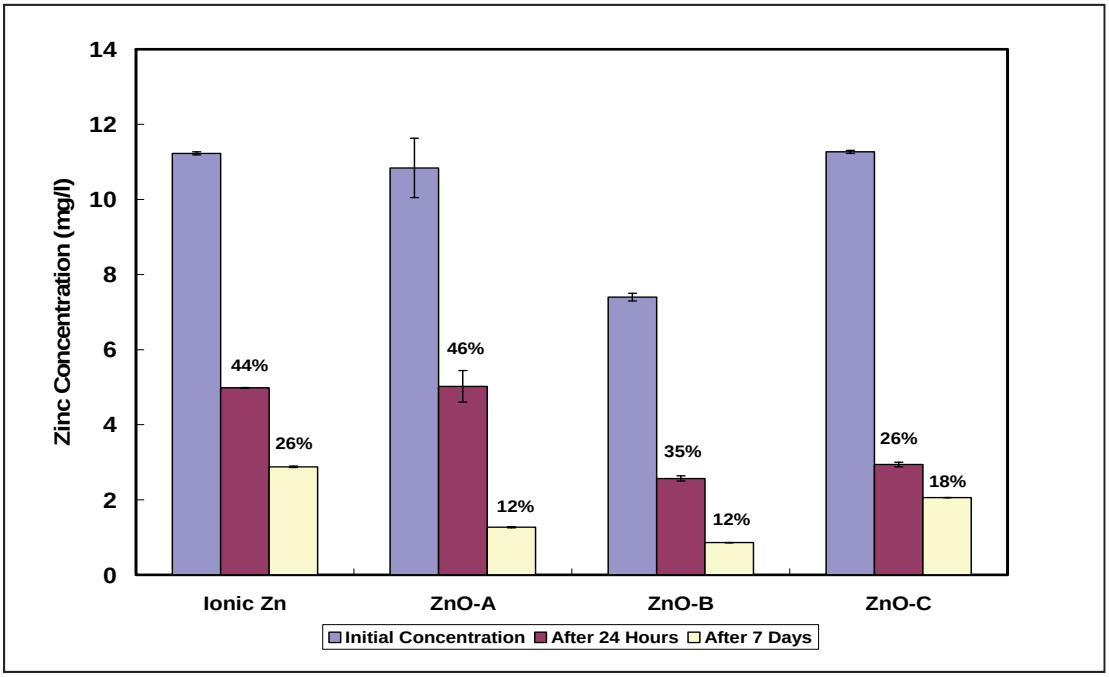

Figure 5.2. Concentration of ionic and nanozinc after equilibration with filtered OCSD effluent for 7 days. Samples were collected after 24 hours and 7 days, filtered, and the filtrate analyzed for zinc levels. The percentage of zinc remaining in the filtrate is shown above the columns.

Figure 5.3 shows abiotic removal when 2 mg/L nano or ionic zinc was added to the activated sludge filtrate. The experimental approach used in this study is similar to that described for 10 mg/L samples (Figure 5.1). The percentage of nano or ionic zinc remaining in the filtrate is shown in the text box above the bars. Only a small fraction of ionic zinc (~ 7%) was removed after 24 hours, whereas approximately 55 to 75% of nanozinc was removed during this period. The amount of ionic zinc precipitated was consistent with that predicted by the speciation model (7.9%). The amount of nanozinc oxide removed was higher than that predicted by the model for ionic zinc. Data from these tests also indicate that nanozinc is removed more effectively than ionic zinc in biomass-free (filtered) wastewaters.

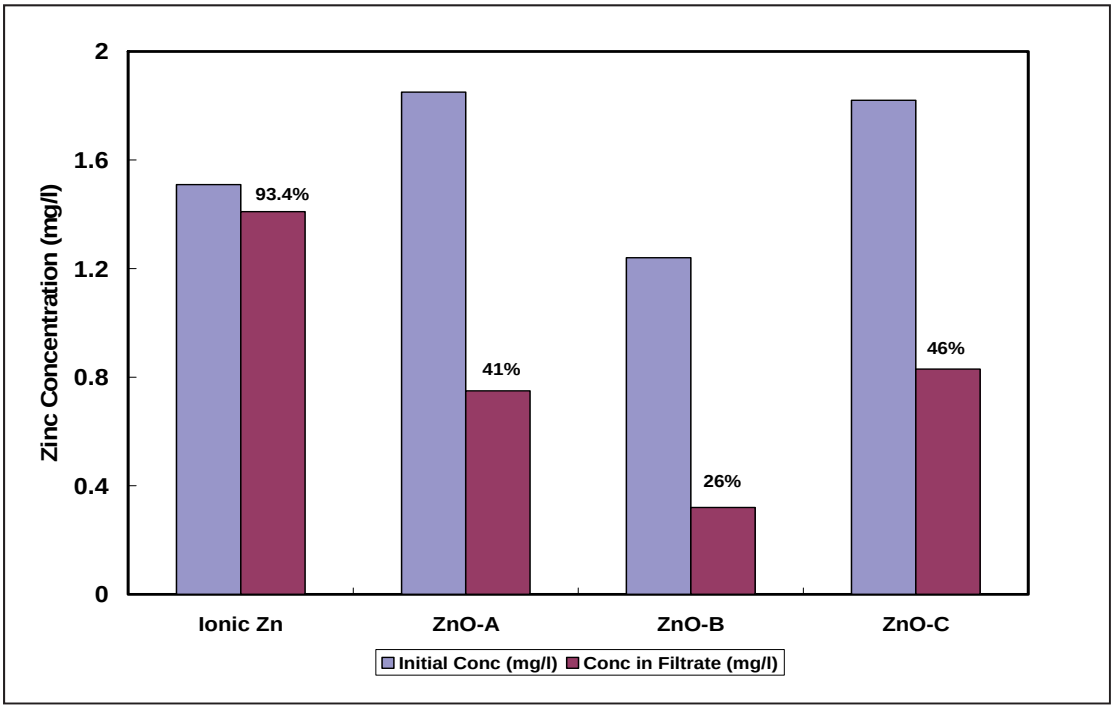

Figure 5.3. Removal of ionic and nanozinc in activated sludge filtrate. Filtered effluent was spiked with 2 mg/L and equilibrated for 24 hours. Equilibrated samples were again filtered, and the filtrate analyzed for copper or zinc levels to estimate abiotic removal. The percentage of zinc remaining in the filtrate is shown above the columns.

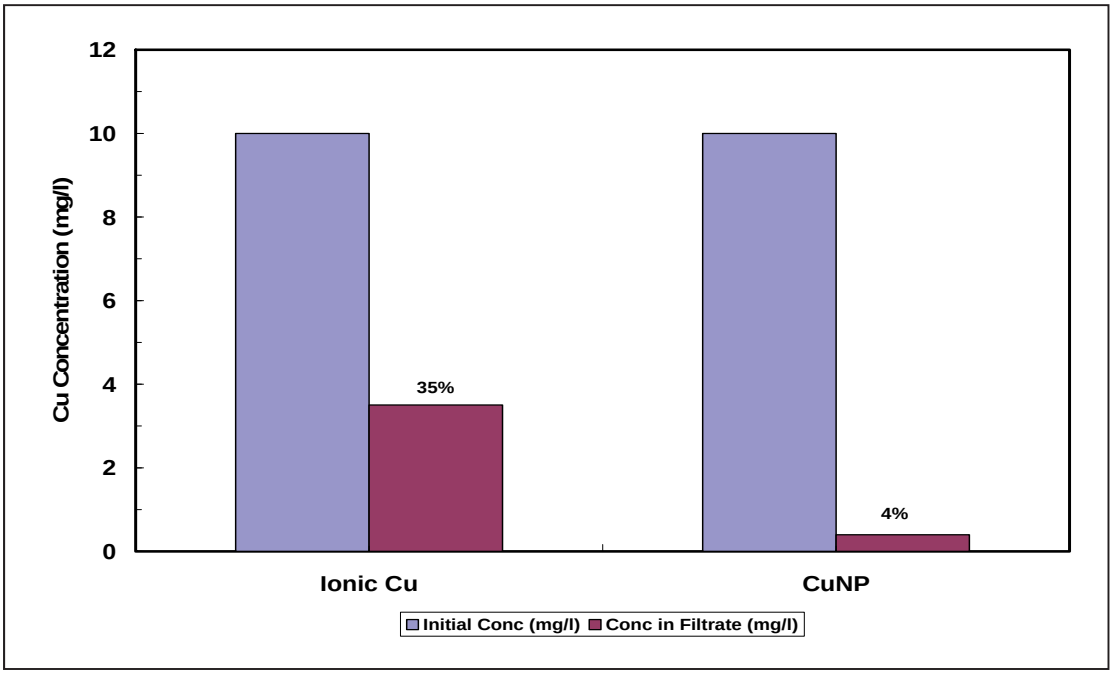

Figure 5.4. Concentration of nano or ionic copper in the filtrate after equilibration with OCSD activated sludge biomass for 24 hours. The percentage of copper remaining in the filtrate is shown above the columns.

Removal of copper and zinc was further investigated in the presence of activated sludge biomass. These tests were similar to the previous tests except that unfiltered activated sludge samples from the OCSD rather than the filtered samples were used. Hence, the removal of copper or zinc from these tests would include the fraction removed by abiotic process (e.g., precipitation, settling) and that removed by biosorption. After equilibration, supernatant samples were collected and filtered prior to analyses. Figure 5.4 shows the removal of nano and ionic copper in the presence of biomass. The data indicated an additional 5% removal of ionic copper and 15% removal nanocopper removal in the presence of biomass. Even in the presence of activated sludge biomass, the extent of nanocopper removal was higher than that of ionic copper.

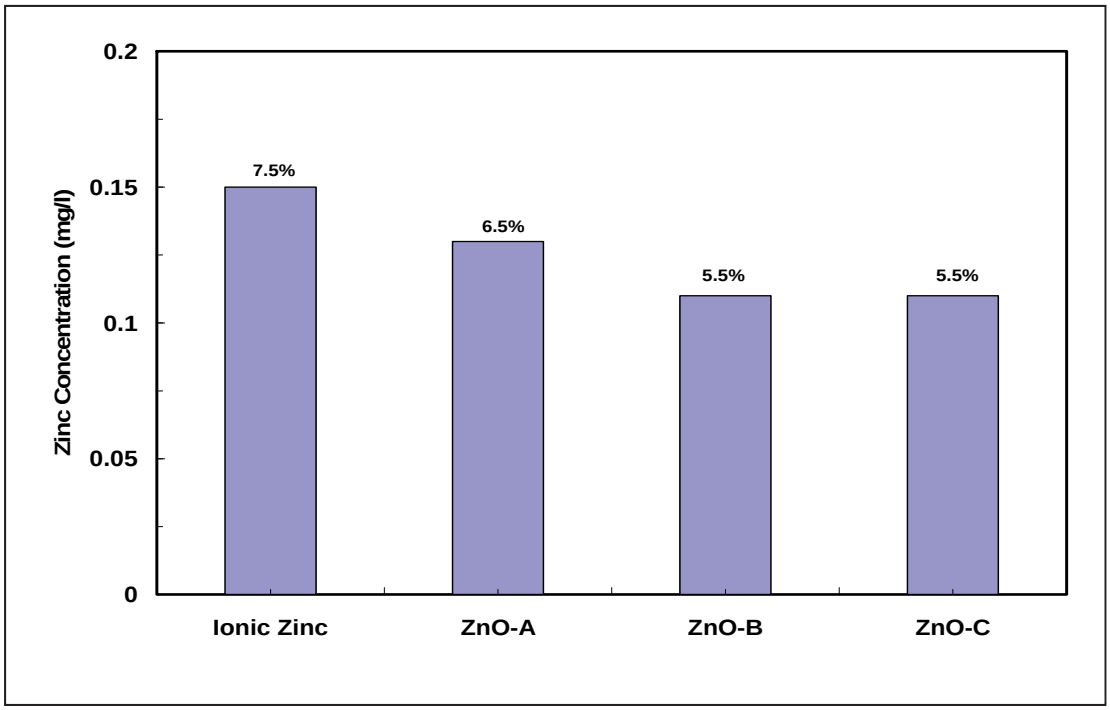

Figure 5.5. Concentration of nano or ionic zinc in the filtrate after equilibration with OCSD activated sludge biomass (MLSS ~ 600 mg/L) for 24 hours. The percentage of zinc remaining is shown above the columns.

Figure 5.5 shows the removal of nano and ionic zinc in the presence of activated sludge biomass. The data indicate that more nanozinc oxide or ionic zinc was removed in the presence of biomass than in the filtered effluent (Figure 5.3). Even in the presence of biomass, the extent of nanozinc removal was slightly higher than that of ionic zinc.

Limited tests were performed to evaluate removal (2 mg/L) of nanosilver in the wastewater. The filtrate samples contained less than 10 % of the added silver. This is consistent with the model-predicted removal of approximately 95.6%. However, the difficulties encountered in nanosilver analyses (Chapter 4) rendered interpretation of the silver data difficult.

5.2 DLS Analyses of Filtrate Samples

Filtered and unfiltered wastewater samples were analyzed by Malvern Zetasizer to evaluate particle size distribution and count (measured as photon count rate). Figure 5.6 shows the particle size distribution in the filtrate samples spiked with 2 or 10 mg/L of ionic or nanocopper after equilibration.

The control samples (not spiked with nano or ionic copper) had the smallest suspended particle size distribution measured as hydrodynamic diameter. The mean particle size for the suspended samples in the filtrate was about 50 nm. The particle size range of the samples spiked with nanocopper was significantly larger than those of the control samples. The average particle size for these samples was approximately 110 nm (range 60 to 300 nm). This indicated that the residual nanocopper in these samples aggregated to this size range in the wastewater samples. The particle size distribution in the ionic copper spiked samples appears to follow a different trend. At a lower residual copper concentration (1.5 mg/L, initial spike of 2 mg/L) the particle size distribution was in the 50 to 100 nm range, with an average particle size of about 60 nm. However, in the filtrate with a higher residual copper (~ 4 mg/L, initial spike of 10 mg/L) the particle size distribution shifted to a range of 70 to 250 nm with an average particle size of about 105 nm. The reasons for this increase of the particle size are not currently known. Formation of colloidal copper or complexation with organic matter in the wastewater may have resulted in an increase in the hydrodynamic diameter of the ionic copper materials.

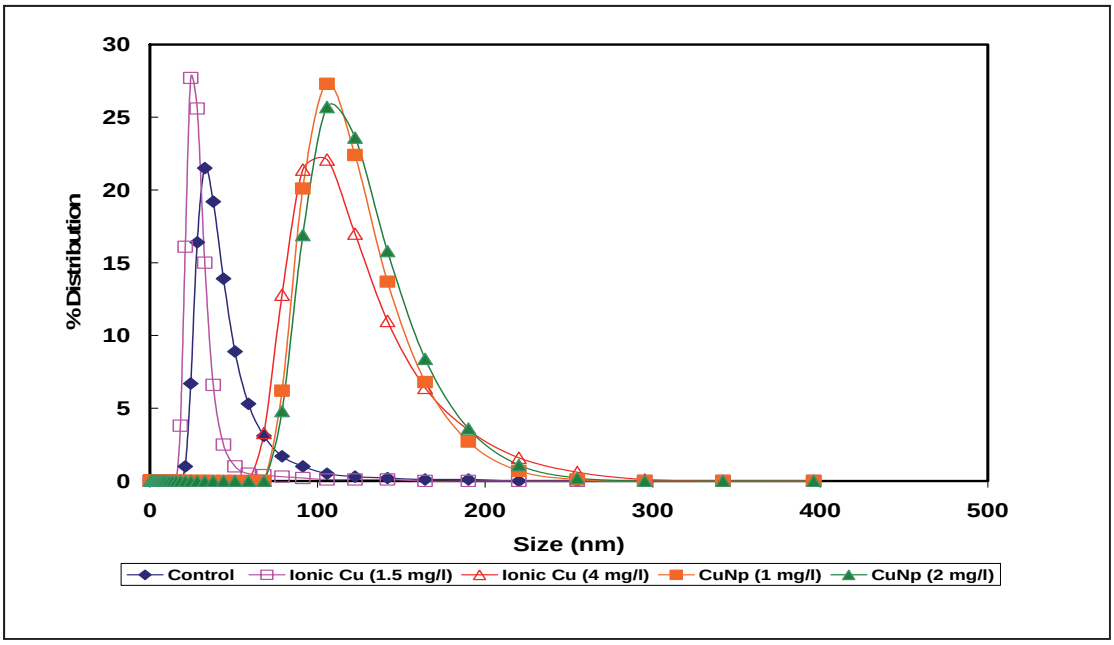

Figure 5.6. Nanoscale particle size distribution of activated sludge filtrate spiked with ionic or nanocopper, after equilibration for 20 hours and filtration. The legend also shows the residual copper concentrations in the filtrate samples.

Figure 5.7 shows the photon count rate measured as a surrogate for number of particles in relation to the residual copper concentration in the filtrate samples (Smeraldi et al., 2012). The data indicated that the particle count rate increased with residual copper concentration for

both ionic and nanocopper spiked samples. However, in general, even at lower residual copper concentrations the particle count rates of nanocopper-spiked samples were higher than those in the ionic copper filtrates. The data appeared to indicate that while some of the ionic copper residuals form colloidal species or complex with organic substances, they were smaller in number compared to particles in the nanocopper suspensions.

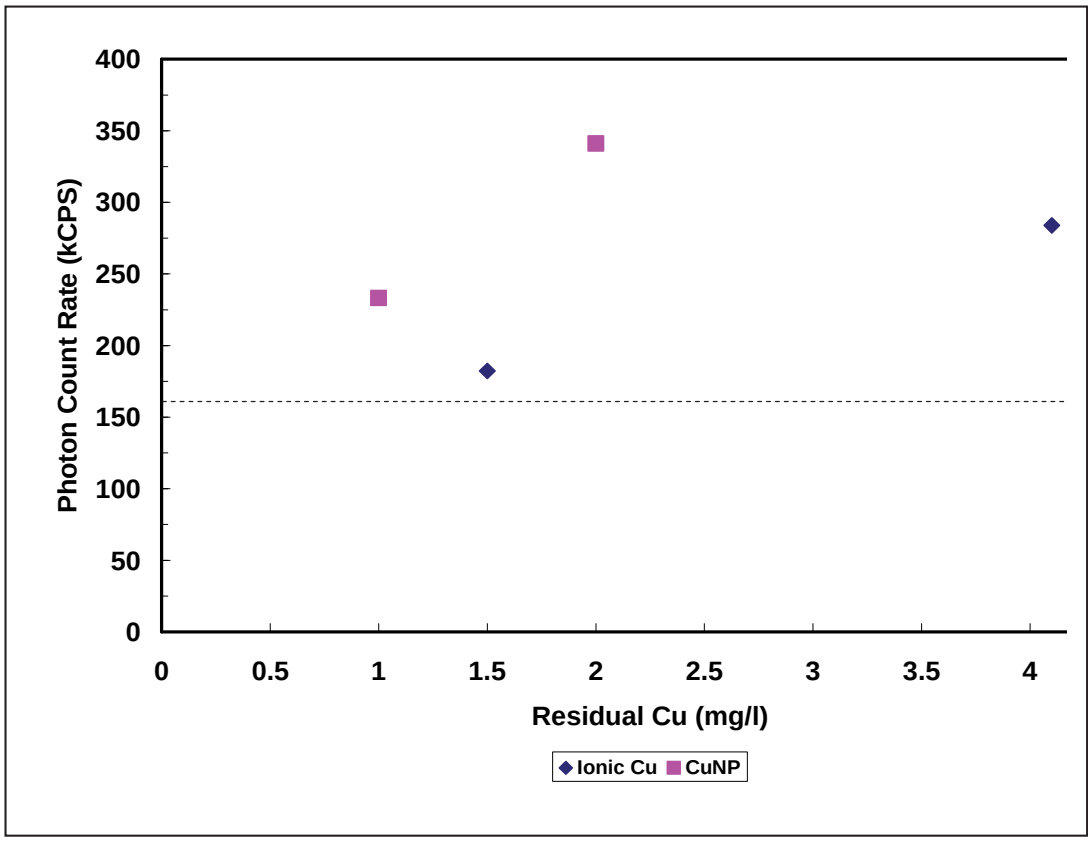

Figure 5.7. Photon count rate and residual copper concentration in the filtered supernatant. The dotted line shows the particle count of the control samples.

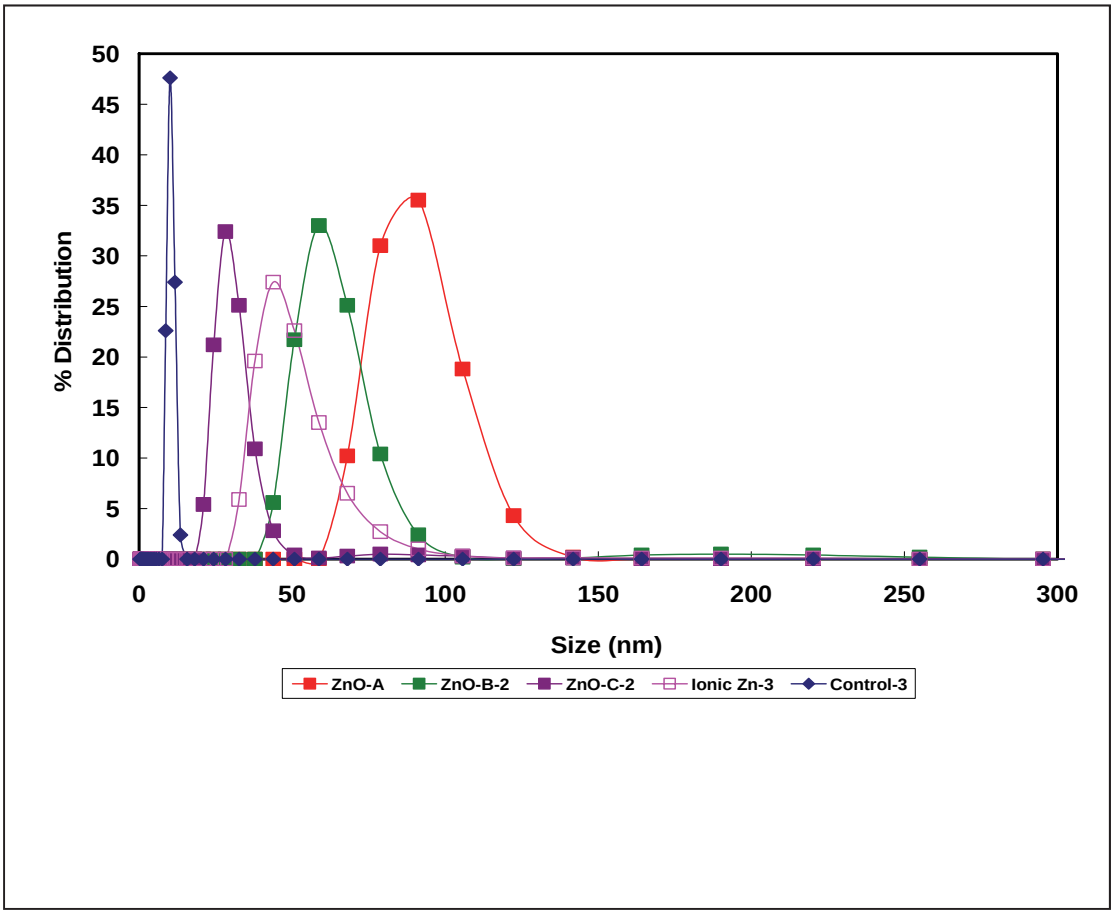

Figure 5.8. Nanoscale particle size distribution of activated sludge filtrate spiked with ionic or nanozinc, after equilibration for 20 hours and filtration.

Figure 5.8 shows the particle size distribution of the filtrate of the ionic- and nanozinc-spiked samples after equilibration. The general trends in the DLS data for ionic and nanozinc were similar to those observed with copper samples. The control sample had an average particle size of about 10 nm. The average particle size of the three different nanozinc-spiked samples varied from 30 to 90 nm. The average particle size for the ionic zinc-spiked samples was about 45 nm. The photon count rate data (Figure 5.9) appears to indicate that based on residual zinc levels, the concentration of nanoscale-suspended particles in nanozinc-spiked samples was higher than that in ionic zinc-spiked samples.

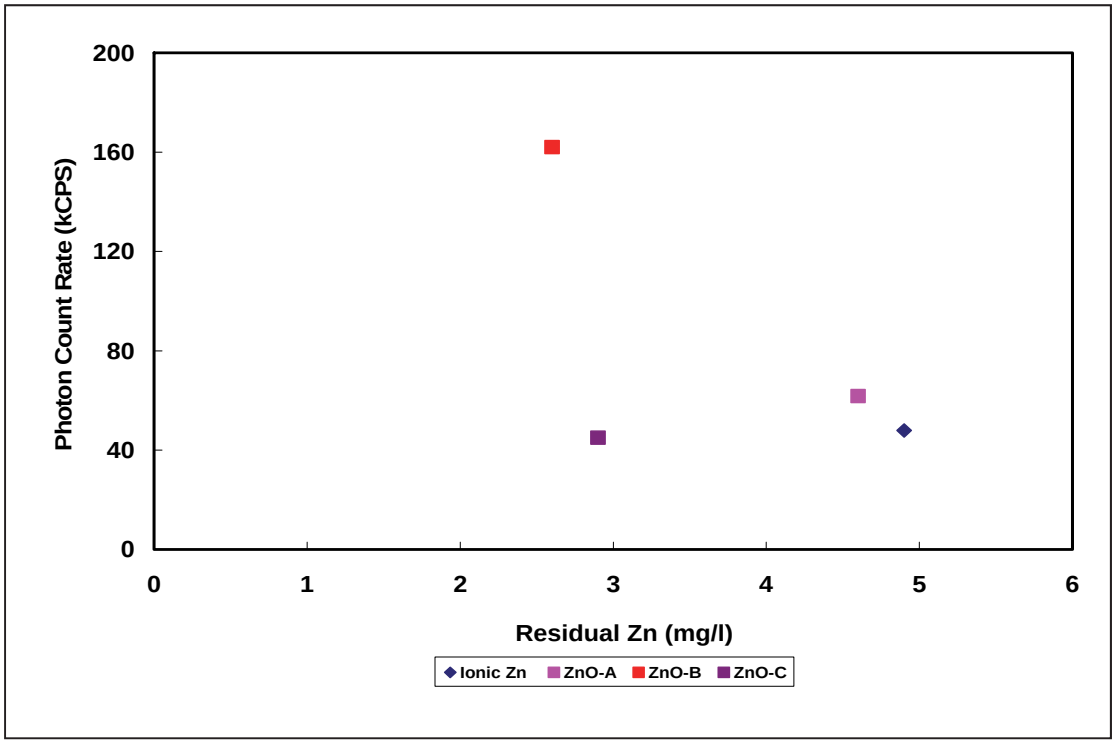

Figure 5.9. Photon count rate and residual zinc concentration in the filtered supernatant.

The differences in the trends observed in the particle size distribution as well as particles count rate indicated that the ionic and nano materials undergo different transformations in the wastewater samples prior to their removal.

5.3 SEM Analyses of the Precipitates

An aliquot of the ionic- and nanomaterials-suspended samples from the equilibration studies were filtered by 0.2 µm nuclepore filters and analyzed by SEM using a Ziess EVO scanning electron microscope. Figure 5.10 shows the SEM pictures of ionic and nanocopper (initial concentration 10 mg/L) immediately after introduction and after 4 hours of incubation in the filtrate. The nanocopper and ionic copper particles showed distinctly different morphologies in the two samples. The nanocopper particles appeared to have aggregated to a larger size (> 1 µm) during their removal. Ionic copper precipitated from the wastewater as finer solids completely covering the filter surface. These observations support the hypothesis that the mechanisms governing the removal of nanocopper and ionic copper are different, thus potentially resulting in the differences in the extent of copper removed from the wastewater. It is likely that the differences in the extent of ionic and nanocopper removed from the OCSD filtered effluent and activated sludge samples are due to the different mechanisms of the nano and ionic copper removal from wastewaters. It is likely that the removal of nanomaterials occurred predominantly because of aggregation and settling, whereas the removal of ionic species occurred because of precipitation.

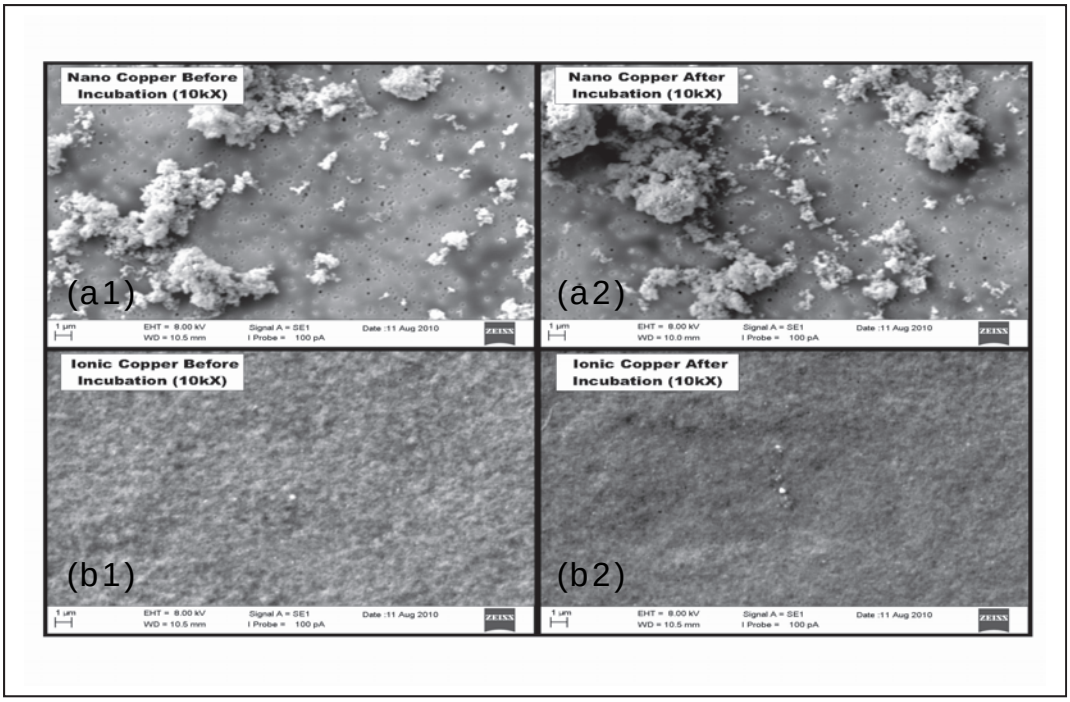

Figure 5.10. SEM of 10 mg/L (a) nanocopper and (b) ionic copper removed by filtration immediately after addition to (a1, b1)and after 4 hours of incubation in wastewater (a2, b2).

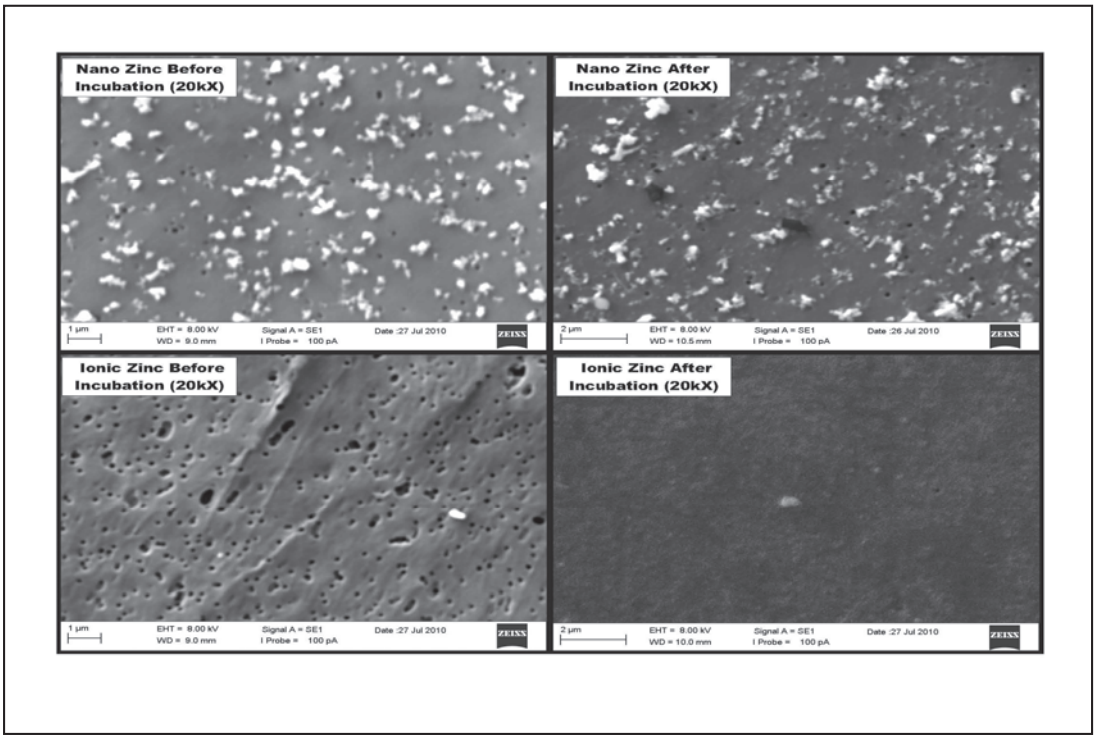

Figure 5.11. SEM of 10 mg/L (a) ZnO-A and (b) ionic zinc removed by filtration immediately after addition to (a1, b1) and after 1 hour of incubation in wastewater (a2, b2).

Figure 5.11 shows the SEM pictures of zinc (initial concentration 2 mg/L) immediately after suspension and after 4 hours of incubation in the filtrate. As observed with copper, the ionic and nanozinc particles showed distinctly different morphologies in the two samples. The nanozinc appeared to have aggregated to larger size particles while ionic zinc precipitated as finer solids. These observations again supported the hypothesis that the mechanisms governing the removal of nanomaterials and ionic salts can be different; therefore, their extent of removal can be different.

5.4 Summary of Nanomaterials Removal Studies

- Results indicated that nanomaterials were removed more effectively than their corresponding ionic salts from the filtered (i.e., biomass-free) OCSD wastewaters.

- More ionic and nanocopper were removed from the wastewater than ionic and nanozinc oxide respectively.

- The higher removal of ionic copper compared to ionic zinc is consistent with the predictions using equilibrium speciation model (MINTEQA2).

- Currently, no information is available on the solubility products for nanomaterials. Therefore, no predictions could be made on their removal using the speciation models. However, the extent of the removal of nanocopper and nanozinc was higher than that predicted for their ionic species.

- The SEM analyses of solids precipitated from nanomaterials (copper, zinc oxide) had distinctly different morphologies than those from ionic copper and zinc suspended samples. The nanozinc oxide or nanocopper appeared to have aggregated to larger size (> 1 μm) during removal. Ionic zinc or copper precipitated from the wastewater as finer solids, completely covering the filter surface.

- Differences in the extent of removal and the morphologies of the removed solids between the ionic and nano forms of zinc oxide and copper support the hypothesis that the mechanisms governing the removal of nano and ionic species are different. It is likely that the removal of nanomaterials occurred predominantly because of aggregation and settling, whereas the removal of ionic species occurred because of precipitation.

- DLS analyses indicated that the filtrate from nanomaterials-added samples contained a higher number of suspended particles than ionic salt-added samples. Furthermore, the average size of the suspended particles was larger in the filtrate from the nanomaterials-added samples.

Removal studies using unfiltered activated sludge (i.e., in the presence of biomass) indicated that compared to studies using filtered wastewater, the presence of biomass increased the removal of ionic and nanozinc oxide by approximately 85 and 35%, and ionic and nanocopper by 5 and 15%, respectively.

Chapter 6

Inhibition of Nanomaterials to Wastewater Microorganisms

6.1 Approach

In these studies, potential inhibitory effects of nanomaterials to wastewater microorganisms were evaluated using the MPN technique. The MPN technique was used to estimate microbial population in a sample as a means to determine inhibitory effects of the constituents in the growth media. The technique does not rely on quantitative assessment of individual cells; instead, it relies on specific qualitative attributes of the microorganism being counted. The methodology for the MPN technique involves dilution and incubation of replicated cultures across several serial dilution steps. This technique relies on the pattern of positive and negative test results following inoculation of a suitable test medium (usually with a pH-sensitive indicator dye). The results are used to derive a population estimate based on the mathematics of Halvorson and Ziegler (1933).

In our current project, the MPN test was performed to evaluate whether introduction of nanomaterials affected the growth of coliform and ammonia oxidizing microbial populations in the OCSD wastewater. Also, the nature of effect (killing of population vs temporary inhibition) was evaluated by monitoring growth of the target microbial population over a period of time after inoculation in the MPN media. The coliform microorganisms were selected because they are the most prevalent group of microorganisms in the wastewaters. The ammonia oxidizing bacteria were chosen because they are often the group that is most vulnerable to toxic upsets.

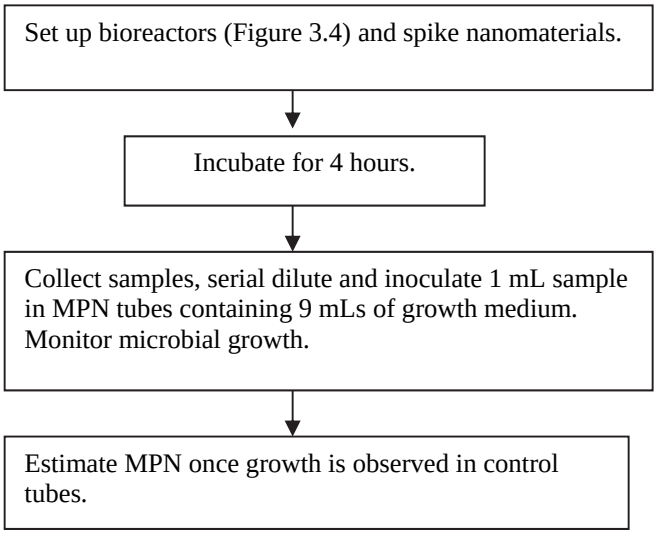

Figure 6.1. Method used for MPN tests using nanomaterials

The composition of media used for MPN tests is described in Section 3. Figure 6.1 shows the procedure used for evaluation of inhibitory effects using MPN tests in this study.

Subsequently, short-term inhibition to wastewater microorganisms that was due to release of nanomaterials was evaluated using respiration rate analyses. The methodology for these analyses is described in Chapter 3. Briefly, respiration rates (i.e., oxygen uptake rate) of the activated sludge samples spiked with 2 mg/L of various nanomaterials or ionic salts were compared with the control samples to evaluate inhibition to microorganisms.

6.2 Inhibition by Nanocopper of Growth of Wastewater Microorganisms

Inhibitory effects to coliform and ammonia oxidizing bacteria were evaluated using 10 mg/L nano or ionic copper. Figure 6.2 shows the results from the MPN studies. Significant growth of coliform bacteria was observed within 24 hours in control (930,000/mL, range 230,000–3,800,000/mL) and copper nanoparticles spiked samples (2,100,000/mL, range 610,000–7, 600,000/mL). Although MPN in nanocopper samples were higher than those for control samples, these were not statistically different at 95% confidence interval (Standard Methods for Examination of Water and Wastewater, 1998). These variations are not uncommon for MPN tests because of various intrinsic and extrinsic variables such as clumping of cells and cell damage (Eisenhart and Wilson, 1943; McBride, 2005). However, the MPNs for ionic copper suspended samples (< 0.3) were significantly lower than that of the control and copper nanoparticles suspended samples (at 95% confidence interval), indicating significant inhibition by ionic copper to coliform bacteria under the test conditions.

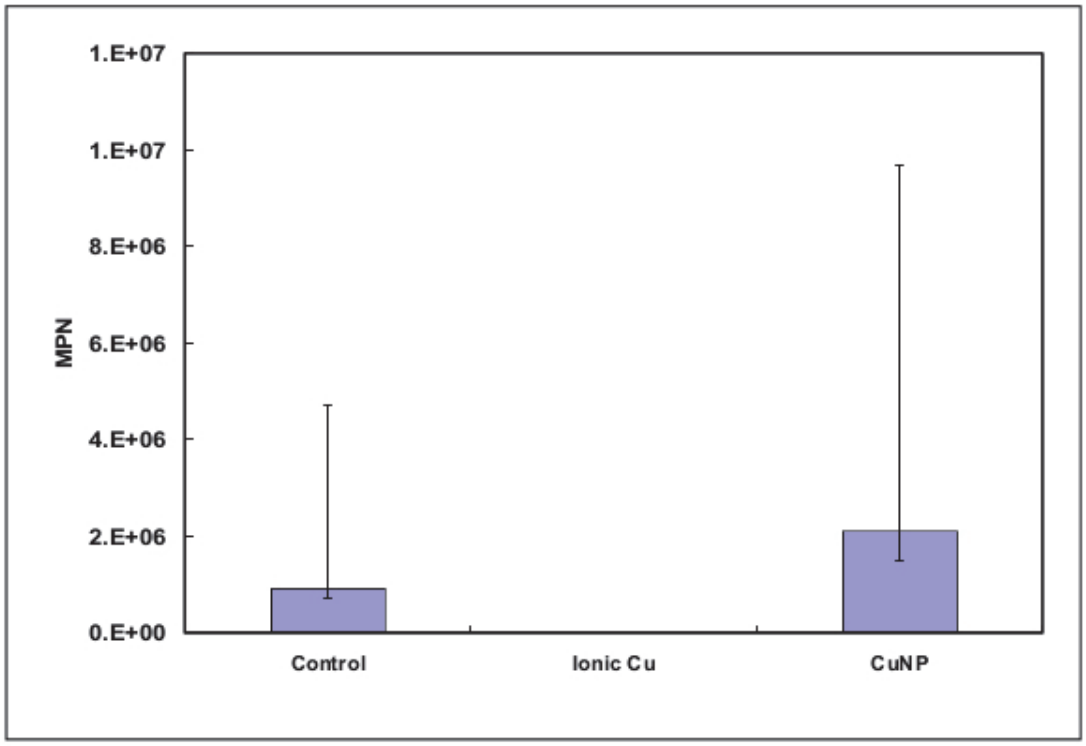

Figure 6.2. MPN data for coliform bacteria in OCSD wastewater spiked with 10 mg/L of ionic or nanocopper. Samples were incubated for 24 hours.

Similar trends were found with MPN data for ammonia oxidizing bacteria also (Figure 6.3). Since the initial ammonia oxidizing bacterial population was low in the OCSD wastewater, nearly 11 days of incubation was required to grow ammonia oxidizing bacteria. As observed with the coliform bacteria, compared to control samples (920/mL, range 210–4,100), the bacterial growth in the samples spiked with copper nanoparticles (920/mL, range 210–4,100) did not vary significantly. However, the growth was significantly lower (55/mL, range 15–200) in the copper ion-spiked samples.

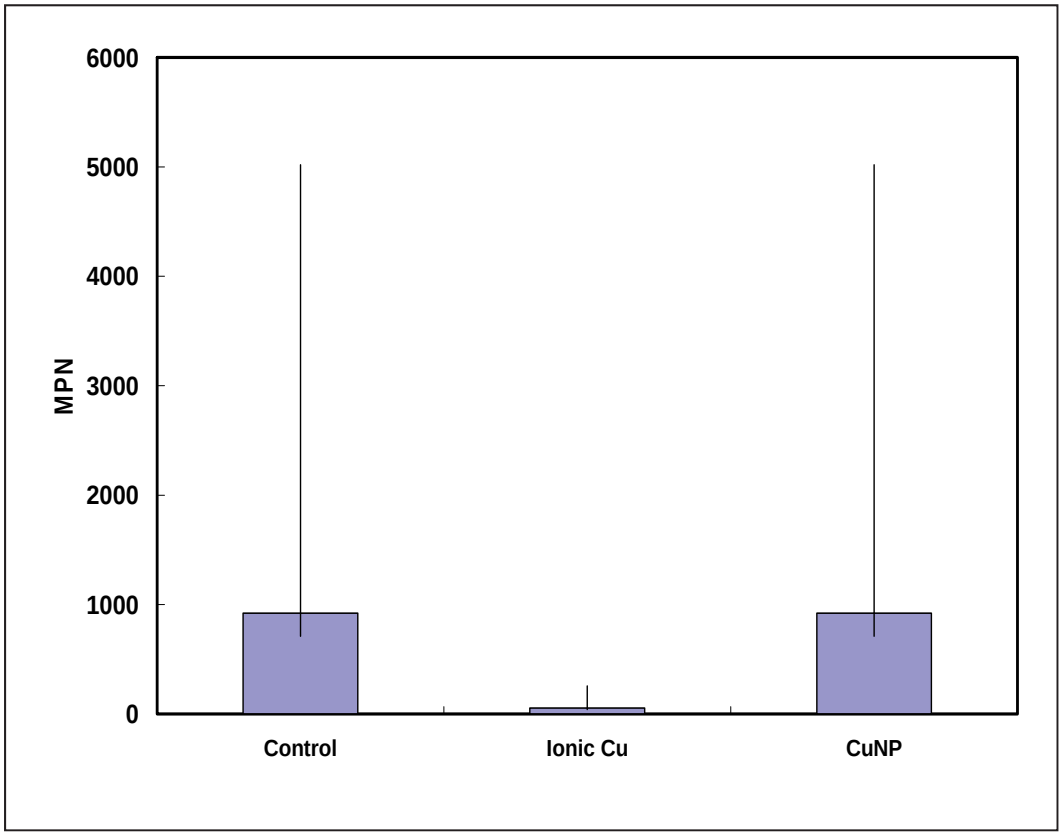

Figure 6.3. MPN data for ammonia oxidizing bacteria in OCSD wastewater spiked with10 mg/L of ionic or nanocopper. Samples were incubated for 11 days.

6.3 Inhibition by Nanozinc Oxide to Growth of Wastewater Microorganisms

MPN tests were performed using ionic and nanozinc oxide at 10 mg/L (coliform bacteria) and 2 mg/L (coliform and ammonia oxidizing bacteria). In general, the inhibitory effects followed a trend similar to that observed using copper. Figures 6.4 to 6.6 summarize the results from the MPN tests. When 10 mg/L zinc was added, significant growth of coliform bacteria was seen in control samples (930,000/mL, range 180,000– 4,200,000/mL) and in the three nanozinc oxide-added samples (ZnO-A: 430,000/mL, range 90,000–4,800,000/mL; ZnO-B: 930,000/mL, range 370,000– 4,200,000/mL; ZnO-C: 430,000/mL, range 90,000–4,300,000/mL) (Figure 6.4). However, the MPN for ionic zinc suspended samples (9,200/mL, range 1,400–38,000/mL) were significantly lower than that of the control and nanozinc oxide suspended samples (at 95% confidence interval), indicating significant inhibition of ionic zinc to coliform bacteria under the test conditions.

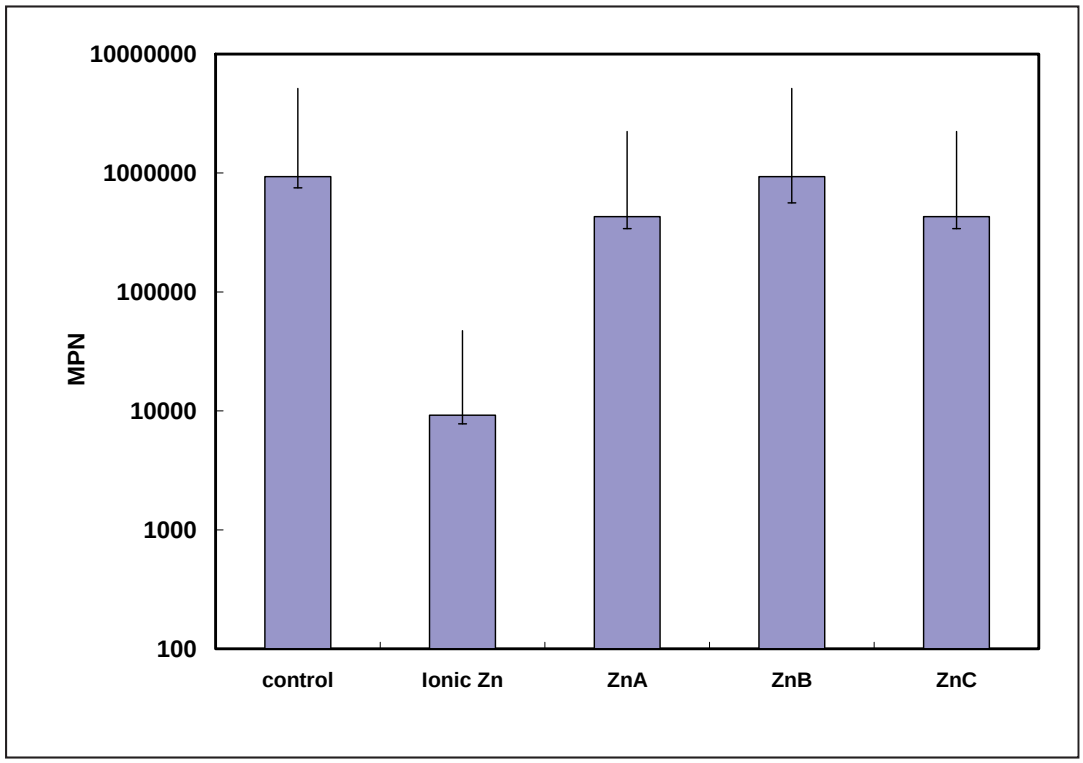

Figure 6.4. MPN data for coliform bacteria in OCSD wastewater spiked with 10 mg/L of ionic or nanozinc. Samples were incubated for 24 hours.

Figure 6.5 shows the MPN data for coliform bacteria at 2 mg/L concentration of nano or ionic zinc. At this lower concentration, coliform bacteria grew well in all of the samples. No significant differences in growth of coliform bacteria were observed among any of the samples (control, nano, or ionic zinc) tested. However, a slightly different trend was observed with ammonia oxidizing bacteria at 2 mg/L zinc concentration (Figure 6.6). After 7 days of incubation, growth was observed in control (48/mL, range 13–170/mL) and nanozinc oxide (ZnO-A: 48/mL, range 13–170/mL; ZnO-B: 48/mL, range 13–170/mL; ZnO-C: 19/mL, range 0.13–1.6/mL) added samples. However, the MPN value for the ionic zinc- added sample (0.46/mL, range 0.13–1.6/mL) was significantly lower. This indicated that even at a dose of 2 mg/L, ionic zinc inhibited the ammonia oxidizing bacteria more than nanozinc oxide. However, after 8 days, significant growth of ammonia oxidizing bacteria was observed in all samples including ionic zinc oxide samples. This indicated that the nature of the observed inhibition at 2 mg/L is not severe.

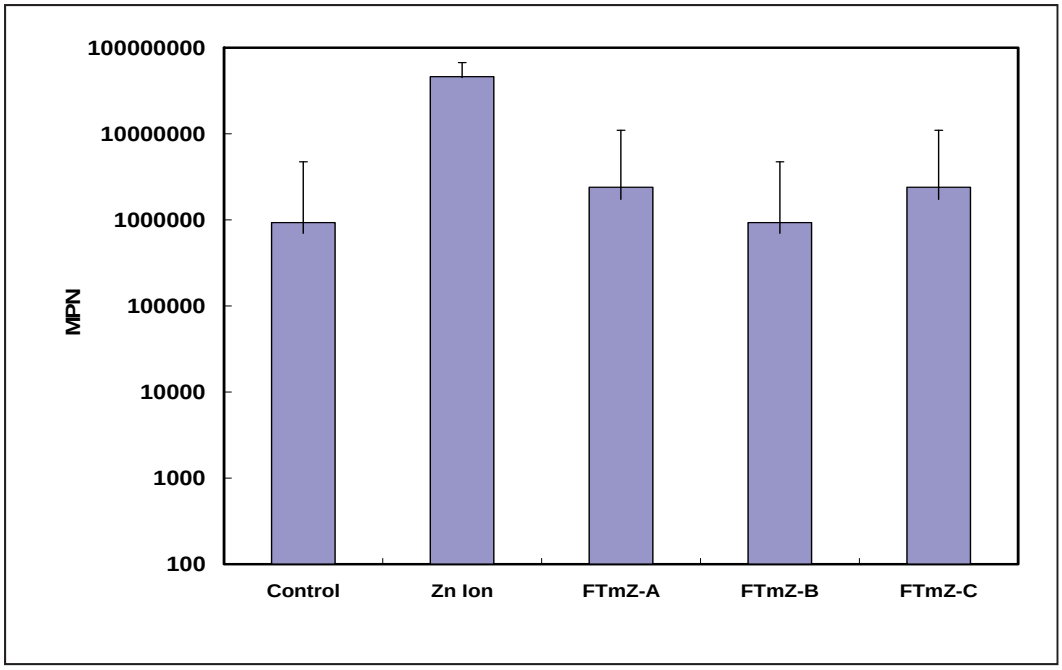

Figure 6.5. MPN data for coliform bacteria in OCSD wastewater spiked with 2 mg/L of ionic or nanozinc. Samples were incubated for 24 hours.

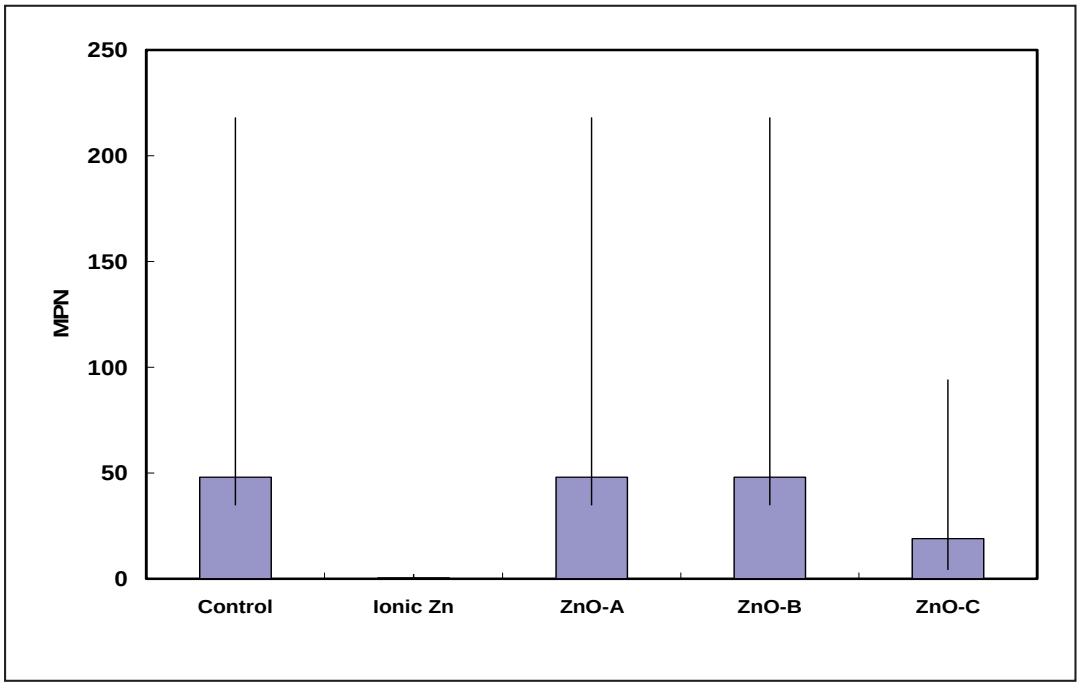

Figure 6.6. MPN data for ammonia oxidizing bacteria in OCSD wastewater spiked with 2 mg/L of ionic or nanozinc. Samples were incubated for 7 days.

6.4 Inhibition by Nanosilver to Growth of Wastewater Microorganisms

MPN tests were performed using ionic and nanozinc oxide at 2 mg/L to coliform and ammonia oxidizing bacteria. Figures 6.7 and 6.8 summarize the results from the MPN tests. At 2 mg/L concentration no significant differences in the MPN data for coliform bacteria were found between control and nanosilver-spiked samples. The growth appeared to be more in the ionic silver-spiked samples. However, the test using ammonia oxidizing medium indicated that one of the nanomaterials (Ag-A) inhibited the growth of ammonia oxidizing bacteria till the 6th day of incubation. No inhibitory effects were observed with ionic silver or nanosilver Ag-C. However, after the 6th day, significant growth of ammonia oxidizing bacteria was observed in all samples, including the Ag-A samples. This indicated that the nature of the observed inhibition at 2 mg/L is not severe, and it was transient in nature.

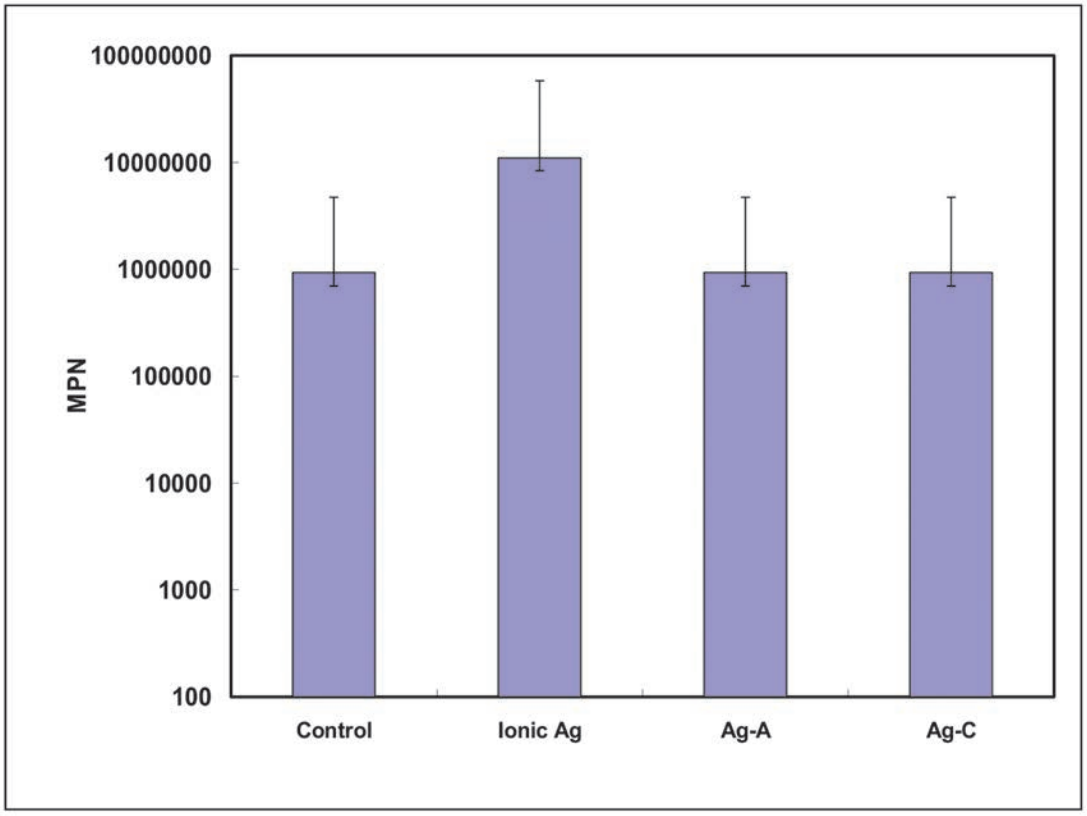

Figure 6.7. MPN data for coliform bacteria in OCSD wastewater spiked with 2 mg/L of ionic or nanosilver. Samples were incubated for 24 hours.

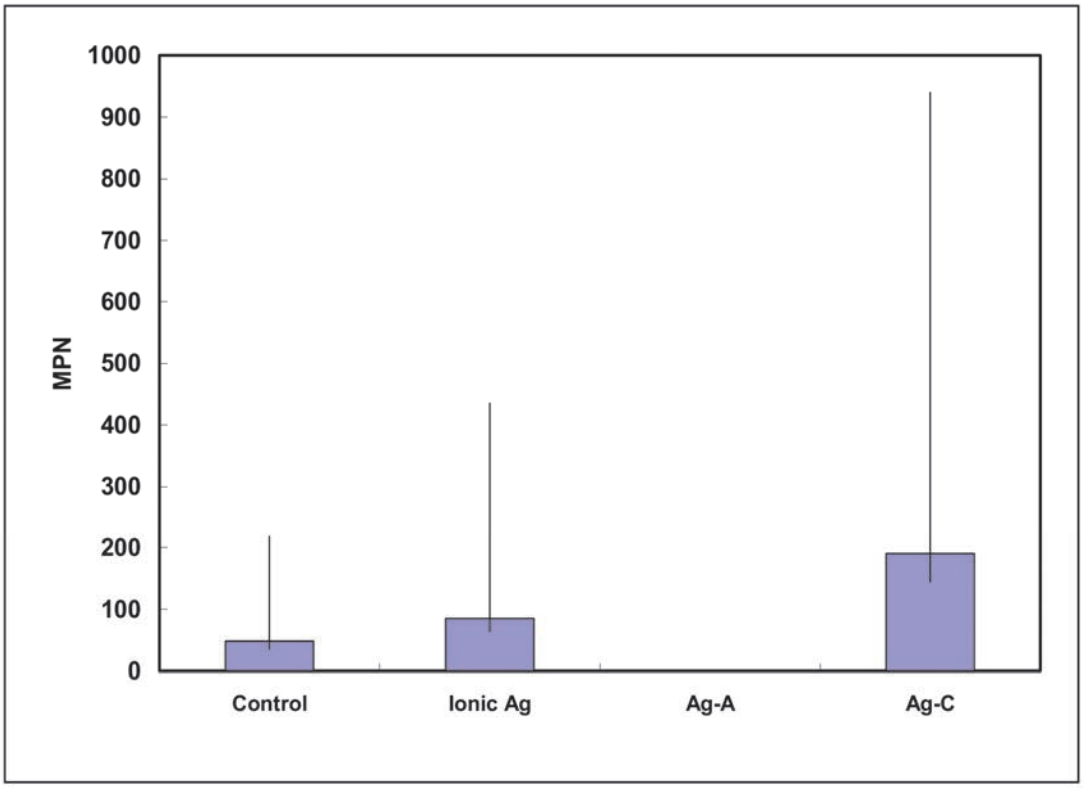

Figure 6.8. MPN data for ammonia oxidizing bacteria in OCSD wastewater spiked with 2 mg/L of ionic or nanosilver. Samples were incubated for 6 days.

6.5 Summary and Discussion

The data indicated that ionic copper or zinc, in general, were more inhibitory to coliform and ammonia oxidizing bacteria in wastewater samples than nanoparticle copper and zinc. The MPN test indicated that at an added concentration of 10 mg/L ionic zinc oxide and copper significantly inhibited the growth of coliform bacteria in the OCSD activated sludge samples. However, no significant differences were observed in the growth of coliform bacteria between the control and nanozinc oxide-or copper-added samples. The addition of 10 mg/L of ionic copper also inhibited the growth of ammonia oxidizing bacteria in OCSD activated sludge. Nanocopper did not inhibit the growth of ammonia oxidizing bacteria.

Lowering the zinc concentration from 10 to 2 mg/L lowered the inhibitory effects of ionic zinc to coliform bacteria in the OCSD activated sludge. However, partial inhibition to ammonia oxidizing bacteria was observed in the ionic zinc-added (2 mg/L) samples, but not in the nanozinc oxide-added samples.

Note that the data from the nanomaterials removal study (Chapter 5) indicated that more nanocopper or zinc oxides were removed than ionic copper or zinc from wastewater samples. It is possible that the inhibitory effects observed in the MPN tests may be due to the presence of a higher concentration of ionic zinc or copper in suspension (i.e., the filtrate samples). As discussed in Chapter 2, literature evidence points to direct toxicity of nanomaterials as well as toxicity occurring through dissolution of nanomaterials. Most of the inhibitory effects

observed in our study (growth of coliform bacteria at 10 mg/L; ammonia oxidizing bacteria at 2 or 10 mg/L) were caused by ionic copper or zinc. This pointed to the toxic effects possibly occurring through dissolution of materials.

Initial inhibition to ammonia oxidizing bacteria was observed in the presence of 2 mg/L nanosilver, but not in the presence of ionic silver. This indicated that nanosilver might be inhibitory to some wastewater microorganisms. However, after the 6th day of incubation, significant growth of ammonia oxidizing bacteria was observed in all samples, including the nanosilver samples. This indicated that the nature of the observed inhibition at 2 mg/L was not severe, and it was transient in nature. Liang et al. (2010) indicated that such toxic effects by nanomaterials are more pronounced in a continuous reactor setup than a batch reactor configuration. Hence, additional investigations are required to document these effects.

Chapter 7

Impact of Process and Operational Parameters During Biological Treatment

7.1 Background

Data from Chapter 6 indicated that although ionic zinc inhibited coliform bacterial growth (10 mg/L) and ammonia oxidizing bacteria (at 2 mg/L), no such inhibition was observed in the presence of nanozinc oxide. Subsequently, additional tests were performed using batch bioreactors to evaluate if any of the process or operational parameters critical to biological treatment processes, such as COD removal efficiency or MLSS concentrations, were affected in the presence of nanozinc oxide or nanosilver. Past studies have shown negative effects on the rate and extent of transformation of these parameters because of release of nanomaterials and other chemicals (Ganesh et al., 1994; Liang et al., 2010).

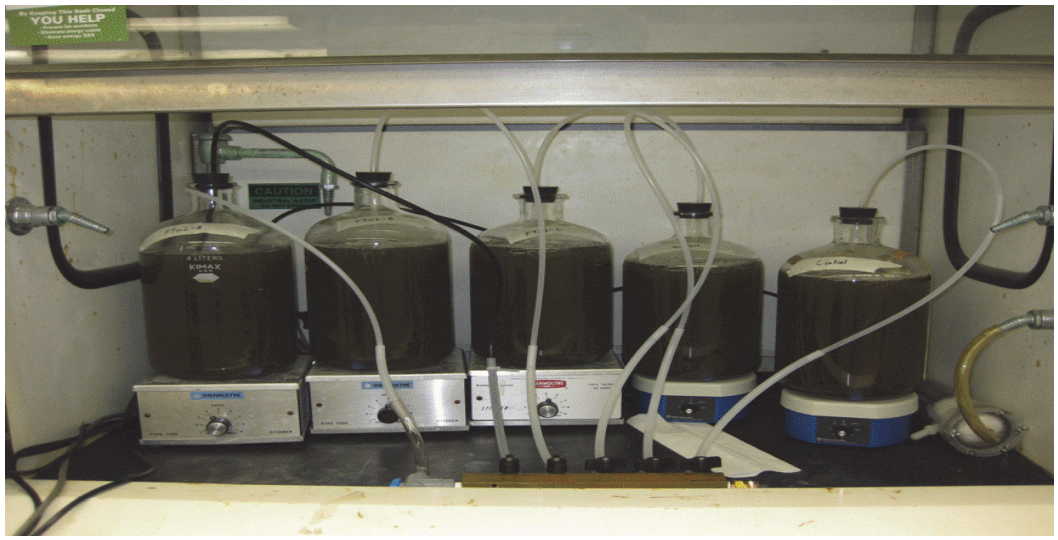

Figure 7.1. Experimental arrangement used for aerobic biological process studies.

Several batch reactors were operated using OCSD activated sludge samples spiked with 2 mg/L of nanozinc oxide (ZnO-A, ZnO-B, ZnO-C) or nanosilver (Ag-A, Ag-B, Ag-C). Figure 3.4 shows the schematic of the bioreactor system and Figure 7.1 shows the bioreactors used in this study. The batch reactor studies performed the parameters analyzed, and the frequency of analyses is shown in Chapter 3 (Tables 3.3 and 3.4). As indicated in Table 3.4, in addition to evaluating process operational parameters, the removal of zinc and silver were also evaluated in these studies. Furthermore, filtrate samples were collected and analyzed for nanoscale suspended particles size distribution and count rate by DLS techniques. Control

reactors with no added zinc or silver and those spiked with 2 mg/L of ionic zinc or silver were also operated. Although the studies performed to evaluate inhibitory effects in Chapter 6 provide the effect of nanomaterials on a specific group of bacteria, the evaluation of parameters in the bioreactor studies yielded information about how the overall microbial community functions because of the release of nanomaterials. The data obtained from the bioreactor studies are discussed in the following subsections

7.2 Effect of Nanomaterials on Organic Degradation

COD analyses were performed to monitor degradation of organic materials in the batch bioreactors. Figure 7.2 shows the COD levels over time in bioreactors spiked with 2 mg/L of ionic zinc or functionalized zinc oxide nanomaterials. The initial COD levels in the bioreactors were about 85 mg/L. Within 4 hours of incubation, the COD levels in all the reactors (including the control and zinc chloride spiked reactors) decreased (presumably biodegraded) to about 40 mg/L. Subsequently, the COD levels increased in all the reactors presumably because of cell lysis. In summary, no significant differences in the COD profile were observed among the control, zinc chloride, and functionalized nanozinc oxide containing reactors. This indicated that at 2 mg/L concentration the functionalized nanozinc oxides used in this study did not significantly inhibit the ability of activated sludge biomass to degrade organic materials (as measured by COD) from OCSD wastewaters. Similar trends in COD degradation were observed using nanozinc oxide with or without functionalization at the concentrations (2 or 0.2 mg/L) used.

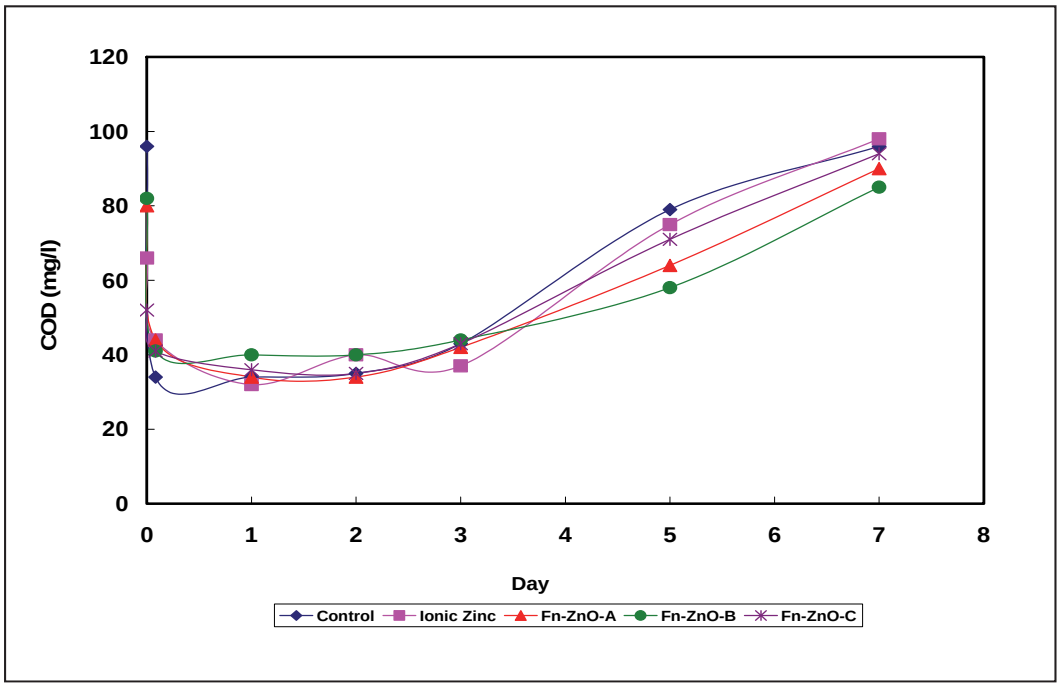

Figure 7.2. COD levels in the bioreactors spiked with 2 mg/L of zinc chloride salt or 3 functionalized nanozinc oxide particles.

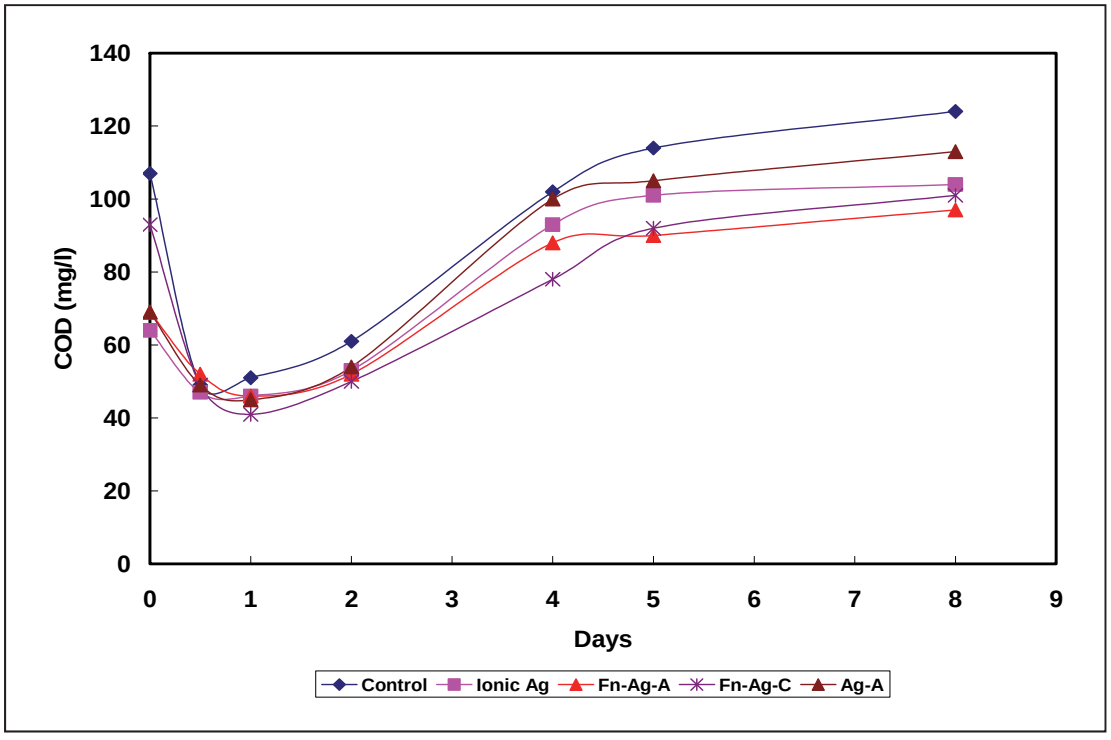

Figure 7.3. COD levels in the bioreactors spiked with 2 mg/L of zinc chloride salt or 3 functionalized nanozinc oxide particles.

Figure 7.3 shows the COD trends in bioreactors spiked with ionic silver and nanosilver with or without functionalization. Similar to that observed in the presence of zinc, the addition of 2 mg/L of nanosilver did not alter the degradation of organic matter (measured as COD) of the activated sludge microorganisms. No significant differences were observed among the control samples, samples spiked with ionic silver, or those spiked with nanosilver. In summary, no significant differences were observed in the degradation of organic materials (as measured by COD) under the test conditions due to the release of zinc oxide or silver nanomaterials used in this study.

7.3 Effect of Nanomaterials on MLSS

MLSS levels were measured to monitor overall biomass concentrations in the bioreactors after the addition of nanomaterials. Figure 7.4 shows the MLSS concentration in the reactors spiked with 2 mg/L of functionalized nanozinc oxide. The initial MLSS level in the bioreactors was approximately 600 mg/L. The MLSS increased slightly (approximately 50 to 100 mg/L) after 24 hours of operation. Subsequently, the MLSS decreased to about 400 mg/L after 7 days. No significant differences were observed between the control and the nanomaterial-containing reactors, which indicated that the observed trends in the MLSS data was not affected by the presence of ionic or nanozinc.

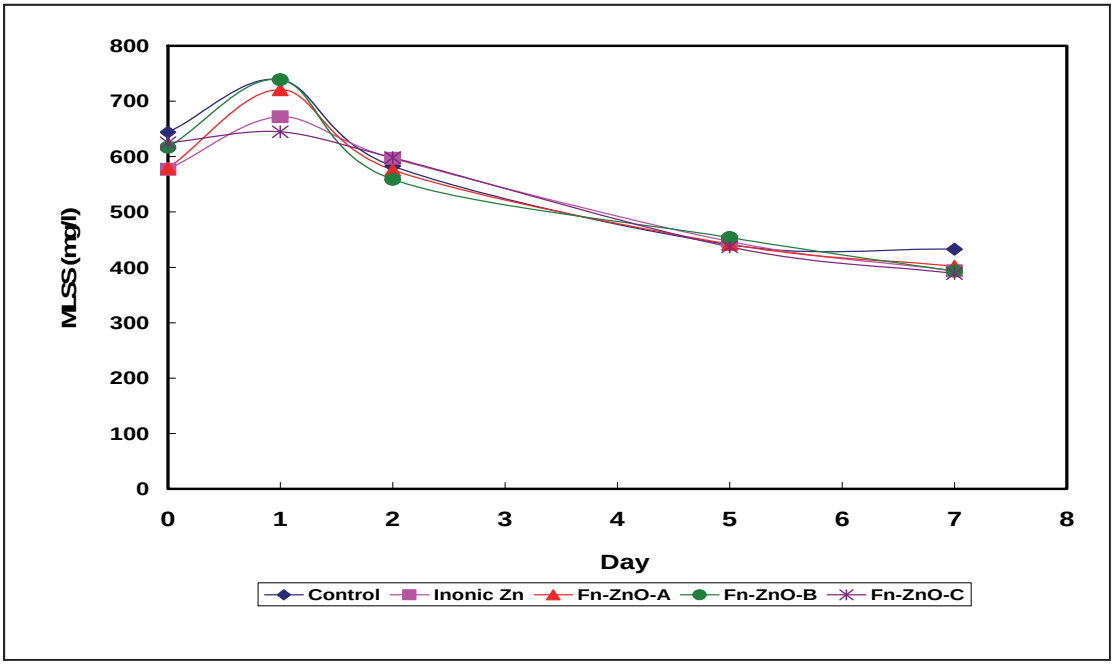

Figure 7.4. MLSS in the reactors spiked with zinc chloride and 3 functionalized nanozinc oxide particles.

Similarly, Figure 7.5 shows the MLSS concentration in reactors spiked with 0.2 or 2 mg/L of nanosilver. No significant differences were observed between ionic silver or nanosilver-spiked samples or between reactors spiked with 0.2 or 2 mg/L nanosilver. There were no differences in the trends observed between the two types of nanosilver.

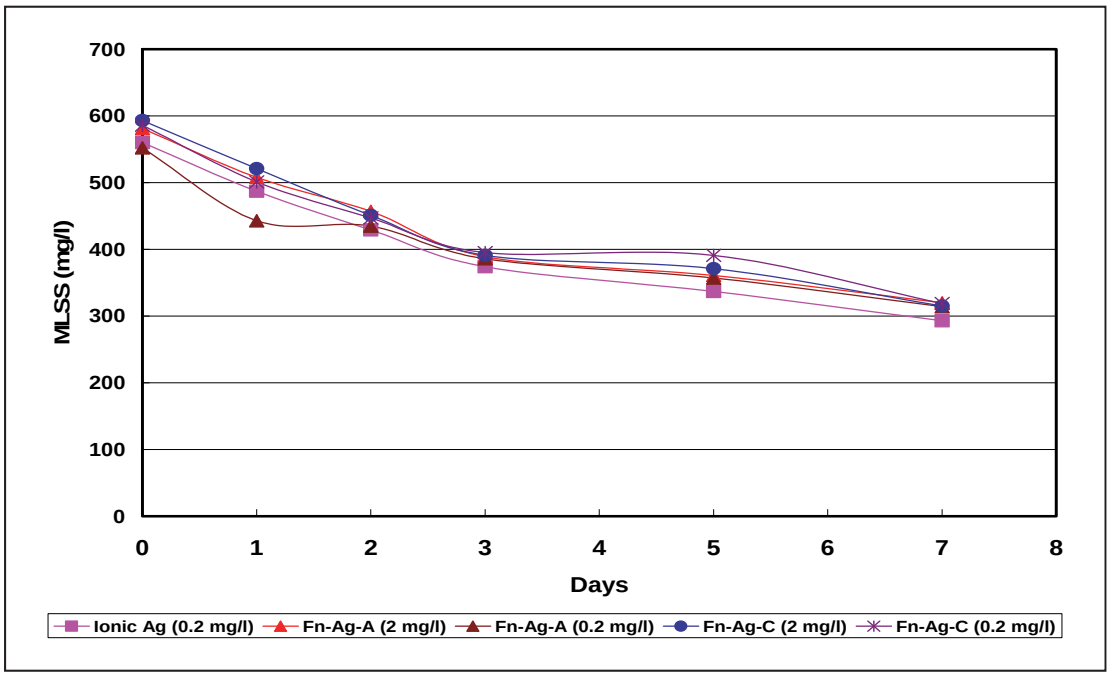

Figure 7.5. MLSS in the reactors spiked with 0.2 mg/L ionic or 0.2 or 2 mg/L nanosilver.

7.4 Effect of Nanomaterials on pH

Figure 7.6 shows the pH profile in the bioreactors spiked with ionic zinc or nanozinc oxide. Figure 7.7 shows the pH profile in the bioreactors spiked with ionic or nanosilver. The initial pH in the reactors varied from 8.3 to 8.5. The pH decreased to approximately 7.4 after 7 days. The decrease in pH during aerobic degradation is anticipated because of oxidation of ammonia to nitrate and whether the alkalinity in the reactors is not sufficient to buffer the system. However, no significant differences in the pH trends were observed among the control and nanomaterial-spiked reactors, indicating that the release of nanomaterials used in this study did not inhibit the collective ability of the microbial community in the bioreactor to oxidize ammonia. Had the nanomaterials affected the oxidation of ammonia, the pH would not have decreased to the same extent as in the control reactors.

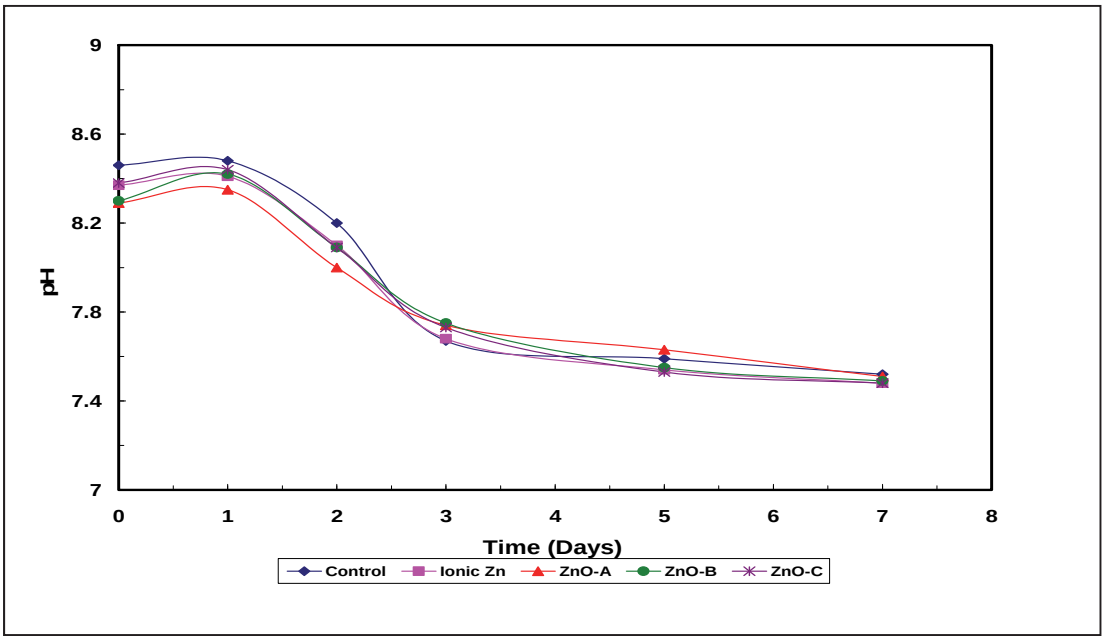

Figure 7.6. pH in the bioreactors spiked with 0.2 mg/L ionic or 0.2 or 2 mg/L nanozinc.

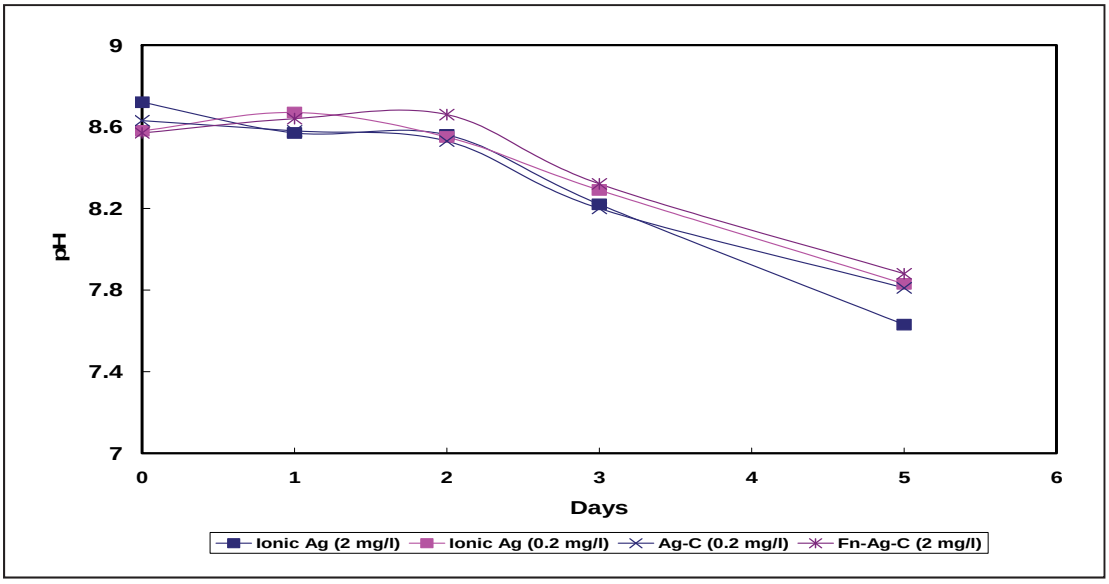

Figure 7.7. pH in the bioreactors spiked with ionic or nanosilver.

7.5 Effect of Nanomaterials on DO, Nitrate, and Ammonia

No significant differences were observed in the DO, nitrate, and ammonia profiles because of the release of nanomaterials. The DO levels in all the reactors remained approximately 2 mg/L over the period of the study. The nitrite levels increased from an initial concentration of approximately 0.02 mg/L to 14 mg/L over 8 days. The nitrate levels increased from approximately 0.02 mg/L to over 2 mg/L during this period. The increase in nitrite and nitrate levels indicated oxidation of ammonia in the reactors. However, no significant differences were observed among the control reactors or the reactors spiked with ionic salts, nanozinc oxide, or silver.

7.6 Removal of Nanomaterials in the Bioreactors

Figure 7.8 shows the zinc concentrations in the filtrate samples from the bioreactors spiked with 2 mg/L of ionic or nanozinc oxide. The data indicated that most of the added zinc (> 90%) aggregated, settled, precipitated, or otherwise removed from the filtrate samples within 4 hours of incubation. The Time 0 samples, which are typically collected within minutes of setting up each reactor, showed a higher level of ionic zinc (~ 1.3 mg/L) than nanozinc (~ 0.2 mg/L) indicating rapid removal of the nanozinc oxide compared to ionic zinc in these samples. These trends are in agreement with the data obtained from the nanomaterials removal studies (Section 5). In general, in all of the batch studies using zinc samples, the Time 0 samples for the ionic zinc reactors contained 20 to 50% higher zinc than the nanozinc oxide-spiked samples.

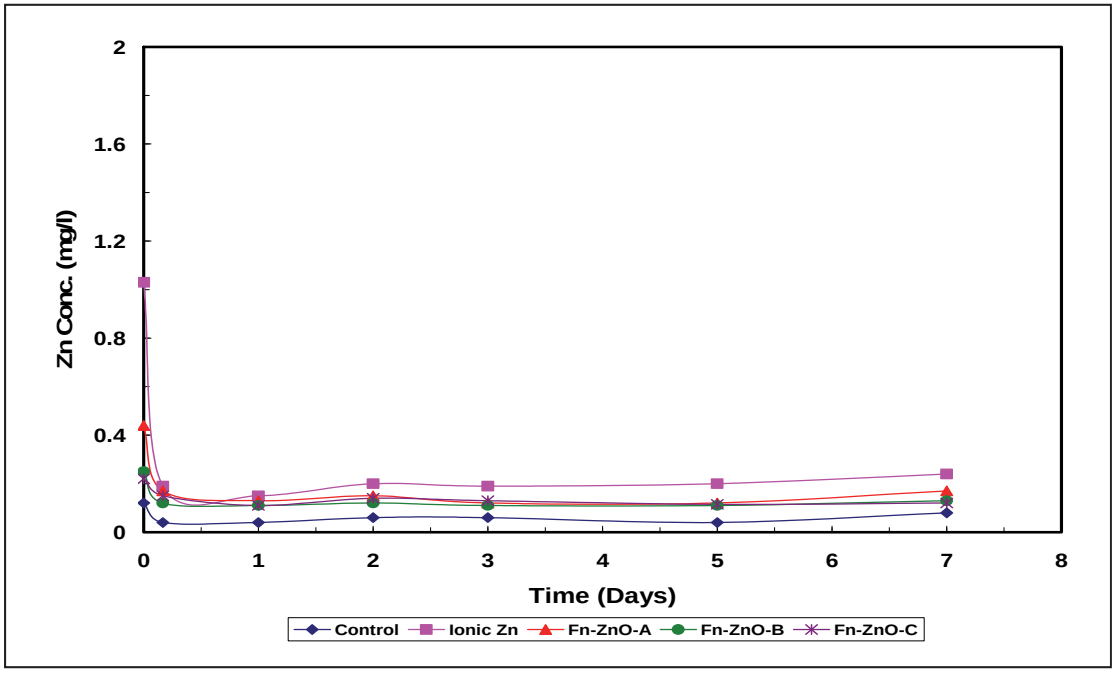

Figure 7.8. Zinc concentrations in filtrate samples in the bioreactors spiked with 2 mg/L ionic or nanozinc.

Figure 7.9 shows silver concentration in the reactors spiked with ionic or nanosilver. Overall, the trends observed with silver removal were similar to those observed with zinc samples. More than 90% of the added silver was removed within 4 hours of incubation. As observed with the zinc samples, the Time 0 samples showed higher levels of ionic silver than nanosilver, which indicated rapid removal of nanosilver.

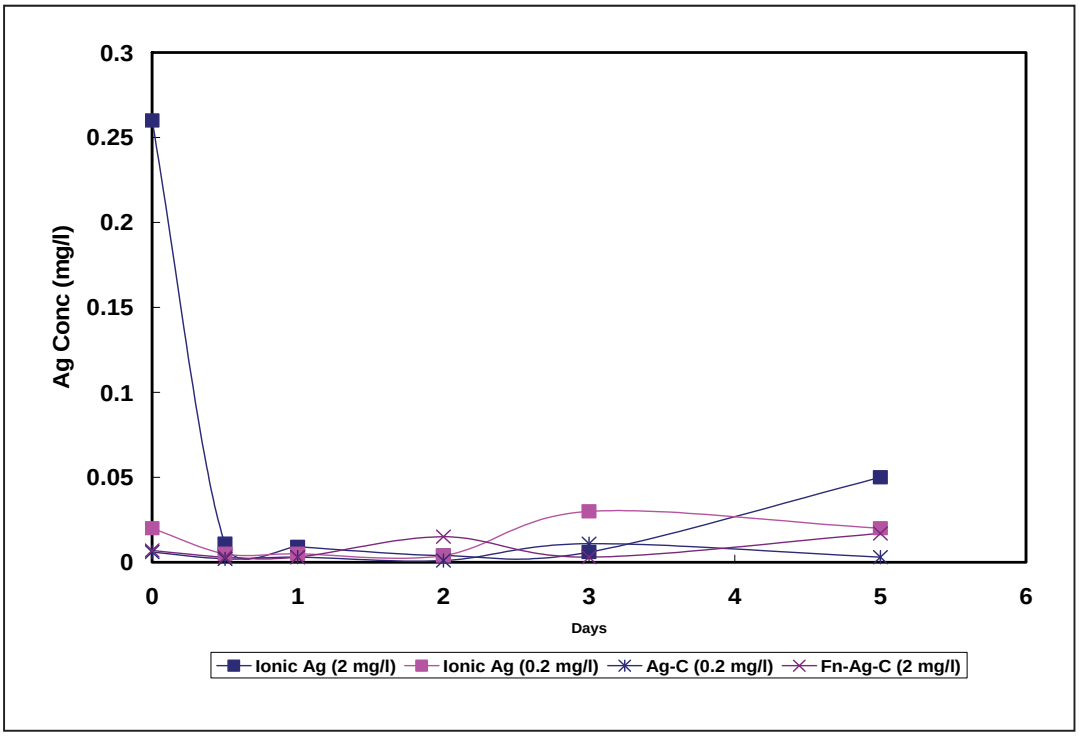

Figure 7.9. Silver concentrations in filtrate samples in the bioreactors spiked with ionic or nanosilver.

7.7 Evaluation of Nanosuspended Particles by DLS Analyses

Filtrate samples from the bioreactors were analyzed using Malvern Zetasizer for particle size distribution and photon count rate. As discussed in Chapters 3 and 5, photon count rate could be a useful measurement to monitor concentration of nanoscale particles and their transformation. The count rates in the filtered samples varied from approximately 175 kCPS to 225 kCPS on Day 0 (Figure 7.10). The count rate gradually decreased over time to approximately 60 to 75 kCPS after 7 days. On Day 0 (i.e., samples collected within minutes of setting up the reactors), the control samples contained the lowest photon count rate (Figure 7.11). In general, the nanozinc oxide-spiked samples had higher count rate that the ionic zinc oxide containing samples (except for Fn-ZnO-C). Note that the zinc concentration in the ionic zinc-spiked samples was higher than that in the nanozinc oxide-spiked samples at Time 0 (Figure 7.8). The higher or equivalent photon count rate in the nanozinc oxide-spiked samples that contained less residual zinc than that in the ionic zinc-spiked samples indicated the differences in the mode of ionic and nanozinc transformations in the reactors. These results are again consistent with the trends observed in the nanomaterials removal studies (Chapter 5). Gradual removal of the remaining zinc as well as other wastewater colloidal constituents apparently resulted in lower photon count rate over time. It is interesting to note that the COD

levels in all the reactors gradually increased after the first day (Figure 7.2). However, the increase in COD did not have any significant effect (i.e., increase) in the count rates. Similar trends were observed with the count rates in all of the batch bioreactors.

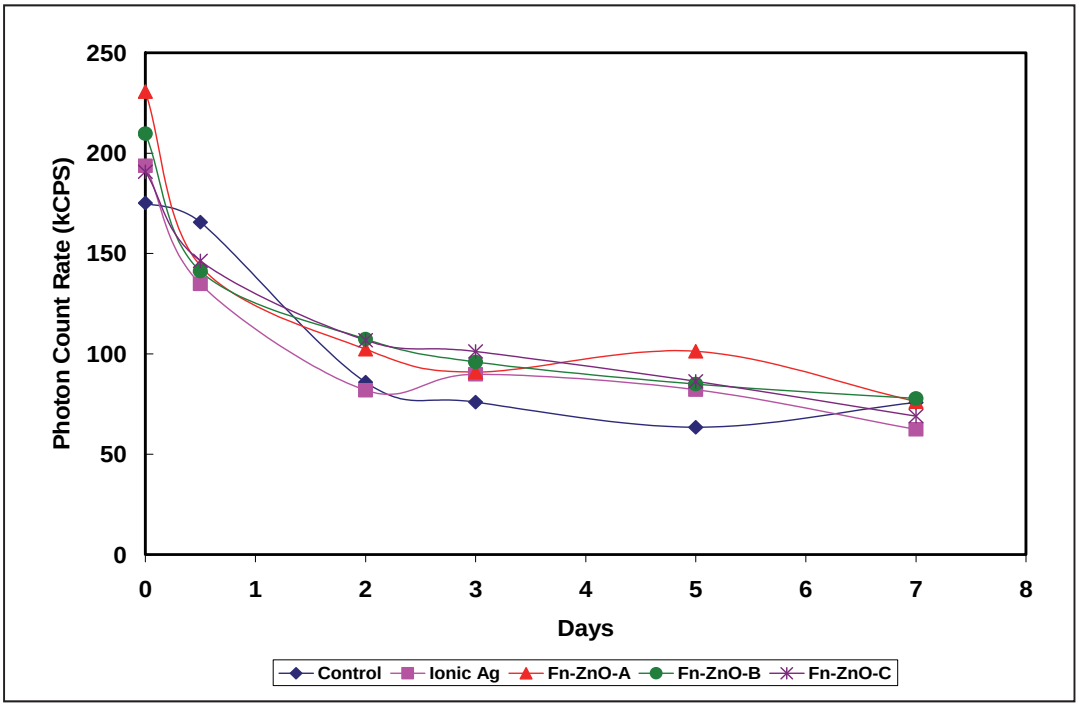

Figure 7.10. Photon count rates in filtrate samples in the bioreactors spiked with 2 mg/L ionic or nanozinc.

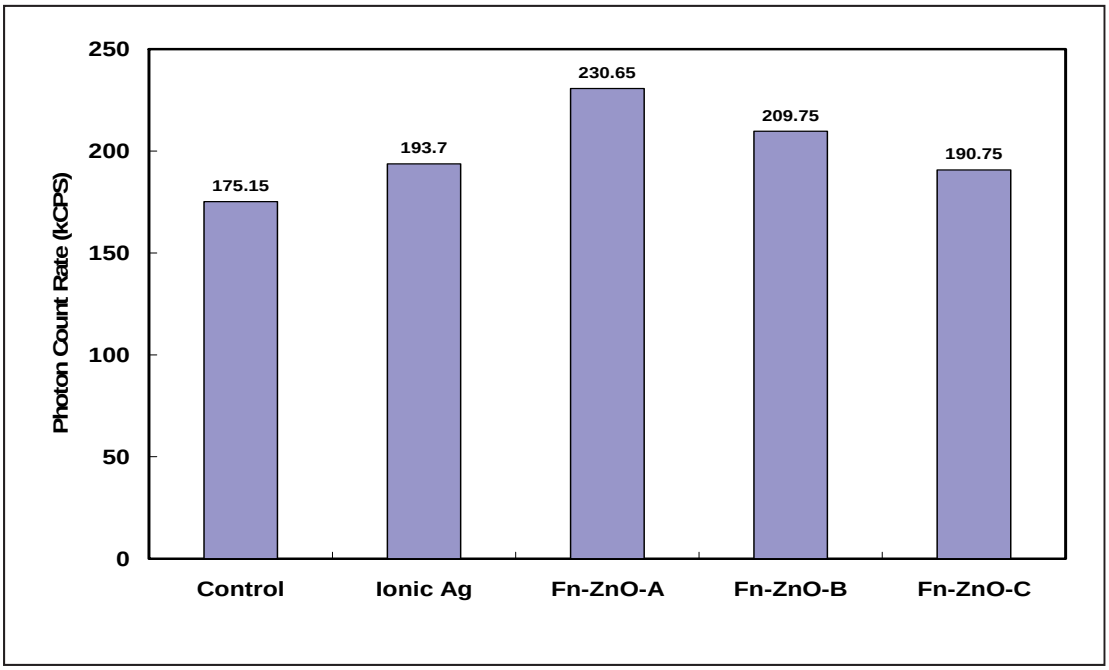

Figure 7.11. Photon count rates in filtrate samples in the bioreactors immediately after spiking with 2 mg/L ionic or nanozinc.

Figures 7.12 and 7.13 show the particle size distribution of the nanoscale suspended particles in the filtrate samples at the beginning and end of the study using 2 mg/L zinc. The particle size ranged from approximately 50 to 200 nm in all the samples at the two time periods. However, no significant contrast could be inferred among the control, ionic zinc, or nanozinc oxide-spiked samples. In general, similar trends were observed in most of the batch reactors.

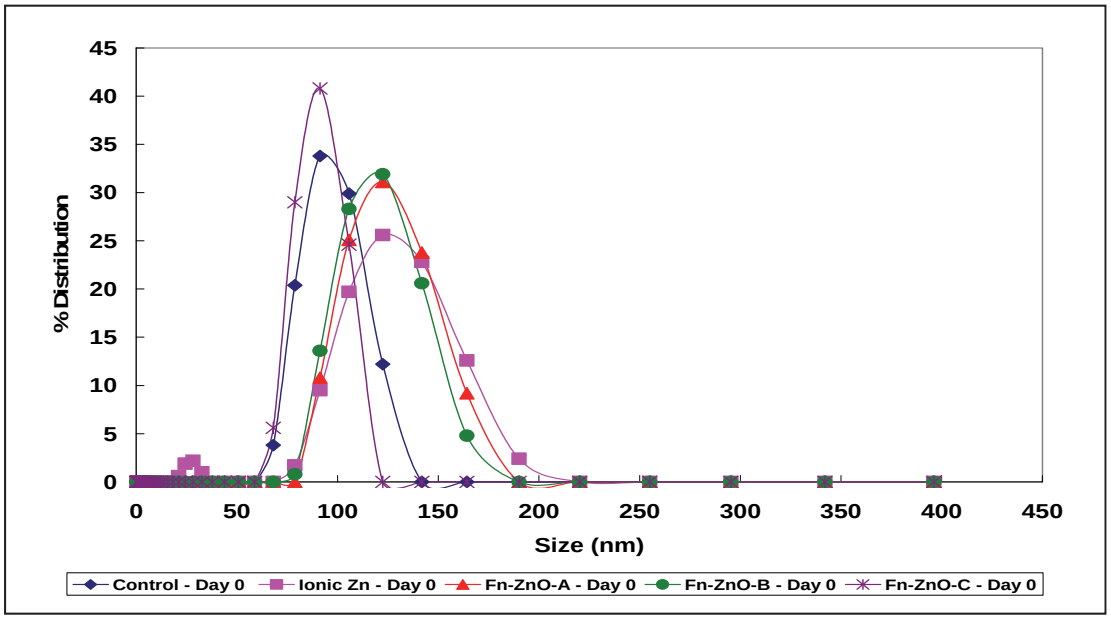

Figure 7.12. Particle size distribution on Day 0 in the filtrate samples spiked with 2 mg/L of ionic or nanozinc oxide.

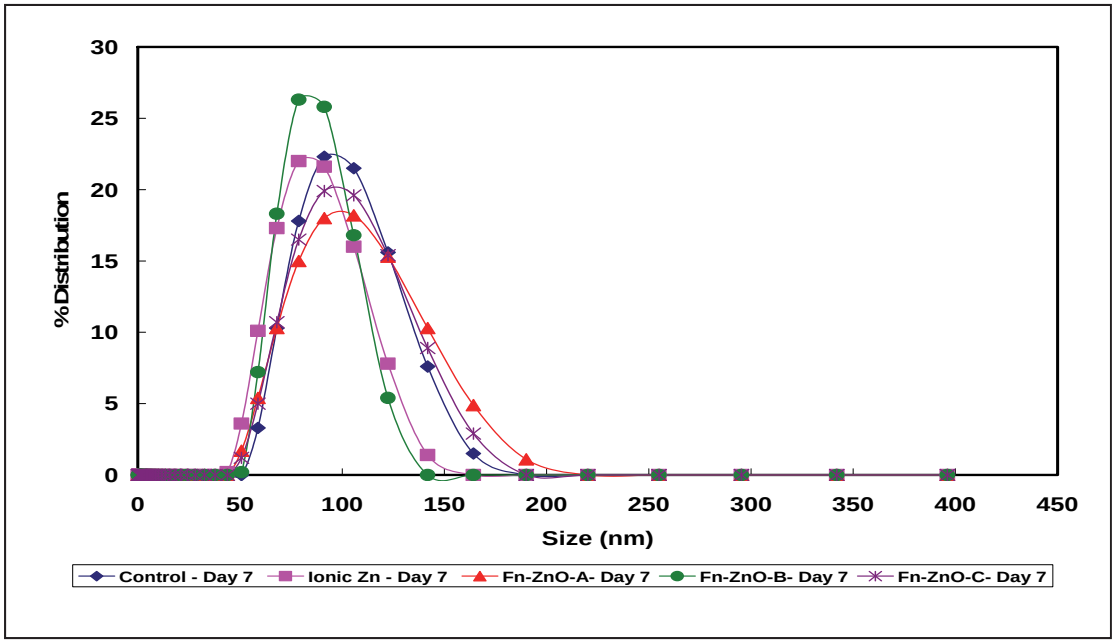

Figure 7.13. Particle size distribution on Day 7 in the filtrate samples spiked with 2 mg/L of ionic or nanozinc oxide.

7.8 Summary of Operational Parameters Evaluation During Biological Treatment

Bench-scale bioreactors were operated by spiking 0.2 or 2 mg/L of nanozinc oxide, nanosilver, or ionic salts ($ZnNO_3$ and $AgNO_3$) in activated sludge samples from the OCSD. Effects of their presence on various parameters critical to biological treatment process were evaluated. In addition, the removal of the added nanomaterials and the nanoscale suspended particles profile in the filtrate samples were also evaluated. The observations from these studies are summarized as follows:

- No significant differences in the filtrate COD profiles were observed among the control and the nanomaterials-spiked reactors, which indicated that at the levels added, the nanomaterials used in this study did not significantly inhibit the ability of the microbial community to degrade organic matter in the wastewater.

- The nitrite and nitrate production increased and the pH decreased in a similar manner in all of the reactors indicating that the ammonia oxidation was not significantly inhibited in the presence of the nanomaterials used in this study. This result slightly differed from the MPN study data (Figure 6.6) using 2 mg/L of nanozinc oxide. The MPN data showed a delay in the growth of ammonia oxidizing bacteria when 2 mg/L of ionic zinc was added. However, the MPN test conditions favor the growth of a targeted group of microbial community through the use of a select growth media. The bioreactor study involves degradation of constituents by a variety of microbial communities using the organic matter in the wastewater as the substrate. Therefore, it is possible that the microbial community that was not the target of the MPN study may have played a role in oxidation of ammonia in the bioreactors.

- More than 90% of the added zinc and silver was removed in all the reactors within 4 hours. However, in the Time 0 sample collected within minutes after starting the reactors, the zinc or silver levels in the ionic salt-spiked samples were consistently higher than those in the nanomaterials-spiked samples. This indicated rapid removal of nanomaterials compared to their ionic salts during biological treatment. Furthermore, at Time 0, despite the higher zinc (or silver) concentrations, the nanoscale particles count (measured as photon count rate) in the filtrate of ionic salt-added samples were lower than those in the nanozinc oxide- (or silver-) added samples. This suggested that the modes of transformation and removal of nanomaterials were different from that for ionic salts.

These results, in general, compared well with the bioreactor study by Liang et al. (2010). Their study evaluated inhibition of nitrifying bacteria to nanosilver in batch and continuous bioreactors using heterotrophic as well as enriched nitrifying bacteria. Their data showed that approximately 90% of the added nanosilver was removed from the solution. Furthermore, there was no significant change in the COD removal rate because of the addition of nanosilver. The addition of nanosilver inhibited respiration of nitrifying bacteria in a batch reactor, but the inhibition to activated sludge system was significantly low. The MPN test data (Chapter 6) as well as the bioreactor data using activated sludge in our studies also followed these general trends. Liang et al. (2010) observed that the inhibition to nitrifying bacterial culture in activated sludge treatment is more pronounced in a continuous reactor system than in a batch reactor system possibly because of "slow kinetics of metal internalization and exacerbation effect on bacteria due to continued metal exposure." (p.

5433) They observed a lower ammonia degradation and higher nitrite accumulation in a continuous reactor and a reduction in *Nitrospira* population and near washout of *Nitrobactor* population in continuous reactors. Our study, however, was limited to evaluation of inhibition only in a batch reactor system.

Chapter 8

Removal of Nanomaterials in Media Filters

8.1 Background

Column studies were conducted to evaluate removal of nanozinc oxide in media filters. Media filters are often used as a polishing treatment for removing suspended particles in water reclamation facilities. As described in Chapter 3, feed samples for the column study were prepared by spiking secondary effluent with 2 mg/L of zinc oxide (ZnO-A, ZnO-B, or ZnO-C) or ionic zinc and allowing it to settle for 1 hour; this facilitated the removal of readily precipitated solids to minimize clogging of the media. The supernatant containing suspended zinc oxide was used as the column feed. Table 8.1 shows the zinc concentrations in the supernatant thus prepared for the column studies.

Table 8.1. Average Zinc Concentrations in the Settled Secondary Effluent used as Column Feed Water[a]

Sample	Average Zinc Concentration in Feed Water (mg/L)
Ionic Zinc	2.05
ZnO-A	1.75
ZnO-B	1.32
ZnO-C	1.81

[a]Represents the feed concentration at Time 0.

Column studies were performed using two different sizes of sand media (0.45 mm, 0.175 mm) to evaluate the effect of pore size. Furthermore, studies were performed using two different flow rates to evaluate the impact of surface loading rate on the removal of nanomaterials. Overall, 16 different combinations of nanomaterials, media size, and flow rates were used for the evaluation of media filtration.

Figure 8.1 shows the zinc concentrations in the feed water and column effluent over time in the samples spiked with ZnO-A nanomaterial. The zinc levels in the first column effluent sample (taken within minutes of starting the column runs) were 70 to 90% lower than the zinc concentrations in the column influent. Following this, the column effluent data appeared to show two distinctive trends during the course of the run. During the first 20 to 30 bed volumes the effluent zinc concentrations increased gradually (Zone A in Figure 8.1). The concentration profile during this phase was similar to typical breakthrough curves for contaminant removal in media filters. The peak effluent zinc concentrations under all column operating conditions were lower than influent zinc concentrations. This indicated aggregation and deposition of nanozinc

in the filter media. This trend is consistent with those observed by others using high ionic strength solutions and heterogenic media (Torkzaban et al., 2010). After this (Zone B in Figure 8.1), the concentration remained unchanged or gradually decreased. Also, resistance to flow occurred marked by gradual decrease in effluent flow rates. This suggested that zinc solids accumulated in the filter media and blocked effluent flow through the columns. The decrease in zinc concentration occurred probably because of straining and settling of zinc solids. Finally, in the runs using 0.3 gpm/ft^2 after nearly 135 bed volumes, the columns were completely plugged by the entrapped zinc, and the flow was completely arrested. For the runs using 0.15 gpm/ft^2, complete plugging of the pores occurred after 115 bed volumes.

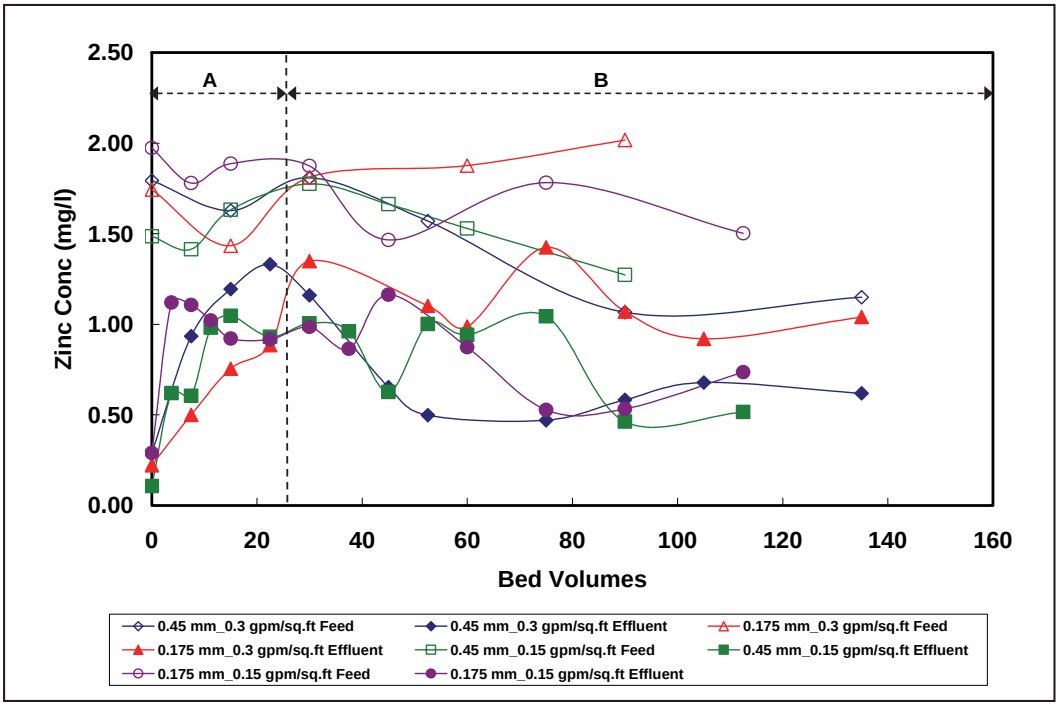

Figure 8.1. Influent and effluent zinc concentration in OCSD wastewater spiked with zinc oxide (ZnO-A) nanomaterial. Open legends represent column influent concentration, and the full legends show zinc levels in column effluents.

Figures 8.2 to 8.6 compare breakthrough curves for nano and ionic zinc materials using different media type and loading rates. A clear distinction was observed in the breakthrough pattern for nano and ionic zinc in all of these runs. The peak effluent zinc concentrations for the ionic zinc samples were always higher than those for nanozinc oxide samples. The zinc concentrations in the ionic zinc effluents were generally high throughout the initial bed volumes (indicated as Zone A in Figure 8.1). These trends are consistent with the DLVO theory and those observed by others (Tian, 2010; Torkzaban et al., 2010). Nanomaterials that tend to aggregate and deposit in the columns exhibit a lower peak effluent concentrations than the constituents (e.g. tracers, stabilized nanomaterials) that do not have the tendency to aggregate and deposit. In our study, ionic zinc is made of smaller size suspensions (Figure 5.6), has a lesser tendency to aggregate and deposit, and thus exhibited higher effluent peak concentrations.

The differences in the breakthrough patterns are more pronounced during filtration using larger media (Figures 8.2 and 8.3) than using smaller media (Figures 8.4 and 8.5). Typically, the pore sizes of the columns packed with larger media tend to be larger than the pore sizes in the columns packed with smaller media. In the columns packed with the larger media (0.45 mm), the pore sizes were large enough for more ionic zinc to pass through. However, nanozinc oxide particles are larger in size, have a higher tendency to aggregate and settle, and thus were removed more effectively in these columns. The pore size in the columns packed with smaller media (0.175 mm) was smaller; as a result, nanozinc oxides as well as ionic zinc were removed in these columns. Hence, the differences in the extent of removal were fewer.

Finally, breakthrough data using ZnO-A nanomaterials indicated smaller effluent peaks during filtration at lower loading rates (~ 1 mg/L at 0.15 gpm/ft^2, Figure 8.1) than those using higher loading rates (~ 1.25 mg/L at 0.3 gpm/ft^2, Figure 8.1). Furthermore, the peak breakthrough occurred early (within 5 to 10 bed volumes) compared to that (25 to 30 bed volumes) at the higher loading rates. These trends are consistent with the data reported by others (Liu et al., 2009; Jeong and Kim, 2009). A lower loading rate allows formation and deposition of more number of aggregates in the media resulting in lower effluent concentrations.

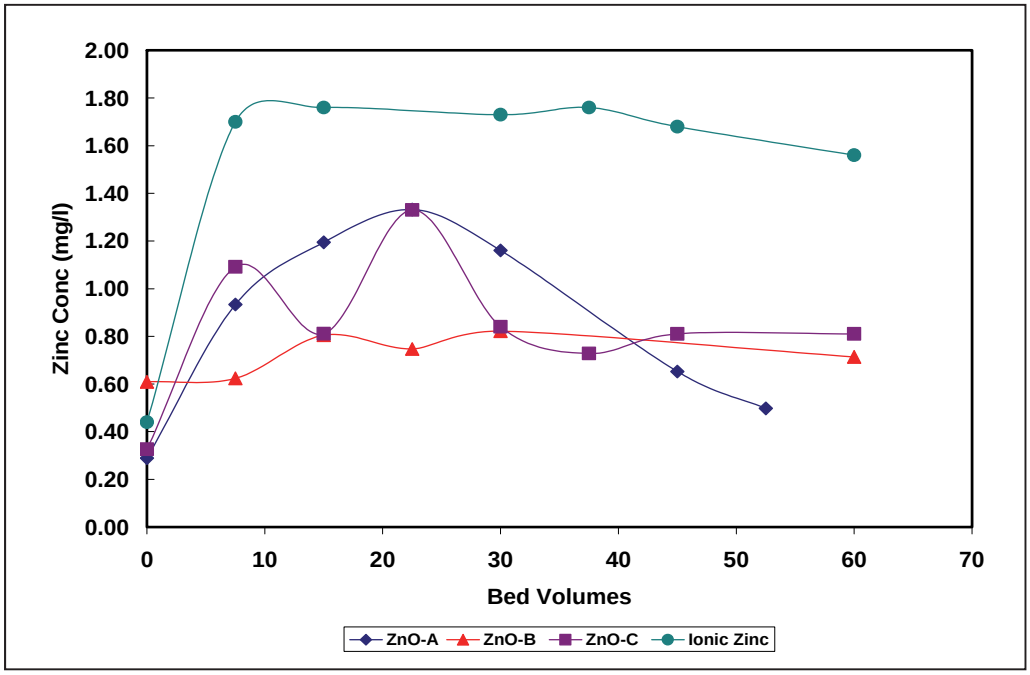

Figure 8.2. Breakthrough curves for nanozinc oxide material and ionic zinc suspended in wastewater effluent at a loading rate of 0.3 gpm/ft^2. The column was packed with 0.45 mm sand media.

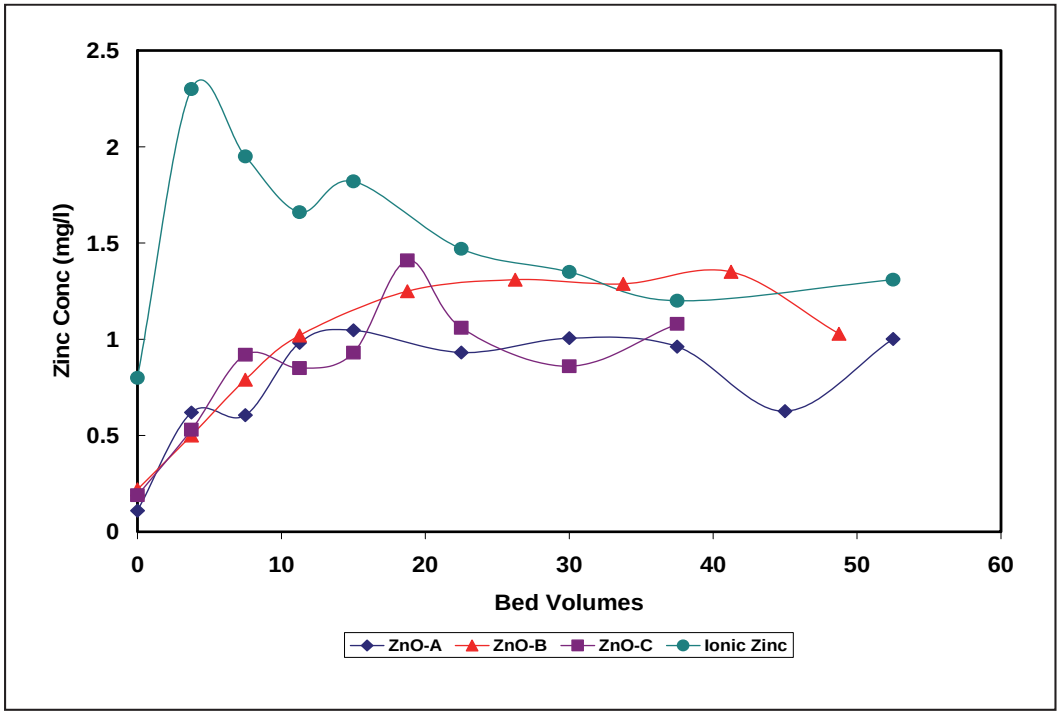

Figure 8.3. Breakthrough curves for nanozinc oxide material and ionic zinc suspended in wastewater effluent at a loading rate of 0.15 gpm/ft^2. The column was packed with 0.45 mm sand media.

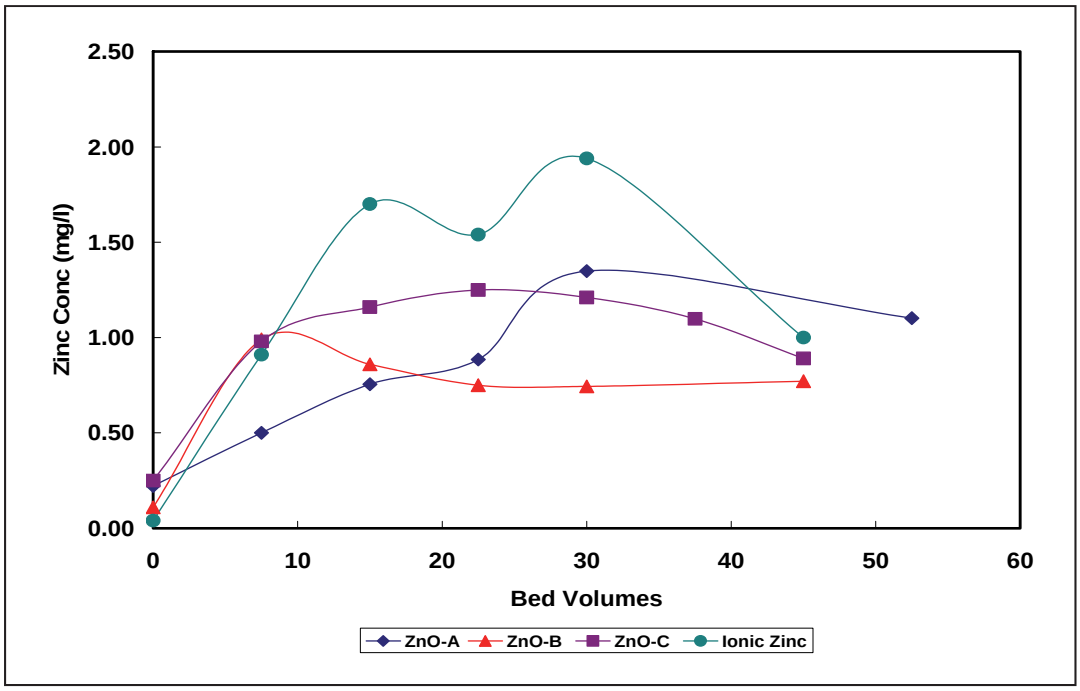

Figure 8.4. Breakthrough curves for nanozinc oxide material and ionic zinc suspended in wastewater effluent at a loading rate of 0.3 gpm/ft^2. The column was packed with 0.175 mm sand media.

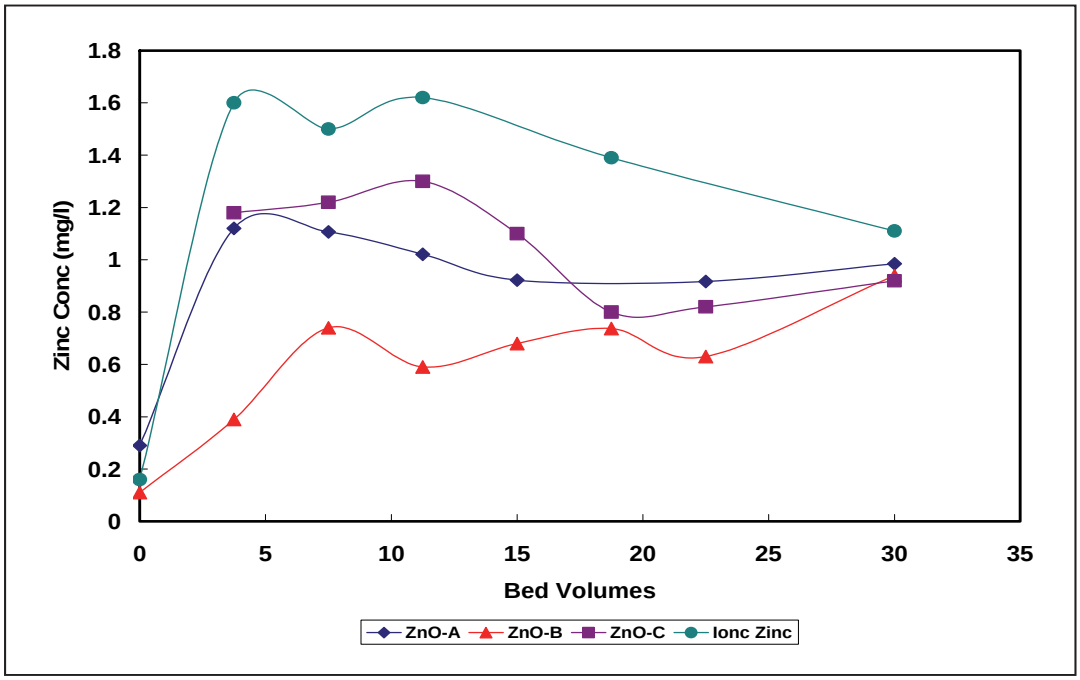

Figure 8.5. Breakthrough curves for nanozinc oxide material and ionic zinc suspended in wastewater effluent at a loading rate of 0.15 gpm/ft^2. The column was packed with 0.175 mm sand media.

Figure 8.6 compares breakthrough curves for nanozinc oxide (ZnO-A) suspended in DI water and in wastewater (OCSD effluent). The breakthrough occurred early, and the peak zinc concentration was also higher in the DI water suspension. These trends indicated that nanozinc oxide in DI water suspension was transported more effectively than in wastewater. This data again demonstrated the role of ionic strength on the transport characteristics of nanomaterials during media filtration. The higher dissolved salts (ionic strength) of the wastewater facilitated aggregation of the nanomaterials and caused their deposition in the column.

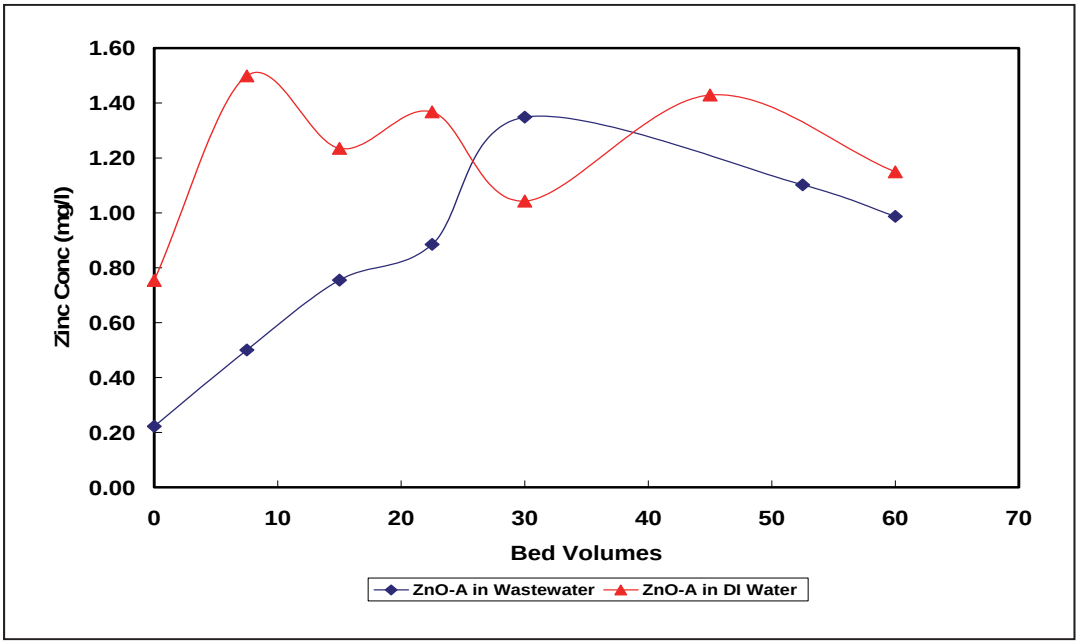

Figure 8.6. Breakthrough curves for nanozinc oxide material in wastewater or DI water suspension at a loading rate of 0.3 gpm/ft^2. The column was packed with 0.175 mm sand media.

Figures 8.7 and 8.8 show the zinc removed (i.e., the difference between influent and effluent zinc concentrations) after 15 and 30 bed volumes, respectively using different nanomaterials, media, and loading rates. The data showed a clear distinction in the extent of zinc removal in samples spiked with nanozinc oxide and ionic zinc. In almost all cases, nanozinc oxide was removed more effectively than ionic zinc. After 15 bed volumes in the column packed with smaller media, the ionic zinc removal was comparable to that of nanozinc oxide (Figure 8.7). This again appears to be due to effective removal of both ionic zinc and nanozinc oxide in the smaller pore sizes in the column packed with smaller-size media.

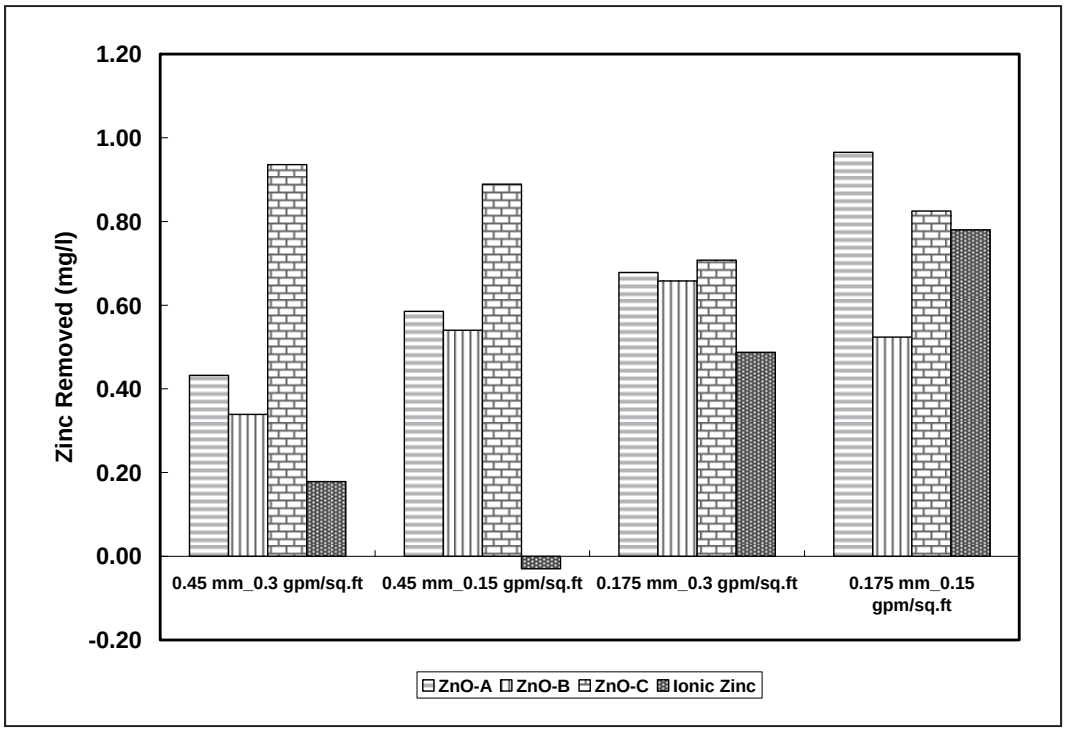

Figure 8.7. Zinc removed in the media filters after 15 bed volumes under various operating conditions.

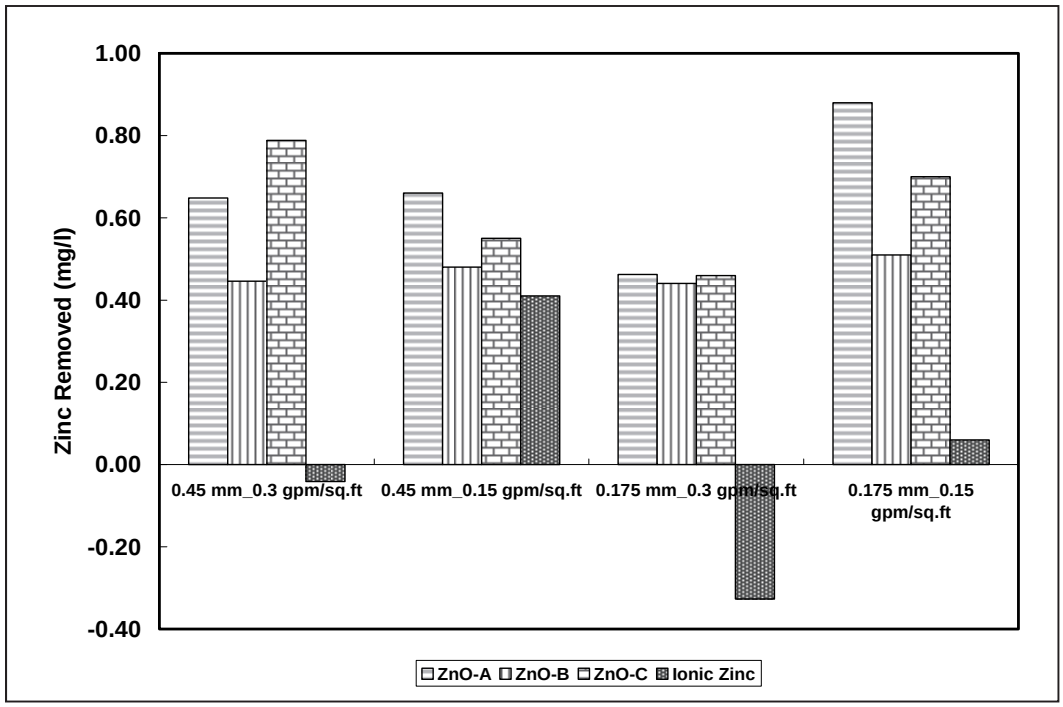

Figure 8.8. Zinc removed in the media filters after 30 bed volumes under various operating conditions.

8.2 Summary of Media Filtration Studies

The results from various media filtration studies are summarized as follows:

- In general, more nanomaterial (zinc oxide) than ionic zinc was removed in the media filters under similar operation conditions (i.e., media size and loading rate).
- A decrease in the loading rate (0.3 to 0.15 gpm/ft^2) or media size (from 0.45 mm to 0.175 mm) increased the removal of nanozinc oxide as well as ionic zinc.
- Column studies indicated that peak effluent zinc concentration for the ionic zinc added samples were always higher than those of nanozinc oxide added samples. It appears that nanomaterial tend to aggregate and are trapped in the media filters while the ionic species do not readily exhibit such behavior.
- Lowering the surface loading from 0.3 to 0.15 gpm/ft^2 resulted in smaller effluent peak (from approximately 1.25 mg/L to 1 mg/L) and early breakthrough (from approximately 30 to 10 bed volumes) of nanomaterial. Lower loading rate appears to allow formation and deposition of more number of aggregates in the media resulting in lower effluent concentrations.
- Media filtration trends for nanozinc oxide suspended in DI water were compared with that of nanozinc suspended in OCSD wastewater filtrates. Media filtration of nanozinc oxide in the wastewater samples produced smaller effluent peaks and more delayed breakthrough than that in DI water. Compared to the DI water, the wastewater contained higher levels of dissolved salts. These salts appeared to have facilitated the aggregation of nanomaterial resulting in lower peaks and a longer period for breakthrough.

Chapter 9

Nanomaterials and Chlorine Demand

9.1 Background

DLS analyses of wastewater samples throughout this study indicated that the addition of nanomaterials increased the levels of nanoscale suspended particles, as measured by photon count rate. The nanoscale particles, in turn, contribute to the turbidity. For example, Figure 9.1 shows the relationship between the turbidity and photon count rates for a group of groundwater wells in northern CA. The correlation co-efficient (R^2) was approximately 0.98 indicating a good fit. Turbidity is known to affect chlorine demand in water and wastewater samples, and thus disinfection efficiency through various mechanisms. Whereas several studies have attempted to evaluate the efficiency of nanomaterials for disinfection, very few studies have investigated the impact of nanomaterials on efficiency. It is known, however, that fullerene molecules undergo transformation in the presence of ozone (a disinfection agent), and this transformation also has an effect on its ability to disinfect. Hence, in this study, preliminary tests were performed to evaluate chlorine demand of the OCSD secondary effluents in the presence of nanomaterials.

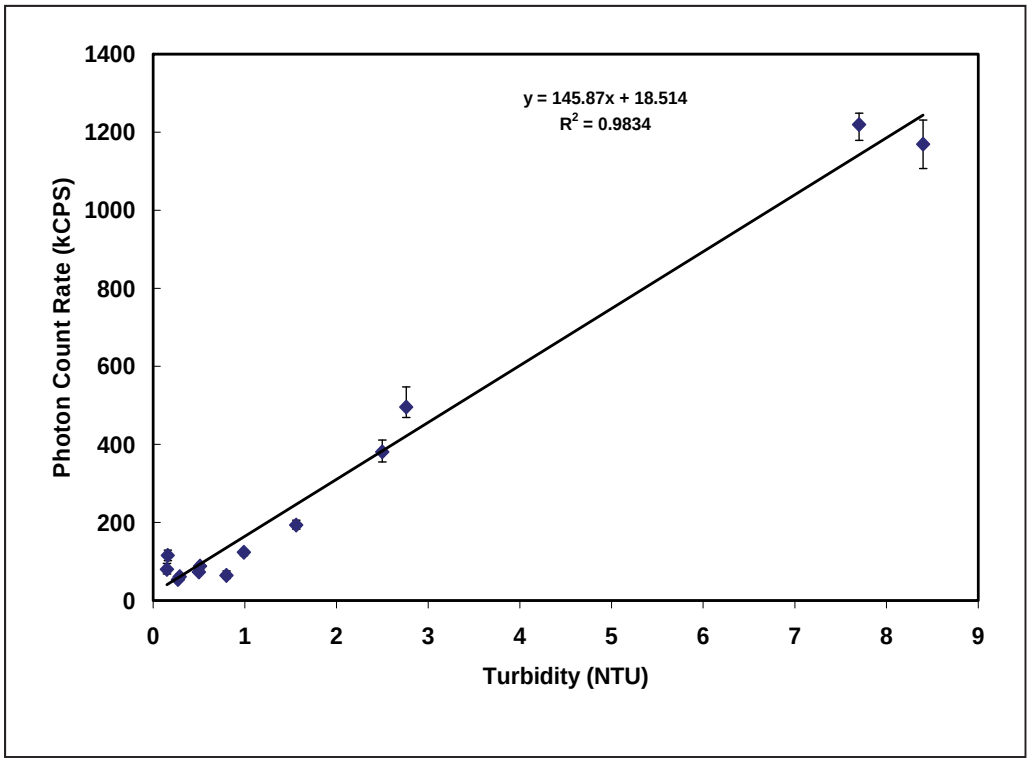

Figure 9.1. Relationship between turbidity and photon count rate for groundwater samples.

9.2 Chlorine Demand of Zinc Oxide Nanomaterial

Nanozinc oxide materials or ionic zinc at a 2 mg/L concentration were used in this study. Similar to the approach used for column studies, effluent samples spiked with 2 mg/L zinc oxide were allowed to settle for an hour, and the supernatant samples were collected for chlorine demand evaluation. Subsequently, a procedure similar to Standard Method 2350 B (Chlorine Demand/Requirement) was used to estimate the chlorine demand exerted by nanomaterials in wastewater. Three-hundred-milliliter glass vials were filled with the OCSD secondary effluent spiked with 2 mg/L chlorine (from bleach). Control vials that received no nanozinc oxide or zinc chloride salts were also used. The vials were then wrapped with aluminum foil, placed in a shaker table, and incubated for 1 hour in a dark room.

The total chlorine levels in control and nanomaterial-containing samples were measured using Hach Colorimetric (DPD, Hach Method No. 8167) method. The chlorine demand of the nanomaterial-containing samples was estimated using the following formula:

$$\text{Chlorine Demand (mg/L)} = (D_s - R_s) - (D_c - R_c)$$

Where,

D_s = Initial Chlorine Dose in the nanomaterial-containing sample (mg/L)

R_s = Residual Chlorine in the nanomaterial-containing sample after the contact time (mg/L)

D_c = Chlorine Dose in the Control Sample (Unspiked OCSD Effluent) (mg/L)

R_c = Residual Chlorine in the Control Sample after the contact time (mg/L)

Table 9.1. Chlorine Levels in Various Samples After Incubation

Sample	**Chlorine Conc. (mg/L)**			
	Replicate 1	***Replicate 2***	***Replicate 3***	***Average***
Control #1	0.34	0.39	0.31	0.35
Zinc Chloride Salt	0.33	0.38	0.32	0.34
ZnO-A	0.34	0.34	0.31	0.33
ZnO-B	0.27	0.31	0.27	0.28
ZnO-C	0.32	0.37	0.27	0.32
Control #2	0.38	0.39	0.33	0.37
Fn-ZnO-A	0.36	0.34	0.33	0.34
Fn-ZnO-B	0.33	0.32	0.32	0.32
Fn-ZnO-C	0.37	0.34	0.3	0.34

Table 9.1 shows the chlorine levels in the samples after incubation for 1 hour. The average residual chlorine concentrations in the control samples spiked with initial 2 mg/L chlorine were 0.35 and 0.37 mg/L after incubation, indicating a chlorine demand of approximately 1.65 mg/L. Except in the samples spiked with nanozinc oxide ZnO-B, the residual concentration in the zinc chloride or nanozinc oxide-spiked samples varied from 0.32 to 0.34 mg/L. This indicated that the addition of 2 mg/L of nanozinc oxide did not significantly alter the chlorine demand of the OCSD effluent. However, residual concentration in the effluent spiked with ZnO-B nanozinc oxide was about 0.08 mg/L lower than that of the control sample, which indicated that this nanomaterial exerted a chlorine demand of 0.08 mg/L.

9.3 Summary

Overall, the data indicated that the zinc oxide nanomaterial did not interact with chlorine and increase the chlorine demand of the effluent.

However, the study did not address whether these materials can affect disinfection efficiency by other mechanisms such as sheltering bacteria from exposure to chlorine, influence of other disinfectants, or during UV or ozone-mediated disinfection processes. More systematic studies may be required to investigate the role of nanomaterials on disinfection of wastewater effluents.

Chapter10

Summary and Recommendations

10.1 Summary of Findings

This study evaluated fate and effect of nanomaterials in key water reclamation processes. Bench-scale studies were performed using three nanomaterials (nanocopper, zinc oxide, and silver) to evaluate their impact during biological treatment, media filtration, and disinfection. The evaluations included the characterization of nanomaterials, the abiotic/biotic removal of nanomaterials in wastewaters, the inhibition of nanomaterials to key wastewater microorganisms, the impact of nanomaterials to key process parameters during biological treatment, the transport of nanomaterials in media filters, and the effect of nanomaterials on chlorine demand. The findings from these are summarized as follows.

The nanomaterials received from the vendors were characterized by various techniques. The data indicated that the measured primary size of the particles, in general, were larger than that reported by the vendors. The reasons for these deviations are not currently known. However, because of various instrument malfunctions and eventual closure of the Zeiss Nanomaterial Lab at the UCI facility, the nanomaterial characterization was performed near the end of the project period rather than on immediate receipt of the nanomaterial stock suspensions. As a result, the nanomaterial stock suspensions were stored for nearly 2 years prior to characterization. Nanomaterials are known to aggregate to a larger size over time. This may have caused the differences in the particle size.

Although good recoveries (compared to vendor-indicated concentrations) were obtained during analyses of nanocopper and zinc oxide by ICP analyses, significant problems were encountered during analyses of nanosilver in aqueous samples.

Studies using filtered wastewater indicated that nanomaterials were removed more effectively than their ionic salts. Nearly 60% and 55% of ionic copper and zinc, respectively, were removed from the wastewater, and 80% and 65% of nanocopper and nanozinc oxide, respectively, were removed. Furthermore, nanocopper was removed more effectively than nanozinc oxide. The trends in nanocopper and zinc oxide removal were similar to those predicted by speciation models (i.e., solubility products for ions). However, the extent of removal was lower than model predictions possibly because of the presence of organic matter in the wastewater. Presence of activated biomass increased nanomaterial removal by 5% to 20%.

MPN tests performed to evaluate microbial inhibition indicated that ionic copper and zinc caused more inhibition to coliform and ammonia oxidizing bacteria than did the nanocopper or zinc oxide. The addition of 10 mg/L ionic copper or zinc significantly lowered the growth of coliform bacteria. Note that the residual copper and zinc concentrations were higher in the samples spiked with ionic copper or zinc. It appears that the dissolved form (i.e., ionic species) of copper or zinc was responsible for inhibition of the microorganisms. However, nanosilver, at 2 mg/L, caused some inhibition to ammonia oxidizing bacteria. This inhibition was transient in nature, and the growth of the ammonia oxidizers was observed with a longer

incubation period. However, this finding indicated that nanomaterials might be directly involved in some inhibitory activities during biological treatment process.

Evaluation of key operational parameters in batch bioreactors did not indicate any adverse effects because of the presence of nanomaterials. Rate and extent of organic degradation, biomass levels, dissolved oxygen, pH, and ammonia oxidation remained similar in the presence or absence of nanomaterials in the batch bioreactors.

Transport of nanozinc oxide in media filters indicated that more nanomaterials aggregated and deposited in the columns than ionic zinc. The peak effluent zinc concentrations in the nanozinc oxide samples were consistently lower than those from the ionic zinc-suspended samples. The results were consistent with DLVO theory for aggregation of charged colloidal particles. Ionic zinc has a lower tendency to aggregate and therefore passed through the columns more readily than nanozinc oxide. These differences are more pronounced in a larger size media (0.45 mm) than a smaller size media since the larger media provides a larger pore space for ionic zinc transport. However, nanozinc oxide particles are aggregated and retained on this media. Smaller media provides smaller pore space where both ionic and nanozinc oxide are more effectively captured. Nanomaterial deposition is higher at lower surface loading rates than at higher loading rates because of the longer duration available for aggregation and deposition.

Finally, data from chlorine demand studies indicated no change in chlorine demand because of the presence of nanoscale-suspended materials (2 mg/L of nanozinc oxide) in the wastewater.

10.2 Recommendations for Future Studies

The following future investigations are recommended to better understand the impact of nanomaterials during water reclamation.

- A major limitation in this study is that the nanomaterials in the stock suspensions were characterized almost 2 years after their procurement and after completion of most of the fate and effect studies. The particle size of the nanomaterials measured by SEM and other techniques were generally larger (50 to 500 nm) compared to the vendor- specified sizes (10 to 100 nm). It is possible that such a long holding time may have altered the nanomaterials characteristics resulting in these discrepancies. Future studies to evaluate environmental fate and effects of nanomaterials should characterize the nanomaterials without significant delay.

- Characterization of nanomaterials used in this study indicated that the primary particles varied in sizes 50 nm or larger. Some of the recent toxicological studies appear to indicate that smaller size nanomaterials (e.g., 5 to 10 nm) are more inhibitory to microorganisms than are larger size nanomaterials. Studies using smaller size nanomaterials must be performed in the future to verify these findings for wastewater microorganisms.

- Some difficulties were encountered during analysis of nanosilver in aqueous samples. In general, techniques to analyze various nanomaterials in wastewater samples must be developed and validated.

- In this study, inhibitory effects of nanomaterials were evaluated using batch systems. Some differences in inhibitory effects have been reported between batch and continuous reactor studies using the nanomaterials (i.e., higher inhibition in continuous reactors). Detailed studies using continuous reactor studies must be performed using various nanomaterials. Moreover, such toxicity studies may initially include (1) nanomaterials such as silica that do not aggregate under DLVO forces and therefore tend to remain in suspension, (2) nanomaterials with novel structures and those with molecular level changes (e.g., new carbon-based nanomaterials), and (3) nanomaterials such as silver or copper that are known to cause toxic effects in their ionic form.

- The inhibitory effects were evaluated in this study by exposing the microorganisms to nanomaterials over a shorter duration of time. Studies must be performed to understand the effects of long-term release of nanomaterials to wastewater microorganisms.

- Data from this study indicated that a significant portion of the nanomaterials were removed from the wastewater and ended up in the biosolids. Studies must be performed to evaluate the long-term effect of nanomaterials in biosolids.

- This WRF study focused on the fate and effect of metal oxide nanomaterials. Literature information indicates that transport of some nanomaterials such as carbon nanotubes do not conform to the DLVO theory of particles aggregation. Studies must be conducted using nanomaterials other than metal oxides to evaluate their effects during water reclamation.

- This study primarily focused on bench-scale studies to evaluate nanomaterials impact. Pilot- and field-scale studies must be performed to verify the effect on biological and media transport observed in this study.

- Studies by other researchers indicate that biogenic nanoscale-suspended particles in wastewaters play a significant role in the fouling of membrane filters during water reclamation. Hence, the effect of nanomaterials in water reclamation processes, such as membrane filtration, must be evaluated.

- Finally, the role of nanomaterials to adsorb and transport other microconstituents (e.g., pharmaceuticals) in wastewater must be evaluated.

References

Atlas, R. *Handbook of Microbiological Media*; CRC Press: Boca Raton, FL, 2004.

Badireddy, A. R. Inactivation of bacteriophanges via photosensitization of fullerol nanoparticles. *Environ. Sci. Technol.* **2007**, *41*, 6627–6632.

Ben-Moshe, T. Transport of metal oxide nanoparticles in saturated porous media. *Chemosphere.* **2010**, *81*, 387–393.

Bian, S.; Mudunkotuwa, I. A.; Rupasinghe, T.; Grassian, V. H. Aggregation and dissolution of 4 nm ZnO nanoparticles in aqueous environments: Influence of pH, ionic strength, size and adsorption of humic acid. *Langmuir.* **2011**, *27*, 6059–6068.

Brunet, L. Comparative photoactivity and antibacterial properties of C60 fullerenes and titanium dioxide nanoparticles. *Environ. Sci. Technol.* **2009**, *43*, 4355–4360

Choi, O.; Deng, K. K.; Kim, N.; Ross, L. Jr.; Surampalli, R. Y.; Hu, Z. The inhibitory effects of silver nanoparticles, silver ions, and silver colloids on microbial growth. *Water Res.* **2008**, *42*, 3066–3074.

Choi, O. K.; Hu., C. Q. Nitrification inhibition by silver nanoparticles. *Water Sci. & Technol.* **2009**, *59*, 1699–1702.

Derjaguin, B. V.; Landau, L. D. Theory of the stability of strongly charged lyophobic sols and of the adhesion of strongly charged particles in solutions of electrolytes. *Acta Physicochim. URSS* **1941**, *14*, 733–762.

Eaton, L. S.; Rice, C.; Greenberg, A. E.; Franson, M. A. H. *Standard Methods for the Examination of Water and Wastewater;* Method 9221B. American Public Health Association: Washington, DC, 2005.

Eisenhart, C.; Wilson, P. W. Statistical methods and control in bacteriology. *Bacteriological Reviews* **1943**, *7* (2), 57–137.

Fabrega, J.; Fawcett, S. R.; Renshaw, J. C.; Lead, J. R. Silver nanoparticles impact on bacterial growth: Effect of pH, concentration, and organic matter. *Environ. Sci. Technol.* **2009**, *43* (19), 7285–7290.

Fortner, J. D.; Lyon, D. Y.; Sayes, C. M.; Boyd, A. M.; Falkner, J. C.; Hotze, E. M.; Alemany, L. B.; Tao, Y. J.; Guo, W.; Ausman, K. D.; Colvin, V. L.; Hughes, J. B. C_{60} in water: Nanocrystal formation and microbial response. *Environ. Sci. Technol.* **2005**, *39* (11), 4307–4316.

French, R. A.; Jacobson, A. R.; Kim, B.; Isley, S. L.; Penn R. L.; Baveye, P. C. Influence of ionic strength, pH, and cation valence on aggregation kinetics of titanium dioxide nanoparticles. *Environ. Sci. Technol.* **2009**, *43* (5), 1354–1359.

Ganesh, R.; Boardman, G. D.; Michelsen, D. Fate of azo dyes in sludges. *Water Res.* **1994**, *28* (6), 1367–1376.

Gangadharan, D. Polymeric microspheres containing silver nanoparticles as a bactericidal agent for water disinfection. *Water Res.* **2010**, *44*, 5481–5487.

Gao, J.; Youn, S.; Hovsepyan, A.; Llaneza, V. L.; Wang, Y.; Bitton, G.; Bonzongo, J. J. Dispersion and toxicity of selected manufactured nanomaterials in natural river water

samples: Effect of water chemical composition. *Environ. Sci. Technol.* **2009**, *43* (9), 3322–3328.

Gottschalk, F.; Nowack, B. The release of engineered nanomaterials to the environment. *J. Environ. Monit.* **2011**, *13*, 1145–1155.

Griffit, R. J.; Luo, J.; Gao, J.; Bonzongo, J.; Barber, D. S. Effects of particle composition and species on toxicity of metallic nanomaterials in aquatic organisms. *Environ. Toxicol. Chem.* **2008**, *27* (9), 1972–1978.

Halvorson, H. O.; Ziegler, N. R. Applications of statistics to problems in bacteriology. A means of determining bacterial populations by the dilution method. *J. Bacteriol.* **1933**, *25*, 101–121.

He, Y. T.; Wan, J.; Tokunaga, T. Kinetic stability of hematite nanoparticles: The effect of particle sizes. *J. Nanopart Res.* **2008**, *10* (2), 321–332.

Jeong, S.; Kim, S. Aggregation and transport of copper oxide nanoparticles in porous media. *J. Environ. Monit.* **2009**, *11*, 1595–1600.

Jiang, X.; Tong, M.; Li, H.; Yang, K. Deposition kinetics of zinc oxide nanoparticles on natural organic matter coated silica surfaces. *J. Colloid Interface Sci*. **2010**, *350*, 427–434.

Kiser, M. A.; Westerhoff, P.; Benn, T.; Wang, Y.; Pérez-Rivera, J.; Hristovski, K. Titanium nanomaterial removal and release from wastewater treatment plants. *Environ. Sci. Technol.* **2009**, *43* (17), 6757–6763.

Klaine, J. S.; Alverez, P. J. J.; Batley, G. E.; Fernandes, T. F.; Handy, R. D.; Lyon, D. Y.; Mahendra, S.; McLaughlin, M. J.; Lead, J. R. Nanomaterials in the environment: Behavior, fate, bioavailability and effects. *Environ. Toxicol. Chem*. **2008**, *27* (9), 1825–1851.

Kowalchuk, G. A.; Stephen, J. R. Ammonia-oxidizing bacteria: A model for molecular microbial ecology. *Annual Review of Microbiology.* **2001**, *55*, 485–529.

Lecoanet, H.; Wiesner, M. Velocity effect on fullerene and oxide nanoparticles deposits in porous media. *Environ. Sci. Technol*. **2004**, *38*, 4377–4382.

Li, Q.; Mahendra, S.; Lyon, D. Y.; Brunet, L.; Liga, M. V.; Li, D.; Alvarez, P. J. J. Antimicrobial nanomaterials for water disinfection and microbial control: Potential application and implications. *Water Res.* **2008**, *42*, 4591–4602.

Liang, Z.; Das, A.; Hu, Z. Bacterial response to a shock load of nanosilver in an activated sludge treatment. *Water Res.* **2010**, *44*, 5432–5438.

Limbach, L. K.; Bereiter, R.; Muller, E.; Krebs, R.; Galli, R.; Stark, W. Removal of oxide nanoparticles in a model wastewater treatment plant: Influence of agglomeration and surfactants on clearing efficiency. *Environ. Sci. Technol.* **2008**, *42* (15), 5828–5883.

Liu, H. L.; Dai, S. A.; Fu, K. Y.; Hsu, S. H. Antibacterial properties of nanoparticles in three different sizes and their nanocomposites with a new waterborne polyurethane. *Int. J. Nanomedicine.* **2010**, *5*, 1017–1028.

Liu, X.; Wazne, M.; Christodoulatos, C.; Jasinkiewicz, K. L. Aggregation and deposition behavior of boron nanoparticles in porous media. *J. Colloid Interface Sci.* **2009**, *330* (1), 90–96.

Long, T. C.; Saleh, N.; Tilton, R. D.; Lowrey, G. V.; Veronesi, B. Titanium dioxide (P25) produces reactive oxygen species in immortalized brain microglia (BV2) : Implications for nanoparticle neurotoxicity. *Environ. Sci. Technol.* **2006,** *40* (14), 4346–4352.

Maynard, A. D.; Aitken, R. J.; Butz, T.; Colvin, V.; Donaldson, K.; Oberdörster, G.; Philbert, M. A.; Ryan, J.; Seaton, A.; Stone, V.; Tinkle, S. S.; Tran, L.; Walker, N. J.; Warheit, D. B. Safe handling of nanotechnology. *Nature* **2006**, *444*, 267–269.

McBride, G. B. *Using statistical methods for water quality management. Issues, problems and solutions;* Wiley: Chichester, UK, 2005.

National Nanotechnology Initiative. http://www.nano.gov (**2011**).

Petosa, A. R. Aggregation and deposition of engineered nanomaterials in aquatic environments: Role of physiochemical interactions. *Env. Sci. Tech.* **2010**, *44*, 6532–6549.

Rolison, D. R. Catalytic nanoarchitectures—The importance of nothing and the unimportance of periodicity. *Science* **2003**, *299* (5613), 1698–1701.

Safarik, J.; Phipps, D.W. *Role of microfiltration cake layer composition and stability in desalination efficiency.* Proceedings of the National American Membrane Society Conference, Chicago, IL, May 12–17, 2006.

Schwegmann, H.; Feitz, H., Frimmel, F. H. Influence of the zeta potential on the sorption and toxicity of iron oxide nanoparticles on S. cerevisiae and E. coli. *J. Colloid Interface Sci.*, **2010**, *347* (1), 43–48.

Smeraldi, J.; Ganesh, R.; Safarik, J.; Rosso, D. Evaluation of ensemble techniques to monitor nanoparticles in wastewater. *International Conference on the Environmental Implications and Applications of Nanotechnology.* Amherst, MA, June 9–11, 2009.

Smeraldi, J.; Ganesh, R.; Safarik, J.; Rosso, D. Statistical evaluation of photon count rate data for nanoscale particles measurement in wastewaters**,** *J. Environ. Monit.* **2012**, *14* (1), 79–84**.**

Standard Methods for the Examination of Water and Wastewater. Part VII. Multiple-tube fermentation technique. Section C. Estimation of coliform group density, 12th ed.; American Public Health Association: Washington, DC, 1998.

Tian, Y. Transport of engineered nanoparticles in saturated porous media. *J. Nanopart. Res.* **2010**, 2371–2380.

Torkzaban, S.; Kim, Y.; Mulvihill, M.; Wan, J.; Tokunaga, T. K. Transport and deposition of functionalized CdTe nanoparticles in saturated porous media. *J. of Contaminant Hydrology*, **2010**, *118*, 208–217.

U.S. Environmental Protection Agency. *Nanotechnology White Paper*. Contract # 100/B-07/001. EPA: Washington, DC, 2007.

Verwey, E. J. W.; Overbeek, J. Th. G. *Theory of the Stability of Lyophobic Colloids*. Elsevier: New York, 1948.

Woodrow Wilson International Center for Scholars (WWICS). *Project on Emerging Nanotechnologies: A Nanotechnology Consumer Products Inventory.* http://www.nanotechproject.org/inventories/consumer/2011.

Zhang, Y.; Chen, Y.; Westerhoff, P.; Hristovski, K.; Crittenden, J. C. Stability of commercial metal oxide nanoparticles in water. *Water Res.* **2008**, *42*, 2204–2212.

Zhang, Y.; Chen, Y.; Westerhoff, P.; Crittenden, J. C. Impact of natural organic matter and divalent cations on the stability of aqueous nanoparticles. *Water Res*. **2009**, *43*, 4249–4257.

Zhou, D.; Keller, A. A. Role of morphology in the aggregation kinetics of zinc oxide nanoparticles. *Water Res*. **2010**, *44*, 2948–2956.

Appendix

Chemical Speciation Model Output for 10 mg/L Ionic Zinc or Copper in OCSD Wastewater

1. WRF Project - OCSD Wastewater with 10 mg/L Zn

```
PART 1 of OUTPUT FILE
MINTEQA2  v4.03   DATE OF CALCULATIONS: 13-MAY-2011  TIME: 15:27: 9
```

WRF Project - OCSD Wastewater with 10 mg/L Zn

```
Component file (COMP.DBS): comp.dbs    COMP v4.00 09/30/1999
Thermodynamic file (THERMO.UNF): thermo.unf  THERMO V4.00 09/30/1999
Gaussian DOM file (GAUSSIAN.DBS):gaussian.dbsGAUSSIAN V4.00
09/30/1999
Solids file (TYPE6.UNF): type6.unf   TYPE6 V4.00 09/30/1999
-----------------------------------------------------------------------
 Temperature (Celsius):  25.00
 Units of concentration: mg/L
 Ionic strength to be computed.
 If specified, carbonate concentration represents total inorganic
carbon.
 Do not automatically terminate if charge imbalance exceeds 30%
 Precipitation is allowed for all solids in the thermodynamic
database and the print option for solids is set to: 1
 Maximum iterations: 200
 The method used to compute activity coefficients is: Davies
equation
 Intermediate output file

-----------------------------------------------------------------------
    330  0.000E+00   -8.00 y
    490  2.300E+01   -2.89 y
    500  3.170E+02   -1.86 y
    180  4.830E+02   -1.87 y
    950  1.000E+01   -3.82

 H2O has been inserted as a COMPONENT
  3   1
    330     8.0000     0.0000
```

INPUT DATA BEFORE TYPE MODIFICATIONS

ID	Name	ACTIVITY GUESS	log GUESS	ANAL TOTAL
330	H+1	1.000E-08	-8.000	0.000E+00
490	NH4+1	1.288E-03	-2.890	2.300E+01
500	Na+1	1.380E-02	-1.860	3.170E+02
180	Cl-1	1.349E-02	-1.870	4.830E+02
950	Zn+2	1.514E-04	-3.820	1.000E+01
2	H_2O	1.000E+00	0.000	0.000E+00

Charge Balance: UNSPECIATED

Sum of CATIONS= 1.538E-02 Sum of ANIONS = 1.364E-02

PERCENT DIFFERENCE = 6.022E+00 (ANIONS - CATIONS)/(ANIONS + CATIONS)

PART 2 of OUTPUT FILE
MINTEQA2 v4.03 DATE OF CALCULATIONS: 13-MAY-2011 TIME: 15:27: 9

CONSTRAINTS ON COMPONENT ACTIVITIES

As specified, this chemical system is OPEN with respect to the following components:

H_2O H+1

Activities of the following components are constrained by the species shown:

COMPONENT	SPECIES	TYPE
H+1	H+1	3
H_2O	H_2O	3

PART 3 of OUTPUT FILE
MINTEQA2 v4.03 DATE OF CALCULATIONS: 13-MAY-2011 TIME: 15:27: 9

PARAMETERS OF THE COMPONENT MOST OUT OF BALANCE:

ITER	NAME	TOTAL mol/L	DIFF FXN	LOG ACTVTY	RESIDUAL
0	Cl-1	1.364E-02	-1.333E-04	-1.87000	1.319E-04
1	Cl-1	1.364E-02	1.762E-03	-1.86567	1.761E-03
2	Cl-1	1.364E-02	1.431E-06	-1.91834	6.780E-08

ITERATIONS= 3: SOLID ZnO (active) PRECIPITATES

PART 2 of OUTPUT FILE
MINTEQA2 v4.03 DATE OF CALCULATIONS: 13-MAY-2011 TIME: 15:27: 9

CONSTRAINTS ON COMPONENT ACTIVITIES

As specified, this chemical system is OPEN with respect to the following components:

H_2O H+1

Activities of the following components are constrained by the species shown:

COMPONENT	SPECIES	TYPE
Zn+2	ZnO (active)	4
H+1	H+1	3
H_2O	H_2O	3

PART 3 of OUTPUT FILE
MINTEQA2 v4.03 DATE OF CALCULATIONS: 13-MAY-2011 TIME: 15:27: 9

PARAMETERS OF THE COMPONENT MOST OUT OF BALANCE:

ITER	NAME	TOTAL mol/L	DIFF FXN	LOG ACTVTY	RESIDUAL
3	Na+1	1.380E-02	-1.581E-03	-1.91295	1.580E-03
4	Na+1	1.380E-02	1.772E-03	-1.86011	1.770E-03

ID No	Name	Total Conc(M)	Conc (M)	log Activity	Diff fxn
180	Cl-1	1.364E-02	1.363E-02	-1.91784	1.127E-06
490	NH4+1	1.276E-03	1.215E-03	-2.96790	1.001E-07
500	Na+1	1.380E-02	1.380E-02	-1.91257	1.140E-06
2	H_2O	0.000E+00	-1.289E-04	-0.00021	0.000E+00
330	H+1	0.000E+00	1.128E-08	-8.00000	0.000E+00
950	Zn+2	1.531E-04	2.504E-05	-4.81139	0.000E+00

Type I - COMPONENTS AS SPECIES IN SOLUTION

ID No	Name	Conc (M)	log Act	Charge	Act Coef	New logK
330	H+1	1.128E-08	-8.00000	1.00	0.88615	0.052
490	NH4+1	1.215E-03	-2.96790	1.00	0.88615	0.052
500	Na+1	1.380E-02	-1.91257	1.00	0.88615	0.052
180	Cl-1	1.363E-02	-1.91784	-1.00	0.88615	0.052
950	Zn+2	2.504E-05	-4.81139	2.00	0.61664	0.210

Type II - OTHER SPECIES IN SOLUTION OR ADSORBED

ID No	Name	Conc (M)	log Act	Charge	Act Coef	New logK
9501804	ZnOHCl (aq)	6.154E-07	-6.20944	0.00	1.00332	-7.481
3304900	NH3 (aq)	6.116E-05	-4.21212	0.00	1.00332	-9.246
3300020	OH-	1.136E-06	-5.99721	-1.00	0.88615	-13.945
9503300	ZnOH+	1.753E-06	-5.80860	1.00	0.88615	-8.945
9503301	Zn(OH)2 (aq)	2.470E-07	-6.60581	0.00	1.00332	-17.795
9503302	Zn(OH)3-	1.411E-09	-8.90303	-1.00	0.88615	-28.039
9503303	Zn(OH)4-2	8.123E-14	-13.30024	-2.00	0.61664	-40.278
9501800	ZnCl+	5.288E-07	-6.32922	1.00	0.88615	0.452
9501801	ZnCl2 (aq)	8.943E-09	-8.04706	0.00	1.00332	0.599

```
9501802 ZnCl3-     9.718E-11  -10.06490   -1.00   0.88615    0.552
9501803 ZnCl4-2    8.438E-13  -12.28374   -2.00   0.61664    0.409
-----------------------------------------------------------------------
Type III - SPECIES WITH FIXED ACTIVITY

  ID No      Name                Conc (M)     New logK    Enthalpy
      2 H2O                   -1.289E-04      0.000       0.000
    330 H+1                    3.149E-04      8.000       0.000

-----------------------------------------------------------------------
Type IV - FINITE SOLIDS (present at equilibrium)

  ID No      Name                Conc (M)     New logK    Enthalpy
2095005 ZnO (active)           1.249E-04    -11.188      88.760

-----------------------------------------------------------------------

 Type V - UNDERSATURATED SOLIDS (not present at equilibrium)

  ID No      Name                Conc (M)     New logK    Enthalpy
2095001 Zn(OH)2                9.732E-02    -12.200       0.000
2095002 Zn(OH)2 (beta)         2.718E-01    -11.754      83.140
2095003 Zn(OH)2 (gamma)        2.846E-01    -11.734       0.000
2095004 Zn(OH)2 (epsilon)      4.510E-01    -11.534      81.800
2095000 Zn(OH)2 (am)           5.178E-02    -12.474      80.620
2095006 ZINCITE                7.152E-01    -11.334      89.620
4195000 ZnCl2                  2.009E-16     -7.050      72.500
4195001 Zn2(OH)3Cl             1.852E-03    -15.191       0.000
4195002 Zn5(OH)8Cl2            4.034E-03    -38.500       0.000
4150000 HALITE                 3.691E-06     -1.603      -3.700

PART 4 of OUTPUT FILE
 MINTEQA2  v4.03   DATE OF CALCULATIONS: 13-MAY-2011  TIME: 15:27: 9

               PERCENTAGE DISTRIBUTION OF COMPONENTS AMONG
             TYPE I and TYPE II (dissolved and adsorbed) species

Cl-1     100.0     Percent bound in species #    180   Cl-1

NH4+1         95.2     Percent bound in species #    490   NH4+1
               4.8    Percent bound in species #3304900   NH3 (aq)

Na+1          100.0     Percent bound in species #    500   Na+1

H2O           15.4     Percent bound in species #9501804   ZnOHCl (aq)
              28.4     Percent bound in species #3300020   OH-
              43.8     Percent bound in species #9503300   ZnOH+
              12.3     Percent bound in species #9503301   Zn(OH)2 (aq)

H+1           93.9     Percent bound in species #3304900   NH3 (aq)
               1.7    Percent bound in species #3300020   OH-
               2.7    Percent bound in species #9503300   ZnOH+

Zn+2          88.8     Percent bound in species #    950   Zn+2
               2.2    Percent bound in species #9501804   ZnOHCl (aq)
               6.2    Percent bound in species #9503300   ZnOH+
               1.9    Percent bound in species #9501800   ZnCl+
```

PART 5 of OUTPUT FILE
 MINTEQA2 v4.03   DATE OF CALCULATIONS: 13-MAY-2011 TIME: 15:27: 9

---------- EQUILIBRATED MASS DISTRIBUTION ----------

IDX	Name	DISSOLVED		SORBED		PRECIPITATED	
		mol/L	percent	mol/L	percent	mol/L	percent
180	Cl-1	1.364E-02	100.0	0.000E+00	0.0	0.000E+00	0.0
490	NH4+1	1.276E-03	100.0	0.000E+00	0.0	0.000E+00	0.0
500	Na+1	1.380E-02	100.0	0.000E+00	0.0	0.000E+00	0.0
2	H_2O	4.003E-06	100.0	0.000E+00	0.0	0.000E+00	0.0
330	H+1	-6.515E-05	100.0	0.000E+00	0.0	0.000E+00	0.0
950	**Zn+2**	**2.819E-05**	**18.4**	**0.000E+00**	**0.0**	**1.249E-04**	**81.6**

Charge Balance: SPECIATED

Sum of CATIONS = 1.507E-02 Sum of ANIONS   1.364E-02

PERCENT DIFFERENCE =   4.991E+00 (ANIONS - CATIONS)/(ANIONS + CATIONS)

EQUILIBRIUM IONIC STRENGTH (m) =   1.438E-02

EQUILIBRIUM pH   =   8.000

DATE ID NUMBER: 20110513
TIME ID NUMBER: 15270957

PART 6 of OUTPUT FILE
 MINTEQA2 v4.03   DATE OF CALCULATIONS: 13-MAY-2011 TIME: 15:27: 9

Saturation indices and stoichiometry of all mineralsID No   Name
SI   Composition by stoich. of Components
2095000 Zn(OH)2 (am)   -1.286 [1.000]950 [2.000] 2 [-2.000]330
2095001 Zn(OH)2   -1.012 [-2.000]330 [1.000]950 [2.000] 2
2095002 Zn(OH)2 (beta) -0.566 [1.000]950 [2.000] 2 [-2.000]330
2095003 Zn(OH)2 (gamma)-0.546 [1.000]950 [2.000] 2 [-2.000]330
2095004 Zn(OH)2(epsilon-0.346 [1.000]950 [2.000] 2 [-2.000]330
2095005 ZnO (active)   0.000 [-2.000]330 [1.000]950 [1.000] 2
2095006 ZINCITE   -0.146 [1.000]950 [1.000] 2 [-2.000]330
4195000 ZnCl2   -15.697 [1.000]950 [2.000]180
4195001 Zn2(OH)3Cl   -2.732 [2.000]950 [3.000] 2 [-3.000]330
                                  [1.000]180
4195002 Zn5(OH)8Cl2   -2.394 [-8.000]330 [5.000]950 [8.000] 2
                                  [2.000]180
4150000 HALITE   -5.433 [1.000]500 [1.000]180

2. WRF Project - OCSD Water pH 7.8_Cu 10 mg/L
PART 1 of OUTPUT FILE _____ MINTEQA2 v4.03 DATE OF CALCULATIONS: 15-MAY-2011 TIME: 12:26:55

WRF Project - OCSD Water pH 7.8_Cu 10 mg/L

Component file (COMP.DBS): comp.dbs COMP v4.00 09/30/1999
Thermodynamic file (THERMO.UNF): thermo.unf THERMO V4.00 09/30/1999
Gaussian DOM file (GAUSSIAN.DBS): gaussian.dbsGAUSSIAN V4.00 9/30/1999
Solids file (TYPE6.UNF): type6.unf TYPE6 V4.00 09/30/1999

Temperature (Celsius): 25.00
Units of concentration: mg/L
Ionic strength to be computed.
If specified, carbonate concentration represents total inorganic carbon.
Do not automatically terminate if charge imbalance exceeds 30%
Precipitation is allowed for all solids in the thermodynamic database and the print option for solids is set to: 1
Maximum iterations: 200
The method used to compute activity coefficients is: Davies equation
Intermediate output file
---
330 0.000E+00 -7.80 y
490 2.300E+01 -2.89 y
500 3.170E+02 -1.86 y
180 4.830E+02 -1.87 y
231 1.000E+01 -3.80

H_2O has been inserted as a COMPONENT
3 1
330 7.8000 0.0000

INPUT DATA BEFORE TYPE MODIFICATIONS

ID	Name	ACTIVITY GUESS	log GUESS	ANAL TOTAL
330	H+1	1.585E-08	-7.800	0.000E+00
490	NH4+1	1.288E-03	-2.890	2.300E+01
500	Na+1	1.380E-02	-1.860	3.170E+02
180	Cl-1	1.349E-02	-1.870	4.830E+02
231	Cu+2	1.585E-04	-3.800	1.000E+01
2	H_2O	1.000E+00	0.000	0.000E+00

Charge Balance: UNSPECIATED

Sum of CATIONS= 1.539E-02 Sum of ANIONS = 1.364E-02

PERCENT DIFFERENCE = 6.051E+00 (ANIONS - CATIONS)/(ANIONS + CATIONS)

| IMPROVED ACTIVITY GUESSES PRIOR TO FIRST ITERATION: |

```
            |       Cu+2        Log activity guess:    -4.64
|
PART 2 of OUTPUT FILE
 MINTEQA2  v4.03   DATE OF CALCULATIONS: 15-MAY-2011  TIME: 12:26:55

CONSTRAINTS ON COMPONENT ACTIVITIES

As specified, this chemical system is OPEN with respect to the
following components:

                H2O           H+1

          ---------------------------------------------------
          Activities of the following components are constrained
          by the species shown:

                  COMPONENT          SPECIES             TYPE
                    H+1            H+1                   3
                    H2O            H2O                   3

PART 3 of OUTPUT FILE
 MINTEQA2  v4.03   DATE OF CALCULATIONS: 15-MAY-2011  TIME: 12:26:55

PARAMETERS OF THE COMPONENT MOST OUT OF BALANCE:

ITER      NAME       TOTAL mol/L   DIFF FXN   LOG ACTVTY    RESIDUAL
0   Cl-1           1.364E-02  -1.449E-04    -1.87000    1.435E-04
1   Cl-1           1.364E-02   1.759E-03    -1.86536    1.757E-03
2   NH4+1          1.276E-03   3.532E-07    -2.96324    2.255E-07
3   Cu+2           1.575E-04   8.958E-08    -4.88710    7.383E-08

  ITERATIONS=   4:  SOLID TENORITE              PRECIPITATES

PART 2 of OUTPUT FILE
 MINTEQA2  v4.03   DATE OF CALCULATIONS: 15-MAY-2011  TIME: 12:26:55

CONSTRAINTS ON COMPONENT ACTIVITIES

          As specified, this chemical system is OPEN with respect
          to the following components:

                H2O           H+1

          ---------------------------------------------------
          Activities of the following components are constrained
          by the species shown:

                  COMPONENT          SPECIES             TYPE
                    Cu+2           TENORITE              4
                    H+1            H+1                   3
                    H2O            H2O                   3

PART 3 of OUTPUT FILE
 MINTEQA2  v4.03   DATE OF CALCULATIONS: 15-MAY-2011  TIME: 12:26:55

PARAMETERS OF THE COMPONENT MOST OUT OF BALANCE:
```

ITER	NAME	TOTAL mol/L	DIFF FXN	LOG ACTVTY	RESIDUAL
4	Na+1	1.380E-02	-1.577E-03	-1.91280	1.575E-03
5	Na+1	1.380E-02	1.771E-03	-1.86011	1.769E-03

ID No	Name	Total Conc(M)	Conc (M)	log Activity	Diff fxn
180	Cl-1	1.364E-02	1.364E-02	-1.91777	1.246E-07
490	NH4+1	1.276E-03	1.237E-03	-2.96012	1.128E-08
500	Na+1	1.380E-02	1.380E-02	-1.91254	1.261E-07
2	H_2O	0.000E+00	-1.582E-04	-0.00021	0.000E+00
330	H+1	0.000E+00	1.788E-08	-7.80000	0.000E+00
231	Cu+2	1.575E-04	1.794E-08	-7.95579	0.000E+00

Type I - COMPONENTS AS SPECIES IN SOLUTION

ID No	Name	Conc (M)	log Act	Charge	Act Coef	New logK
330	H+1	1.788E-08	-7.80000	1.00	0.88628	0.052
490	NH4+1	1.237E-03	-2.96012	1.00	0.88628	0.052
500	Na+1	1.380E-02	-1.91254	1.00	0.88628	0.052
180	Cl-1	1.364E-02	-1.91777	-1.00	0.88628	0.052
231	Cu+2	1.794E-08	-7.95579	2.00	0.61699	0.210

Type II - OTHER SPECIES IN SOLUTION OR ADSORBED

ID No	Name		Conc (M)	log Act	Charge	Act Coef	New logK
3304900	NH3 (aq)		3.929E-05	-4.40434	0.00	1.00331	-9.246
2314901	CuNH3+2		7.241E-09	-8.34991	2.00	0.61699	-5.024
3300020	OH-		7.165E-07	-6.19721	-1.00	0.88628	-13.945
2313300	CuOH+		2.509E-08	-7.65300	1.00	0.88628	-7.445
2313301	Cu(OH)2 (aq)		2.808E-09	-8.55021	0.00	1.00331	-16.195
2313302	Cu(OH)3-		4.140E-12	-11.43543	-1.00	0.88628	-26.827
2313303	Cu(OH)4-2		2.972E-17	-16.73664	-2.00	0.61699	-39.770
2313304	Cu2(OH)2+2		3.458E-11	-10.67094	2.00	0.61699	-10.149
2311800	CuCl+		2.393E-10	-9.67356	1.00	0.88628	0.252
2311801	CuCl2 (aq)		8.856E-13	-12.05133	0.00	1.00331	-0.261
2311802	CuCl3-		1.131E-16	-15.99910	-1.00	0.88628	-2.238
2311803	CuCl4-2	1	9.837E-21	-20.21687	-2.00	0.61699	-4.380

Type III - SPECIES WITH FIXED ACTIVITY

ID No	Name	Conc (M)	New logK	Enthalpy
2	H_2O	-1.582E-04	0.000	0.000
330	H+1	3.549E-04	7.800	0.000

Type IV - FINITE SOLIDS (present at equilibrium)

ID No	Name	Conc (M)	New logK	Enthalpy
2023101	**TENORITE**	**1.574E-04**	**-7.644**	**64.867**

Type V - UNDERSATURATED SOLIDS (not present at equilibrium)

ID No	Name	Conc (M)	New logK	Enthalpy
2023100	Cu(OH)2	9.328E-02	-8.674	56.420
4123100	MELANOTHALLITE	8.943E-19	-6.257	63.407
4123101	ATACAMITE	1.510E-02	-7.391	93.430
4150000	HALITE	3.691E-06	-1.603	-3.700

_____ PART 4 of OUTPUT FILE
MINTEQA2 v4.03 DATE OF CALCULATIONS: 15-MAY-2011 TIME: 12:26:55

PERCENTAGE DISTRIBUTION OF COMPONENTS AMONG
TYPE I and TYPE II (dissolved and adsorbed) species

Cl-1	100.0	Percent bound in species # 180	Cl-1
NH4+1	96.9	Percent bound in species # 490	NH4+1
	3.1	Percent bound in species #3304900	NH3 (aq)
Na+1	100.0	Percent bound in species # 500	Na+1
H_2O	95.9	Percent bound in species #3300020	OH-
	3.4	Percent bound in species #2313300	CuOH+
H+1	98.2	Percent bound in species #3304900	NH3 (aq)
	1.8	Percent bound in species #3300020	OH-
Cu+2	33.6	Percent bound in species # 231	Cu+2
	13.6	Percent bound in species #2314901	CuNH3+2
	47.0	Percent bound in species #2313300	CuOH+
	5.3	Percent bound in species #2313301	Cu(OH)2 (aq)

PART 5 of OUTPUT FILE
MINTEQA2 v4.03 DATE OF CALCULATIONS: 15-MAY-2011 TIME: 12:26:55

---------- EQUILIBRATED MASS DISTRIBUTION ----------

IDX	Name	DISSOLVED		SORBED		PRECIPITATED	
		mol/L	percent	mol/L	percent	mol/L	percent
180	Cl-1	1.364E-02	100.0	0.000E+00	0.0	0.000E+00	0.0
490	NH4+1	1.276E-03	100.0	0.000E+00	0.0	0.000E+00	0.0
500	Na+1	1.380E-02	100.0	0.000E+00	0.0	0.000E+00	0.0
2	H_2O	7.473E-07	100.0	0.000E+00	0.0	0.000E+00	0.0
330	H+1	-4.002E-05	100.0	0.000E+00	0.0	0.000E+00	0.0
231	**Cu+2**	**5.339E-08**	**0.0**	**0.000E+00**	**0.0**	**1.574E-04**	**100.0**

Charge Balance: SPECIATED

Sum of CATIONS = 1.504E-02 Sum of ANIONS 1.364E-02
PERCENT DIFFERENCE = 4.888E+00 (ANIONS - CATIONS)/(ANIONS + CATIONS)

```
     EQUILIBRIUM IONIC STRENGTH (m) =   1.434E-02

     EQUILIBRIUM pH                 =   7.800

     DATE ID NUMBER:        20110515
     TIME ID NUMBER:        12265594

_ PART 6 of OUTPUT FILE
 MINTEQA2  v4.03   DATE OF CALCULATIONS: 15-MAY-2011  TIME: 12:26:55


Saturation indices and stoichiometry of all minerals

 ID No     Name           SI    Composition by stoich. of components
 2023100 Cu(OH)2       -1.030 [  1.000]231 [  2.000]  2 [ -2.000]330
 2023101 TENORITE       0.000 [  1.000]231 [  1.000]  2 [ -2.000]330
 123100 MELANOTHALLITE -18.049 [  1.000]231 [  2.000]180
 4123101 ATACAMITE    -1.821 [  2.000]231 [  3.000]  2 [ -3.000]330
                                        [  1.000]180
 4150000 HALITE                -5.433 [  1.000]500 [  1.000]180
```

Advancing the Science of Water Reuse and Desalination

WATEREUSE RESEARCH

1199 North Fairfax Street, Suite 410
Alexandria, VA 22314 USA
(703) 548-0880
Fax (703) 548-5085
E-mail: Foundation@WateReuse.org
www.WateReuse.org/Foundation